Multiplexed DNA-mediated Electrochemistry

Thesis by
Catrina Gale Pheeney

In Partial Fulfillment of the Requirements for the Degree of Doctor of Philosophy

California Institute of Technology
Pasadena, California
2014
(August 22, 2013)

ACKNOWLEDGEMENTS

Without the support of my many mentors, colleagues, friends, and family this degree would not have been possible. Most importantly I would like to thank my advisor, Jackie, who has been an amazing mentor and role model over the years. Her unwavering belief in my capabilities helped me to become the scientist I am today. Her passion and drive for success are contagious and have taught me the value of striving for lofty goals. I hope I have adopted her zeal for dreaming big. Overall, the balance of her drive and her compassion made her a mentor who I will never forget and has played a critical role in shaping who I am and where I go from here.

I would like to thank my committee chair, Dave Tirrell, whose supportive and engaging demeanor made every milestone feel all the more significant. I learned to count on him to make every interaction a learning experience, and I felt he always had my best interest at heart. I would like to thank Jim Health and Dennis Dougherty, who were also valuable members of my committee. Together they created a committee that was supportive and enthusiastic about me throughout the degree and beyond.

I would like to acknowledge the invaluable mentorship that Natalie Muren provided me throughout the degree. She took me under her wing when I arrived in grad school and taught me how to do bench work from the ground up. I could never imagine completing this degree without her continued supportive presence throughout all the bumps in the road. Through working side-by-side with her I have learnt a lot not only about science but also about myself. I will miss her, not only as a colleague, but as a friend.

I would like to thank all the additional people I have collaborated with over the years. Specifically, I would like to thank Anna Arnold and Mike Grodick for their work on the multiplexed endo project. Thank you for being willing to teach me even the basics of protein

handling and for being a truly collaborative team. I couldn't imagine a more pleasant and skilled group to have done this project with. Additionally, I would like to thank Luis Guerra, who was a dedicated SURF and a valuable addition to the hemoglobin project. I would like to also thank subgroup 3 and multiplexed Bartonites, especially Natalie, Ariel, and Phil, because without our collaborative environment none of our projects would have been possible.

I would like to thank the many skilled and influential Bartonites that I have had the pleasure to overlap with; some have not only been excellent mentors and colleagues but have also been great friends. In particular I would like to thank Joey Genereux, Eric Olmon, Katie Schaefer, Anna McConnell, Anna Arnold, and Helen Segal, as they have helped shape my graduate experience and given me many fond lasting memories.

I would like to thank Mo Renta for her continued efforts in keeping everything moving forward and never forgetting about us. I always counted on her for a good dose of reassurance or a quick reality check, whichever the current situation required. I will miss being able to count on her to know exactly what to do to fix my latest predicament.

I would like to thank the staff of the Kavli Nanoscience Institute, most of all Melissa Melendez, for taking countless hours to teach me and guide me into the world of fabrication. I will always be thankful for Melissa's patience and care while teaching this chemist how to do fabrication properly. I could count on her to be genuinely supportive and enthusiastic for both my work and life. I would also like to thank the CCE staff members, whose continued dedication to the division makes it possible to do the work that we do.

I would like to thank all the Caltech friends that I have made over the years; they have not only been supportive but have created many fun times that I will never forget. Particularly, I would like to thank my husband Matthew for making life a team sport and being the best partner I could ask for. I would like to thank the McDaffies for being an

awesome pair and for never letting late night brawls affect us the next day. I would like to thank the invention of Skype and Gchat for allowing me to feel the continued presence of Deb and Leah in my life. Their continued support has always provided me perspective on why I am where I am. Also, I couldn't be more grateful for the supportive friends I have back home (Heather, Nadine, Bruce, Joel, Tye, etc. …) who, despite seeing me so infrequently, are constant cheerleaders. Finally, I want to give my love and greatest thanks to my parents. Thank you for raising me to be inquisitive, quirky, and to strive to be the best I can. I see elements of both of you in who I am today and I thank you for that.

ABSTRACT

The aromatic core of double helical DNA possesses the unique and remarkable ability to form a conduit for electrons to travel over exceptionally long molecular distances. This core of π-stacked nucleobases creates an efficient pathway for charge transfer to proceed that is exquisitely sensitive to even subtle perturbations. Ground state electrochemistry of DNA-modified electrodes has been one of the major techniques used both to investigate and to harness the property of DNA-mediated charge transfer. DNA-modified electrodes have been an essential tool for both gaining insights into the fundamental properties of DNA and, due to the exquisite specificity of DNA-mediated charge transfer for the integrity of the π-stack, for use in next generation diagnostic sensing. Here, multiplexed DNA-modified electrodes are used to (i) gain new insights on the electrochemical coupling of metalloproteins to the DNA π-stack with relevance to the fundaments of *in vivo* DNA-mediated charge transfer and (ii) enhance the overall sensitivity of DNA-mediated reduction for use in the detection of low abundance diagnostic targets.

First, Methylene Blue (MB′) was covalently attached to DNA through a flexible C12 alkyl linker to yield a new redox reporter for DNA electrochemistry measurements with enhanced sensitivity. Tethered, intercalated MB′ was reduced through DNA-mediated charge transport. The redox signal intensity for MB′-dT-C12-DNA was found to be at least 3 fold larger than that of previously used Nile Blue (NB)-dT-DNA, which is coupled to the base stack via direct conjugation. The signal attenuation, due to an intervening mismatch, and therefore the degree of DNA-mediated reduction, does, however, depend on the DNA film morphology and the backfilling agent used to passivate the surface. These results highlight two possible mechanisms for the reduction of MB′ on the DNA-modified electrode that are distinguishable by their kinetics: reduction mediated by the DNA base pair stack and direct

surface reduction of MB′ at the electrode. The extent of direct reduction at the surface can be minimized by overall DNA assembly conditions.

Next, a series of intercalation-based DNA-mediated electrochemical reporters were developed, using a flexible alkane linkage to validate and explore their DNA-mediated reduction. The general mechanism for the reduction of distally bound redox active species, covalently tethered to DNA through flexible alkyl linkages, was established to be an intraduplex DNA-mediated pathway. MB, NB, and anthraquinone were covalently tethered to DNA with three different covalent linkages. The extent of electronic coupling of the reporter was shown to correlate with the DNA binding affinity of the redox active species, supporting an intercalative mechanism. These electrochemical signals were shown to be exceptionally sensitive to a single intervening π-stack perturbation, an AC mismatch, in a densely packed DNA monolayer, which further supports that the reduction is DNA-mediated. Finally, this DNA-mediated reduction of MB occurs primarily via intra- rather than inter duplex intercalation, as probed through varying the proximity and integrity of the neighboring duplex DNA.

Further gains to electrochemical sensitivity of our DNA-modified devices were then achieved through the application of electrocatalytic signal amplification using these solvent accessible intercalative reporters, MB-dT-C8, and hemoglobin as a novel electron sink. Electrocatalysis offers an excellent means of electrochemical signal amplification, yet in DNA based sensors, its application has been limited due to strict assembly conditions. We describe the use of hemoglobin as a robust and effective electron sink for electrocatalysis in DNA sensing on low density DNA films. Protein shielding of the heme redox center minimizes direct reduction at the electrode surface and permits assays on low density DNA films. Electrocatalysis of MB that is covalently tethered to the DNA by a flexible alkyl linkage allows for efficient interactions with both the base stack and hemoglobin. Consistent

suppression of the redox signal upon incorporation of single CA mismatch in the DNA oligomer demonstrates that both the unamplified and the electrocatalytically amplified redox signals are generated through DNA-mediated charge transport. Electrocatalysis with hemoglobin is robust: it is stable to pH and temperature variations. The utility and applicability of electrocatalysis with hemoglobin is demonstrated through restriction enzyme detection, and an enhancement in sensitivity permits femtomole DNA sampling.

Finally, we expanded the application of our multiplexed DNA-modified electrodes to the electrochemical characterization of DNA-bound proteins containing [4Fe-4S] clusters. DNA-modified electrodes have become an essential tool for the characterization of the redox chemistry of DNA repair proteins that contain redox cofactors. Multiplexed analysis of EndonucleaseIII (EndoIII), a DNA repair protein containing a [4Fe-4S] cluster known to be accessible via DNA-mediated charge transport, elucidated subtle differences in the electrochemical behavior as a function of DNA morphology. *DNA-bound* EndoIII is seen to have two different electron transfer pathways for reduction, either through the DNA base stack or through direct surface reduction. Closely packed DNA films, where the protein has limited surface accessibility, produce electrochemical signals reflecting electron transfer that is DNA-mediated. The electrochemical comparison of EndoIII mutants, including a new family of mutations altering the electrostatics surrounding the [4Fe-4S] cluster, was able to be quantitatively performed. While little change in the midpoint potential was found for this family of mutants, significant variations in the efficiency of DNA-mediated electron transfer were apparent. Based on the stability of these proteins, examined by circular dichroism, we propose that the electron transfer pathway can be perturbed not only by the removal of aromatic residues, but also through changes in solvation near the cluster.

TABLE OF CONTENTS

LIST OF FIGURES

CHAPTER 1.

CHAPTER 2.

CHAPTER 3.

LIST OF TABLES

CHAPTER 1

DNA-mediated electrochemistry

INTRODUCTION

DNA-mediated charge transport

The aromatic core of double helical DNA possesses the unique and remarkable ability to form a conduit for electrons to travel over exceptionally long molecular distances (*1-8*). The conductive properties of DNA have long been predicted due to the similarities of the π-stacking character of the aromatic nucleobases to that of sheets of graphene (*9*) (Figure 1.1). The inter-base pair spacing in duplex DNA is 3.4 Å, the same as the spacing between sheets of graphene, highlighting their potential electronic similarities (*9*). Since these conductive properties of DNA were first predicted, decades of experimental evidence has demonstrated the ability of DNA to function as a molecular wire.

Through the use of a variety of platforms, including solution phase and solid phase as well as excited state and ground state experiments, many of the fundamental properties of DNA-mediated charge transport (DNA CT) have been elucidated. This core of π-stacked nucleobases not only creates a highly efficient pathway for charge transfer with an exceptionally shallow distance dependence (*7, 8*), but is also exquisitely sensitive to even subtle perturbations (*10, 11*).

DNA-modified electrodes

DNA-modified electrodes have proved to be an invaluable tool for the characterization of ground state DNA CT (*8, 10-14*) as well as in the development of next generation biosensors (*15-20*). Electrochemistry provides an affordable and simple means of performing these surface-based studies. DNA-modified electrodes are formed through the immobilization of DNA with a chemical moiety that covalently attaches it to the surface (Figure 1.2). Most commonly, DNA is modified with an alkane thiol appended off the 5′ end

Figure 1.1. The structure of double helical DNA. The nucleobases are depicted using a space filling model (grey) and the sugar-phosphate backbone is depicted using a ribbon (black). Both the axes parallel (top) and perpendicular (bottom) to the direction of DNA CT propagation are presented. The perpendicular axis (bottom) highlights the extensive degree of overlap between the base pairs.

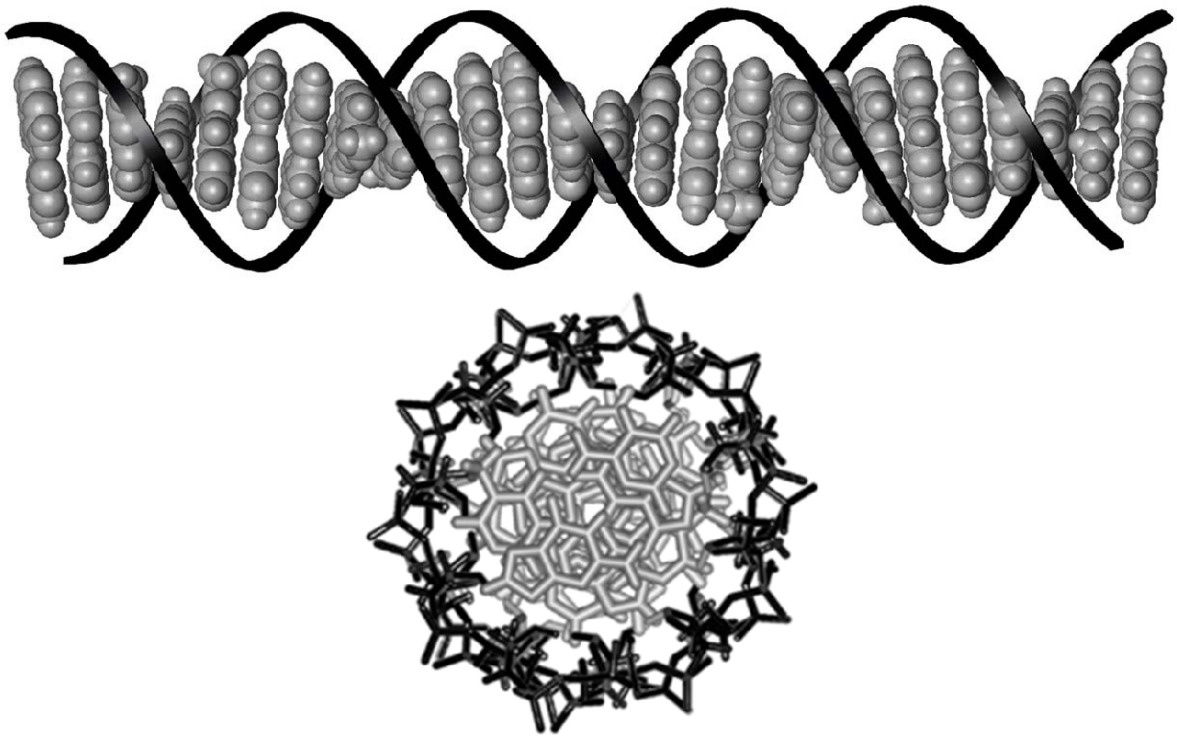

Figure 1.2. Thiol-modified duplex DNA is self-assembled on gold surfaces using a $(CH_2)_6$ alkane linkage. The distal end is modified with an intercalative redox active reporter. In the case of a well-matched duplex (left), DNA CT is able to occur and reduce the reporter as the π–stack is uninterrupted. Incorporation of a single intervening base mismatch (right) disrupts the DNA π-stack such that electrons can no longer efficiently reduce the reporter and the electrochemical signal is attenuated.

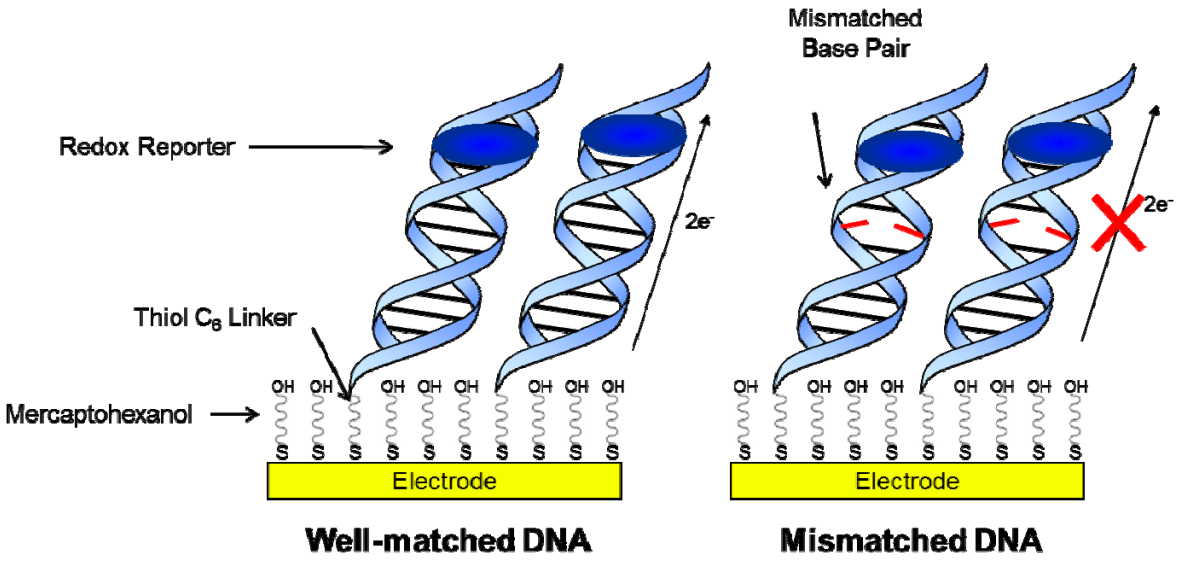

of the duplex, driving the self-assembly of DNA on gold electrodes (*14*). These electrodes are then backfilled with mercaptoalkanes to fill in all remaining areas of exposed electrode surface. This serves to reduce background oxygen contributions and allows the DNA to adopt an upright position (*21*). The two most common means of altering the morphology of the DNA monolayer formed are the addition of $MgCl_2$ (*16, 22*) or backfilling agents during DNA self-assembly (*23*). $MgCl_2$ has been shown to screen the negative charge of the sugar phosphate backbone of DNA, allowing the formation of much more densely packed DNA monolayers. The co-deposition of mercaptoalkanes with the DNA has been shown to yield more extensively passivated surfaces with enhanced signal to noise ratios.

The final component to these DNA-modified electrodes is a redox-active moiety that can be electrochemically monitored. Many different electrochemical reporters have been used for the investigation of these DNA-modified electrodes, including redox active metals, aromatic organic compounds, and proteins (*24*). The choice of the redox-active reporter depends on the properties that one wishes to investigate. Ruthenium hexamine, which electrostatically associates with DNA, is ideal for the quantification of immobilized DNA, while intercalative organic dyes, such as Methylene Blue, Nile Blue, and Daunomycin are ideal for reporting on the integrity of the π-stack and therefore the DNA-mediated electrochemistry. Ultimately, the successful electrochemical characterization of DNA CT by theses platforms depends on the extent and specificity of the electronic coupling of the reporter to the π-stack (*25*). More recently, the covalent tethering of these redox-active reporters has been developed to control the placement and electronic coupling of these reporters (*11, 19, 20, 22, 25*). A variety of means of coupling to the π–stack have been developed, including end capping, intercalation, and direct conjugation (*14, 25, 26*).

Putting all these components together yields a platform where DNA is immobilized on an electrode surface in an upright position with a distally bound redox-active species. At a potential negative enough to reduce the reporter, electrons will travel through the π-stack

of the DNA, yielding an electrochemical signal. This is a reversible signal and will persist as long as the π-stack remains unperturbed. Upon introduction of even a single base pair mismatch or lesion, the observed DNA-mediated signal will be drastically attenuated (*10, 11*). These DNA-mediated signals have been characterized to be rate-limited by tunneling through the alkane thiol (*13*), to have minimal lateral diffusion throughout the monolayer (*12*), and to be capable of proceeding over exceptionally long molecular distances, 34 nm (*8*).

Multiplexed analysis

Multiplexed platforms for these DNA-modified electrodes have been developed to detect an extensive range of targets, including small molecules, DNA, RNA, and proteins (*15, 19, 20, 27-29*). These devices are all designed to achieve the same goals of enhanced sensitivity, faster detection times, and tolerance to cell lysates (*19, 28, 30*). Despite a variety of designs for these multiplexed DNA-modified electrodes, they all possess the same intrinsic benefits of statistical comparisons and parallel experimentation. These advantages have proven to be essential for the electrochemical characterization of complex systems. Ultimately, these technologies possess ideal attributes for performing the next generation of fundamental electrochemical measurements, as they have been optimized for low variability, real-time monitoring, and complex substrates. The use of multiplexed analysis for the fundamental studies of DNA CT has been demonstrated through the characterization of the biologically relevant conformation of the surface immobilized duplex DNA (*19, 20*), as well as the exceptionally shallow distance dependence of this DNA-mediated electrochemistry (*8*). Multiplexed DNA-modified electrodes allow for subtleties of DNA-mediated electrochemistry to be elucidated and for the direct comparisons necessary for diagnostic applications.

The thesis work described here utilizes multiplexed DNA-modified electrodes to further both our fundamental understanding of the properties of DNA CT and their development in sensing applications. Chapter 2 describes the initial synthesis and electrochemical characterization of a new redox-active DNA CT reporter that interacts with the π-stack through an intercalative mechanism allowing for enhanced sensitivity. This new class of intercalative redox-active reporter for DNA CT was then generalized in Chapter 3 and the mechanism of reduction was further explored and demonstrated to be via an intraduplex DNA-mediated pathway. Chapter 4 harnesses the solvent accessibility of the reporter and a novel electron sink, hemoglobin, to electrocatalytically amplify the DNA-mediated signal, yielding a 100-fold enhancement to the sensitivity of these devices. Finally, Chapter 5 describes the extension of these multiplexed DNA-modified electrodes to the electrochemical characterization of DNA-bound metalloproteins. This body of work brings us one step closer to addressing the challenges of harnessing DNA CT for next generation biosensing and the question of the biological role for DNA CT *in vivo*.

REFERENCES

1. Murphy, C.J., Arkin, M. R., Jenkins, Y., Ghatlia, N. D., Bossmann, S. H., Turro, N. J., Barton, J. K. *Science* **1993**, *262*, 1025.

2. Holmlin, E. R., Dandliker P.J., Barton J.K. *Angew. Chem. Int. Ed.* **1997**, *36*, 2714.

3. Long Range Charge Transfer in DNA II edited by Schuster, G.B,; Topics in Current Chemistry; Springer-Verlag, Berlin, Heidelberg,; 237, 103 (**2004**).

4. Charge Transfer in DNA:From Mechanism to Application edited by Wagenknecht, H.A. (Wiley-VCH Verlag GmbH & Co KGaA, Weiheim, **2005**).

5. Genereux, J.G., Barton, J.K. *Chem. Rev.* **2010**, *110*, 1642.

6. Kelley, S.O., Barton, J.K. *Science* **1999**, *283*, 375.

7. Delaney, S., Barton, J.K. *J. Org. Chem.,* **2003**, *68*, 6475.

8. Slinker, J., Muren, N., Renfrew, S., Barton, J.K. *Nature Chemistry* **2011**, *3*, 228.

9. Eley D.D., Spivey D.I. *Trans. Faraday Soc.* **1962**, *58*, 411.

10. Kelley, S. O., Boon, E., Barton, J. K., Jackson, N., Hill, M. *Nucleic Acids Research* **1999**, *27*, 4830.

11. Boon, E., Ceres, D., Drummond, T., Hill, M., Barton, J. K. *Nature Biotechnology* **2000**, *18*, 1096.

12. Kelley, S.O., Jackson, N.M., Hill, M.G., Barton, J.K. *Angew. Chem. Int. Ed.* **1999**, *38*, 941.

13. Drummond, T.G., Hill, M.G., Barton, J.K. *J. Am. Chem. Soc.* **2004**, *126*, 15010.

14. Kelley, S. O., Barton, J. K., Jackson, N., Hill, M. G. *Bioconjugate Chem.* **1997**, *8*, 31.

15. Lam, B., Fang, Z., Sargent, E.H., Kelley, S.O *Anal. Chem.* **2012**, *84*, 21.

16. Lapierre, M.A., O'Keefe, M., Taft, B.J., Kelley, S.O. *Anal Chem.* **2003**, *75*, 6327.

17. Zhao, S., Yang, W., Lai, R.Y. *Biosens. Bioelectron.* **2011**, *26*, 2442.

18. Kwon, S.J., Bard, A.J. *J. Am. Chem. Soc.* **2012**, *134*, 10777.

19. Pheeney, C.G., Guerra, L.F, Barton, J.K. *Proc. Natl. Acad. Sci.* **2012**, *109*, 11528.

20. Slinker, J.D, Muren, N.B., Gorodetsky, A.A., Barton, J.K. *J. Am. Chem. Soc.* **2010**, *132*, 2769.

21. Gorodetsky A. A., Barton, J. K. *Langmuir* **2006**, *22*, 7917.

22. Boon E.M., Salas, J. E., Barton, J. K. *Nat. Biotechnol.* **2002**, *20*, 282.

23. Muren N. B., Olmon, E.D., Barton, J.K. *Phys. Chem. Chem. Phys.* **2012**, *14*, 13754.

24. Ricci, F., Zari, N., Caprio, F., Recine, S., Amine, A., Moscone, D., Palleschi, G. Plaxco, K.W. *Bioelectrochemistry*, **2009**, *76*, 208.

25. Gorodetsky, A.A., Green, O., Yavin, E., Barton, J.K. *Bioconjugate Chem.* **2007**, *18*, 1434.

26. Boon, E., Jackson, N., Wightman, M., Kelley, S., Hill, M., Barton, J.K. *J. Phys. Chem. B.* **2003**, *107*, 11805.

27. Hsieh, K., Patterson, A.S., Ferguson, B.S, Plaxco, K.W., Soh, H.T. *Angew. Chem. Int. Ed.* **2012**, *51*, 4896.

28. Vasilyeva, E., Lam, B., Fang, Z., Minden, M.D., Sargent, E.H., Kelley, S.O. Angew. *Chem. Int. Ed.* **2011**, *50*, 4137.

29. Das, J., Cederquist, K.B., Zaragoza, A.A., Lee, P.E., Sargent, E.H. and Kelley, S.O. *Nat. Chem.* **2012**, *4*, 642.

30. Bonham, A.J., Hsieh, K., Ferguson, B.S, Vallee-Belisle, A., Ricci, F., Soh, H.T., Plaxco, K.W. *J. Am. Chem. Soc.* **2012**, *134*, 3346.

CHAPTER 2

DNA Electrochemistry with Tethered Methylene Blue

Adapted from Pheeney, C.G., Barton, J. K. (2012) *Langmuir* 28, 7063.

ABSTRACT

Methylene Blue (MB′), covalently attached to DNA through a flexible C12 alkyl linker, provides a sensitive redox reporter in DNA electrochemistry measurements. Tethered, intercalated MB′ is reduced through DNA-mediated charge transport; the incorporation of a single base mismatch at position 3, 10, or 14 of a 17-mer causes an attenuation of the signal to 62 ± 3 % of the well-matched DNA, irrespective of position in the duplex. The redox signal intensity for MB′-DNA is found to be at least 3 fold larger than that of Nile Blue (NB)-DNA, which is coupled to the base stack via direct conjugation, suggesting that intercalation, as opposed to direct conjugation, is a stronger mode of coupling to the π-stack. The signal attenuation, due to an intervening mismatch, and therefore the degree of DNA-mediated reduction, does, however, depend on DNA film density and the backfilling agent used to passivate the surface. These results highlight two possible mechanisms for the reduction of MB′ on the DNA-modified electrode: reduction mediated by the DNA base pair stack and direct surface reduction of MB′ at the electrode. These two mechanisms are distinguished by their rates of electron transfer that differ by 20 fold. The extent of direct reduction at the surface can be controlled by assembly and buffer conditions

INTRODUCTION

Since the discovery that DNA can efficiently serve to conduct an electrical current, its properties have been exploited across numerous platforms (*1-14*). DNA-mediated charge transport (CT) is exquisitely sensitive to perturbations in the intervening base stack, including single base mismatches, lesions, or structural changes caused by proteins (*14-16*).

Electrochemistry experiments on DNA-modified electrodes have been particularly valuable in probing ground state DNA CT and in the development of new DNA-based sensors (*11-19*). To study and exploit the sensitivity of DNA CT, it is essential that the redox-moiety makes an electronic interaction with the base stack of the DNA (*17, 20*).

Over the past decade, various reporters have been used for DNA electrochemistry; some redox reporters have been well-coupled, others, not at all (*14-38*). Early applications of DNA-modified electrodes primarily depended on the use of noncovalent redox reporters. Noncovalent Methylene Blue (MB) was widely used as a reporter for DNA CT, as it intercalates into the base stack (*11, 13*). Studies with noncovalent MB demonstrated the exquisite sensitivity of the π–stack to subtle perturbations, and MB had the additional advantage that it undergoes electrocatalytic signal amplification (*38*).

However, noncovalent reporters incurred a number of constraints, including the inability to control probe placement and the stringent requirement for high quality DNA films. As such, covalent tethering has been explored to address these issues. Covalent tethering of the reporter results in its restricted mobility; therefore it must be ensured that coupling between the reporter and base stack is still feasible. The degree of coupling varies based on the mechanism of interaction between the reporter and the base stack (*17*). Coupling to the base stack has been shown to be possible through various mechanisms, including intercalation (*18*), end-capping (*20*), and direct conjugation to a nucleic acid base (*17*). The

degree to which the reporter is coupled to the base stack determines the overall efficiency of DNA CT.

Daunomycin, when covalently tethered to the DNA through a short alkyl linkage, has been shown to yield exceptionally strong electrochemical signals (*14, 16, 21*). This evidence of strong coupling agrees with the crystal structure that shows daunomycin is tightly intercalated into the base stack (*39, 40*). Despite the exceptional coupling of daunomycin, the field of DNA-mediated based sensors has evolved to use other reporters, as DNA modified with daunomycin is difficult to prepare, is unstable, and has sequence constraints.

More recently Nile Blue (NB) has been used as an electrochemical reporter of DNA CT (*12, 19*). The preparation of NB-DNA does not possess the synthetic limitations of daunomycin, and it is well coupled to the base stack through direct conjugation of NB with a modified uracil (*12*). In the present study, we built upon this work by developing a system to covalently tether MB, as it has previously been shown to strongly intercalate into the base stack.

MB′-DNA was tethered through a flexible C12 alkyl linkage to a modified uracil (Figure 2.1). This linkage further improves the coupling of the reporter by providing the conformational freedom for MB′ to interact with the base stack through intercalation. However, with the enhanced flexibility of the reporter, its ability to be reduced directly at the surface of the electrode must be taken into account.

Various probes, including both MB and ferrocene, have been covalently tethered to the DNA through flexible alkyl linkages and shown to be reduced directly at the electrode surface (*20, 22-37*). This has led to a new class of DNA-modified biosensors, based upon the binding of either oligonucleotides (*22-32*) or DNA-binding proteins (*33*) which cause conformational changes that attenuate the observed signal by physically diminishing the surface accessibility of the reporter. These biosensors are based on the surface reduction

Figure 2.1. On the left: Schematic illustration of MB′-DNA (top) and NB-DNA (bottom) monolayers bound to an electrode. The reporter is appended to the distal base of the duplex. The intended path for electrochemical reduction is indicated. On the right: The chemical structure of both MB′ and NB covalently tethered to a modified uracil.

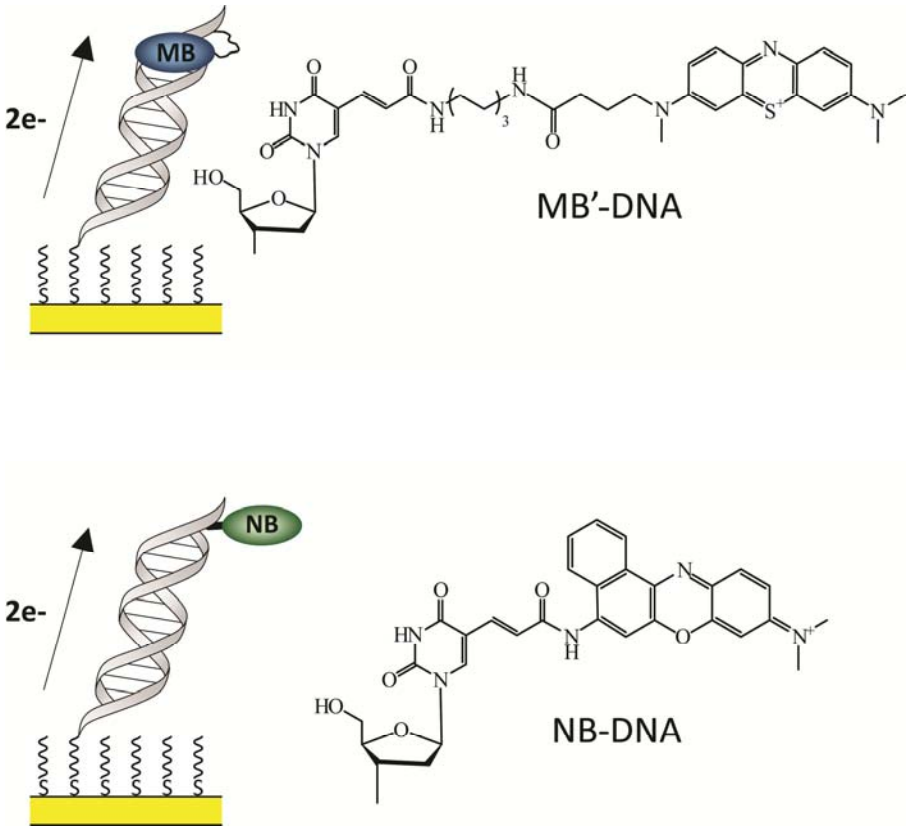

of the reporter, and thus the reporter does not couple with the base stack. Ferrocene has been shown to be a common reporter for this platform, given its poor coupling to the base stack, and yielding efficient reduction at the electrode surface (*37*). More recently, MB′-modified DNA has been frequently used (*22-33*).

In this work, the mechanism of reduction for MB′ covalently tethered to DNA through a flexible C12 alkyl linkage to a modified uracil is investigated (Figure 2.1). MB′-DNA, covalently tethered through this flexible linkage, couples to the base stack through intercalation. This is compared to the previously established reporter, NB-DNA, which is covalently tethered through a short rigid linkage and couples to the base stack through direct conjugation. MB′-DNA is shown not only to be reduced via DNA CT, but is also capable of being reduced directly at the surface (Figure 2.2). We describe the conditions under which DNA CT is the primary mechanism for MB' reduction.

MATERIALS AND METHODS

Synthesis of Modified NHS Ester Activated Methylene Blue' (Figure 2.3).

All materials were used as purchased from Sigma-Aldrich. See Appendix I for further details.

*2-Amino-5-dimethylaminophenylthiosulfonic acid (**3**) preparation.* **3** was prepared according to the procedure described by Wanger (*41*) by separately dissolving aluminum sulfate octadecahydrate (43.6 mg, 65 mmol), sodium thiosulfate (22.0 g, 140 mmol), and zinc chloride (8.8 g, 63 mmol) in 100 mL, 80 mL, and 12 mL of water respectively, which was then added to N,N-dimethylphenylene diamine (**1**) (10 g, 73 mmol) in a 500 mL round bottom flask. The reaction mixture was then cooled to 0 °C while continuously stirring. Potassium dichromate (5.0 g, 17 mmol) was dissolved in 30 mL of water and added

Figure 2.2. Schematic illustration of the different proposed mechanisms for MB′-DNA reduction on DNA-modified electrodes.

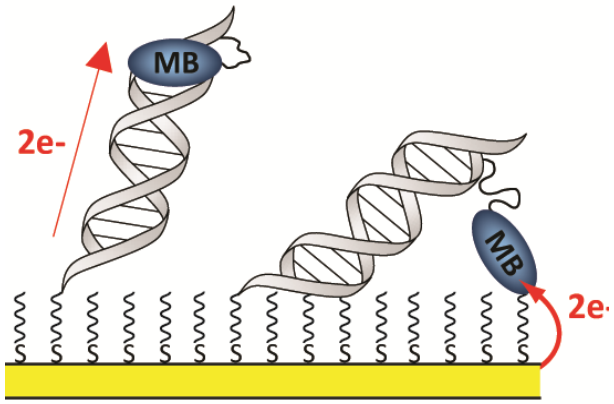

Figure 2.3. Synthetic strategy for the preparation of N-carboxypropyl Methylene Blue (MB′)

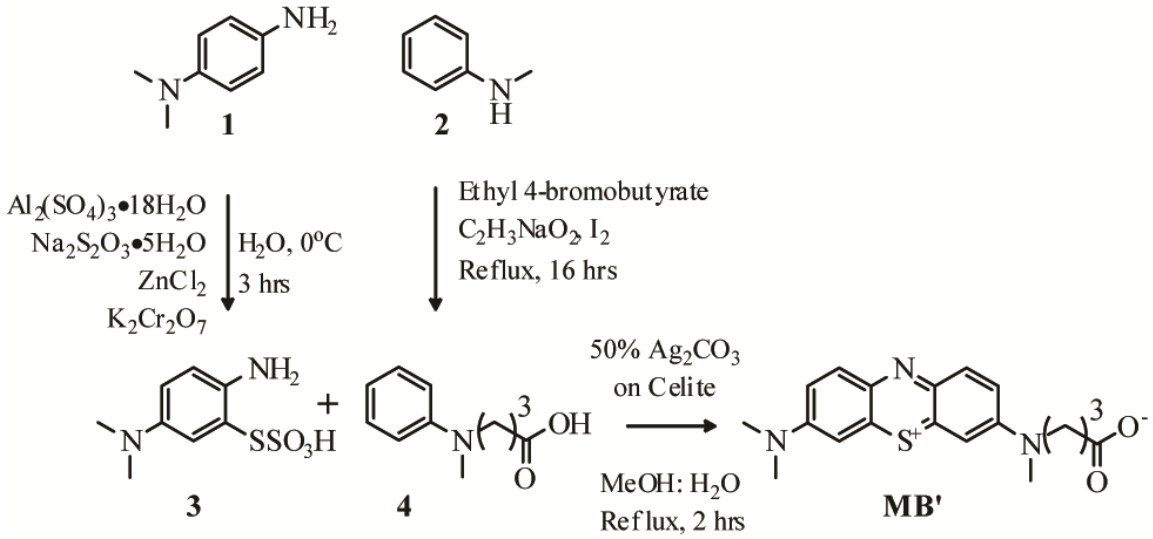

dropwise to the reaction mixture over 15 min. The reaction was kept at 0 °C for 2 hr and then slowly allowed to warm to room temperature. The precipitate was isolated by vacuum filtration and washed with water, acetone, and ether. The purple solid (7.4 g, 30 mmol, 41 % yield) was confirmed as the desired product by ^{1}H-NMR (DMSO-d_6) and was used in subsequent reactions without further purification.

*N-methyl-N-(carboxypropyl)aniline (**4**) preparation.* **4** was prepared according to the procedure described by Whitten (*42*). N-methylaniline (**2**) (15.17 mL, 140 mmol) was refluxed with ethyl-4-bromobutyrate (20.0 mL, 140 mmol) for 16 hr in a 100 mL round bottom flask. The reaction mixture was then cooled to room temperature and water (15 mL) was added. The crude reaction mixture was then made basic by the dropwise addition of saturated sodium hydroxide and extracted with ether (3 x 50 mL). The extract was washed with water, dried over $MgSO_4$, and the ether was removed under reduced pressure. Pure N-methyl-N-ethyl-4-butanoate aniline (16.3 g, 74 mmol, 53 % yield) was isolated, as a clear liquid, by vacuum filtration at 110 °C at 0.2 mm Hg. The product was confirmed by ^{1}H-NMR and ^{13}C-NMR ($CDCl_3$) and an observed mass of 221.3 g/mol (calculated mass of 221.3 g/mol) in ESI-MS in acetonitrile:water:acetic acid (1:1:0.1 %).

The ester product (9.4 g, 43 mmol) was subsequently hydrolyzed in 5 % KOH (150 mL) by refluxing for 2 hr to form the desired carboxylic acid. The reaction was cooled to room temperature and washed with ether (2 x 70 mL). Concentrated hydrochloride acid was added dropwise to the aqueous layer to adjust the pH to 5.5, and then the product was extracted with ether (3 x 100 mL), dried over $MgSO_4$, and the solvent was removed under reduced pressure. The desired product, **4** (5.1 g, 26 mmol, 62 % yield) was confirmed by ^{1}H-NMR and ^{13}C-NMR ($CDCl_3$) and an observed mass of 193.2 g/mol (calculated mass of 193.2 g/mol) with ESI-MS in acetonitrile:water:acetic acid (1:1:0.1 %).

*N-(carboxypropyl)-Methlyene Blue (**MB'**) preparation.* **MB′** was prepared using an adapted procedure from Wagner (*41*). **3** (2.4 g, 9.7 mmol) and **4** (1.87 g, 9.7 mmol) were combined and dissolved in a methanol:water mixture (200 mL : 80 mL). The reaction was heated to just below reflux (60 °C) and 50 % w/w silver carbonate on Celite (10 g) was slowly added. The reaction was then refluxed for 2 hr. The reaction was left to cool to room temperature, was vacuum filtered, and the solvent was removed under reduced pressure. The desired product **MB′** (0.9 g, 2.5 mmol, 26 % yield) was isolated by dry chromatography (*43*) as conventional chromatography techniques were unsuccessful. Impurities were eluted using 20 mL portions of chloroform:methanol:acetic acid (100:15:1.5), and the blue band (**MB′**) was eluted using portions of chloroform:methanol:acetic acid (100:30:1.5). The final product was confirmed by an observed mass of 356.3 g/mol (calculated mass of 357.13 g/mol) with ESI-MS in acetonitrile:water:acetic acid (1:1:0.1 %).

MB'-NHS ester preparation. **MB′** (8 mg, 0.022 mmol) was dissolved in DMF (1 mL) and combined with N,N'-dicyclohexylcarbodiimide (9.3 mg, 0.045 mmol) and N-hydroxysuccinimide (5.2 mg, 0.045 mmol). The reaction proceeded at room temperature for 24 hr. The solvent was removed under reduced pressure and the material was re-suspended in DMSO. Successful ester activation was confirmed by a mass of 454.5 g/mol (calculated mass of 454.54 g/mol) in ESI-MS in acetonitrile:water:acetic acid (1:1:0.1 %). Activated ester was not found to be stable for extended periods of time, and therefore it was freshly prepared directly before tethering to amino-modified DNA.

Synthesis of Modified Oligonucleotides

The synthesis and purification of NB and thiol-modified oligonucleotides were carried out following the previously reported protocol (*19, see Appendix II*). Thiol-modified and NHS-ester uracil analog phosphoramidites were purchased from Glen Research.

MB'-modified oligonucleotides were synthesized similarly to NB-DNA with the substitution of an amino-$(CH_2)_6$-uracil analogue purchased from Glen Research. Amino-modified DNA was purified using standard protocols and then coupled in solution to MB'-NHS ester.

Amino-modified DNA was suspended in 200 µl of a 0.1 M $NaHCO_3$ solution in order to buffer the reaction to a pH of 8.3-8.4. MB'-NHS ester was suspended in DMSO (100 µl) and added to the DNA solution in roughly a 10 fold excess of MB'-NHS ester to amino-modified DNA. The reaction was left to proceed for 12-24 hr. A final round of purification was performed by high-performance liquid chromatography (HPLC) using a 50 mM ammonium acetate buffer/acetonitrile gradient with a PLRP-S Column (Agilent). The MB'-DNA mass was confirmed by matrix-assisted laser desorption/ionization-time of flight mass spectrometry. A mass of 5695 g/mol was found for well-matched MB'-DNA, agreeing with the calculated mass of 5695 g/mol (Figure 2.4).

DNA stock solutions were prepared in low salt buffer (5.0 mM phosphate, 50 mM NaCl, pH 7) and quantified as previously reported. The extinction coefficient for single-stranded MB'-DNA at 260 nm was corrected for the absorbance of MB'. This correction was performed by adding the extinction coefficient of MB' at 260 nm (10,300 $M^{-1}cm^{-1}$) to the calculated extinction coefficient for single-stranded DNA. All DNA solutions were thoroughly deoxygenated with argon prior to annealing. Equimolar amounts of thiol-modified and probe-modified oligonucleotides were combined and annealed by heating to 90 ºC and cooling to ambient temperature over 90 min to form duplexes.

Preparation of DNA Monolayers and Electrochemical Measurements

Multiplex chips, previously reported (*19*), were employed for the electrochemical experiments. Each chip contains 16 gold electrodes (2 mm^2 area) which were prepared with up to four different kinds of DNA. Equimolar amounts of single-stranded thiol-modified and

probe-modified DNA were annealed prior to the electrode assembly. HPLC analyticals of duplex DNA stocks were performed prior to electrode assembly to ensure that there were no single-stranded impurities (data not shown). The duplex DNA (25 µl of 25 µM) was then assembled on the electrode surface overnight (20-24 hr) in a humid environment to allow for monolayer formation with or without 100 mM $MgCl_2$. Once DNA films were assembled and thoroughly washed with low salt buffer, the electrodes were backfilled with either 1 mM 6-mercaptohexanol (MCH) or 6-mercaptohexanoic acid (MHA) for 45 min in low salt buffer with 5 % glycerol. The electrodes were again washed to ensure removal of trace alkanethiols. The electrodes were scanned in a common running buffer of either low salt buffer (5.0 mM phosphate, 50 mM NaCl, pH 7) or spermidine buffer (5.0 mM phosphate, 50 mM NaCl, 4 mM $MgCl_2$, 4 mM spermidine, 50 µM EDTA, 10 % glycerol, pH 7). An analogous buffer to spermidine buffer was prepared that lacked spermidine, and minimal changes were observed in the electrochemistry compared to the low salt buffer (data not shown). Thus, electrochemical differences are best attributed to the effect of adding spermidine. Electrochemical measurements were performed with a CHI620D Electrochemical Analyzer and a 16-channel multiplexer from CH Instruments. A three-electrode setup was used, with a common Ag/AgCl reference and Pt wire auxiliary electrodes placed in the central buffer solution.

Cyclic voltammetry (CV) data was collected at 100 mV/s, with the exception of the scan rate dependence experiments where the scan rate is indicated. In order to minimize errors associated with thiol oxidation and surface quality, all CVs overlaid and compared were acquired on the same multiplexed chip with the thiol-modified strand being equivalent in all duplexes.

The film density (Γ) of MB'-DNA and NB-DNA was calculated by the area under the reductive peaks of CVs at 100 mV/s (Equation 2.1).

(Equation 2.1) $\Gamma = Q / nFA$

In Eq. 2.1, Q is the area of the reductive signal, n is the number of electrons per redox event (n = 2 for both NB and MB'), F is Faraday's constant, and A is the area of the gold electrode.

RESULTS

Electrochemistry of MB'-DNA with Intervening Mismatches

In this investigation MB' has been confined to the distal end of the duplex through a flexible C12-linker appended off the terminally modified uracil (Figure 2.1). As seen in Figure 2.4, the resulting CVs from scanning the electrodes in spermidine buffer exhibit strong reductive and oxidative peaks with a midpoint potential of -290 mV versus Ag/AgCl. This is the same reduction potential as freely diffusing MB, indicating that covalently tethering MB' to the DNA through a flexible alkyl does not alter its electronic properties (*44*). The areas of the reductive and oxidative signals were 7.8 ± 0.4 nC and 7.5 ± 0.3 nC, respectively. Surface bound species reduced by DNA CT have previously been shown to have cathodic/anodic signals with ratios of near unity, which we have ascribed to the fact that the binding affinity of MB for duplex DNA is lowered upon reduction (*19, 38*).

In order to demonstrate that the reduction of MB'-DNA occurs via DNA CT, the signal attenuation from the introduction of a single mismatched base pair (CA) intervening between the surface and the probe was compared to that of well-matched MB'-DNA. By performing these experiments on multiplexed chips, any variation that can be observed from backfilling the electrodes is removed. Under these conditions, any signal differential obtained between well-matched and mismatched DNA on the same multiplexed chip can be attributed to deficiencies in the CT properties of the mismatched DNA (*19*). Introduction of a signal base

Figure 2.4. Electrochemistry of MB'-DNA with a single intervening AC mismatch. Top: Cyclic voltammetry was acquired at 100 mV/s with either a well-matched sequence (blue) or a sequence containing a single mismatch (red). Bottom: All four sequences (left) of MB'-DNA were assembled on the same multiplexed chip and assembled without $MgCl_2$, passivated with MHA, and scanned in spermidine buffer. The area of the reductive signal (right) was used to quantify the signals observed and the errors denoted are determined from the variation across four different electrodes.

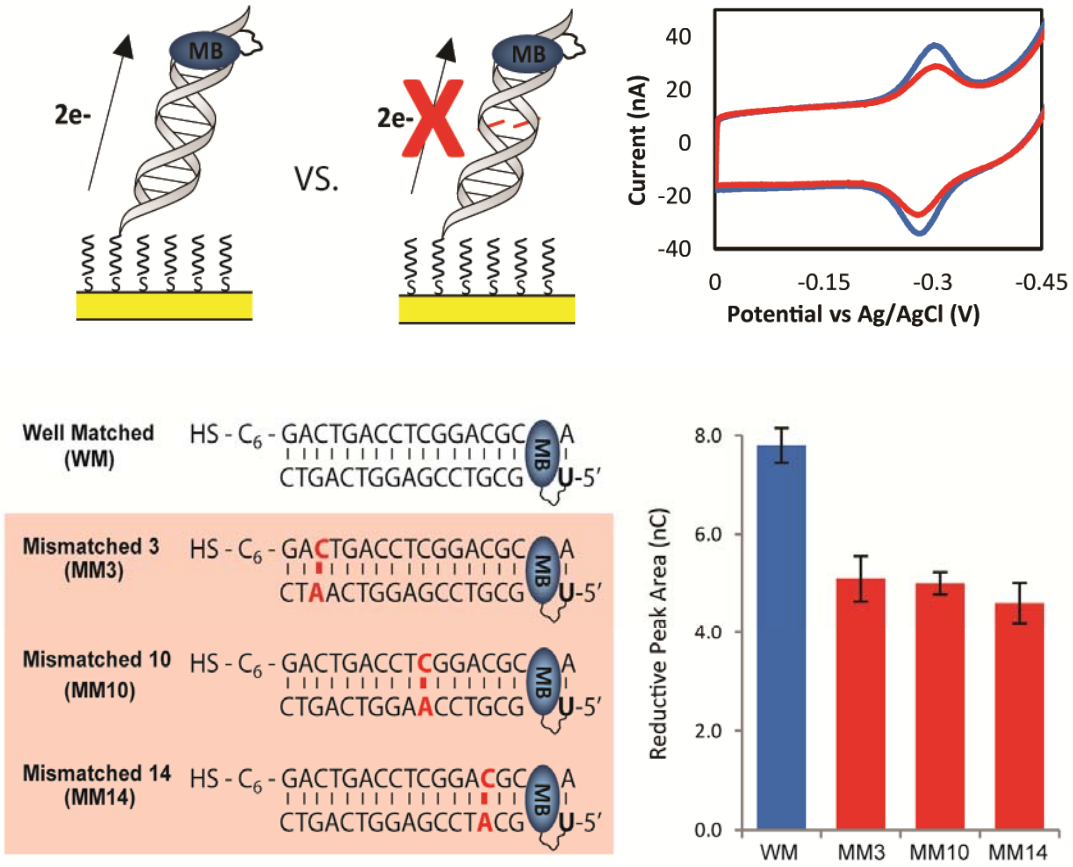

mismatch has been well documented to cause attenuations in DNA CT in both photophysical studies and DNA electrochemistry studies (*1-16*).

Thiol-modified DNA was annealed to the complementary well-matched (WM) DNA sequence and three different mismatched DNA sequences, where the position of the mismatch was varied. The mismatches varied from proximal to the electrode (MM3), in the middle (MM10), and at the distal end (MM14) of the duplex (Figure 2.4). The four quadrants of a multiplexed chip were used to simultaneously assemble each type of DNA overnight without $MgCl_2$ (Figure 2.4). In this case the electrodes were passivated by backfilling with MHA and scanned in spermidine buffer. The ratio of the mismatched to well-matched reduction signal areas was quantified in all cases to determine the percent mismatch signal. The signal area of well-matched MB'-DNA was found to be 7.8 ± 0.4 nC. For the various mismatches, the percent signal remaining was 65 %, 64 % and 59 % for a mismatch incorporated at position 3, 10, or 14, respectively. Under these assembly conditions, the percent signal remaining was essentially equivalent regardless of the position in the duplex, due to the incorporation of the CA mismatch. The suppression of the MB' signal from a single CA mismatch validated that MB' is well coupled to the π-stack and the electrons that reduce MB' are traveling through the intervening DNA.

It should be noted that we observed signal attenuation from a CA mismatch at the 14th position of the 17-mer, indicating that MB' must intercalate within three base pairs of where it is covalently tethered; if MB' intercalates further away there would be no observed signal attenuation. This confinement of MB' is also consistent with what is predicted from model building. Therefore, when MB' is tethered to the distal end of the duplex, any perturbation to the base stack occurring below the top 7.2 Å will be reported.

Comparison with NB-DNA

MB'-DNA was then compared with the previously described DNA CT reporter, Nile Blue (NB). This comparison used electrodes assembled with 100 mM $MgCl_2$, passivated with MCH, and scanned in spermidine buffer. The area of the reductive signal for MB'-DNA is significantly larger than the signal observed with NB-DNA, 12.5 ± 1.2 nC compared to 4.3 ± 0.2 nC, respectively (Figure 2.5).

Additionally, when the same electrodes are scanned in low salt buffer, NB-DNA has an average signal area of 0.2 ± 0.1 nC (Figure 2.5). While the reductive peak areas for MB'-DNA remains relatively unchanged at 11.8 ± 0.5 nC. Despite the area of MB' remaining minimally affected, other peak characteristics were significantly altered. Switching to a low salt buffer resulted in a broadening of the peak and an increase in the peak splitting. The sharper peaks in spermidine buffer indicate that the film is more homogenous. The peak splitting between the oxidative and reductive peaks decreases from 140 mV in low salt buffer to 30 mV in spermidine buffer. These peak changes are largely reversible; there is however not a complete restoration of the peak observed in low salt buffer, indicating that the spermidine is not fully removed.

Optimized Mismatch Discrimination

The degree of signal attenuation upon introduction of a single mismatched base (MB'-MM10 DNA) was compared in low salt buffer and spermidine buffer. The DNA was assembled with 100 mM $MgCl_2$ and backfilled with MHA. Well-matched MB'-DNA shows a reductive signal area of 11.1 ± 0.2 nC while mismatched MB'-DNA shows a signal area of 4.0 ± 0.4 nC in spermidine buffer. The percent signal remaining after the introduction of a CA mismatch is 36 ± 6 % (Figure 2.6). When the same experiment is performed with NB-DNA in spermidine buffer, a 50 ± 10 % decrease is observed (data not shown). This result

Figure 2.5. Comparison of the signal from NB-DNA (dotted) and MB'-DNA(solid). The electrodes were assembled with 100 mM $MgCl_2$ and passivated with MCH. CVs were acquired at 100 mV/s and all electrodes were scanned in both a low salt buffer (5.0 mM phosphate, 50 mM NaCl, pH 7) (grey) and a spermidine buffer (5.0 mM phosphate, 50 mM NaCl, 4 mM $MgCl_2$, 4 mM spermidine, 50 µM EDTA, 10 % glycerol, pH 7) (black). The CVs shows the overall signal changes in response to the running buffer. The reductive peak areas were quantified to show that the amount of MB'-DNA being reduced is relatively unchanged regardless of the buffer. The errors denoted are determined from the variation across four different electrodes.

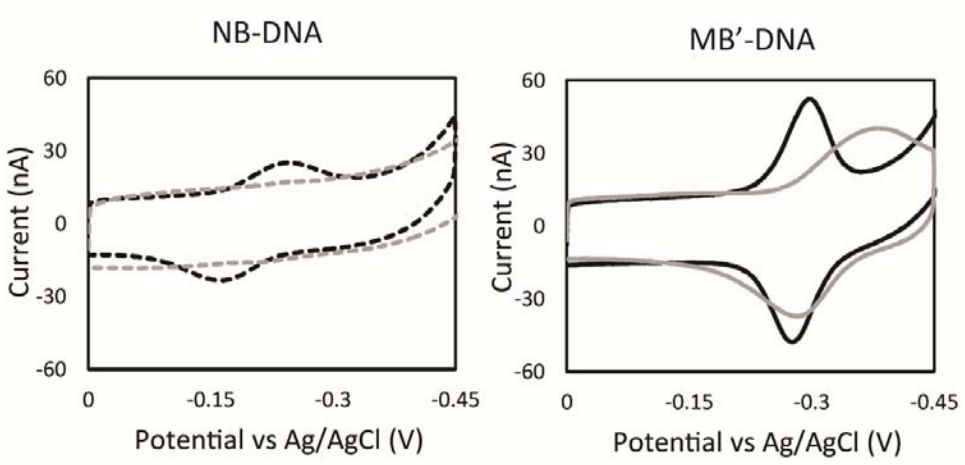

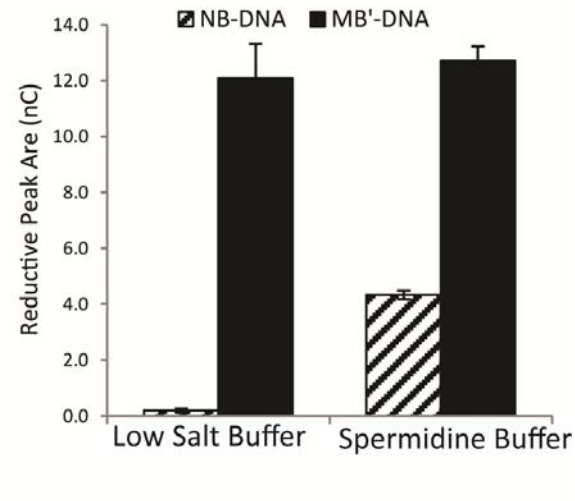

Figure 2.6. Optimization of mismatch discrimination depending on the running buffer. Both WM MB'-DNA (solid) and MM10 MB'-DNA (dotted) modified electrodes were assembled with 100 mM $MgCl_2$, passivated with MHA, and scanned in both low salt buffer (5.0 mM phosphate, 50 mM NaCl, pH 7) (left) and spermidine buffer (5.0 mM phosphate, 50 mM NaCl, 4 mM $MgCl_2$, 4 mM spermidine, 50 μM EDTA, 10 % glycerol, pH 7) (right). The area of the reductive peaks were used to quantify the reductive signal size (black) and determine the percent signal remaining ([MM]/[WM] *100) (grey) from the incorporation of a single mismatch. The grey arrows denote the decrease in signal area with the optimal percent signal attenuation being in low salt buffer. The errors denoted were determined by the standard deviation from four electrodes averages, for each sequence of DNA, across three chips.

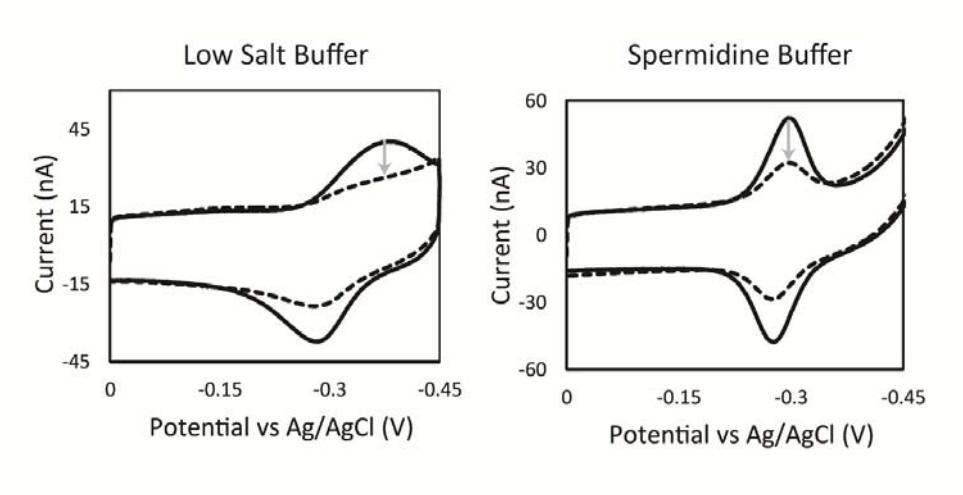

agrees with the previously reported values with NB-DNA, in that the percent signal remaining due to a CA mismatch ranges from 30-60 % (*12,19*).

When the same MB'-DNA electrodes were then examined in low salt buffer, the mismatched reductive signal was significantly broadened and decreased in intensity, yielding an area of 0.5 ± 0.1 nC. This broadening decreased the percent signal remaining to only 7 ± 2 % of the well-matched signal (9.1 ± 1.2 nC) (Figure 2.6). Spermidine binds in the grooves of duplex DNA, which rigidifies the duplex, resulting in sharper peaks. However, spermidine should also decrease the binding affinity of MB', which may account for the decreased signal attenuation.

Variation in Assembly Conditions

In addition to buffer conditions, the effect of varying the assembly conditions on mismatch discrimination was investigated. The varying densities of DNA were obtained by assembling with and without 100 mM $MgCl_2$. In the absence of $MgCl_2$, the negatively charged phosphate backbone of DNA duplexes repel each other, yielding significantly lower film densities (*13, 20*). MB'-DNA and NB-DNA films were therefore examined with and without incubation with 100 mM $MgCl_2$. With these assembly conditions, we find for MB'-DNA and NB-DNA film densities of 1.3 – 3.2 pmol/cm^2 and 0.8 – 1.6 pmol/cm^2, respectively.

The percent of signal remaining after incorporation of a CA mismatch was then compared as a function of film density in both low salt and spermidine buffer (Figure 2.7). When the percent signal remaining is plotted against the film density, a roughly linear correlation is observed. The mismatch signal attenuation improves with increasing density. This trend for MB'-DNA is present in both low salt buffer and spermidine buffer.

The dependence of the mismatch signal attenuation on the film density suggests that there might be a contribution of the signal that originates from direct reduction at the

Figure 2.7. Dependence of mismatch signal attenuation on film density for both MB'-DNA (black) and NB-DNA (grey). Percent MB'-DNA signal remaining due to the incorporation of a CA mismatch was determined in both low salt buffer (x) and spermidine buffer (squares).

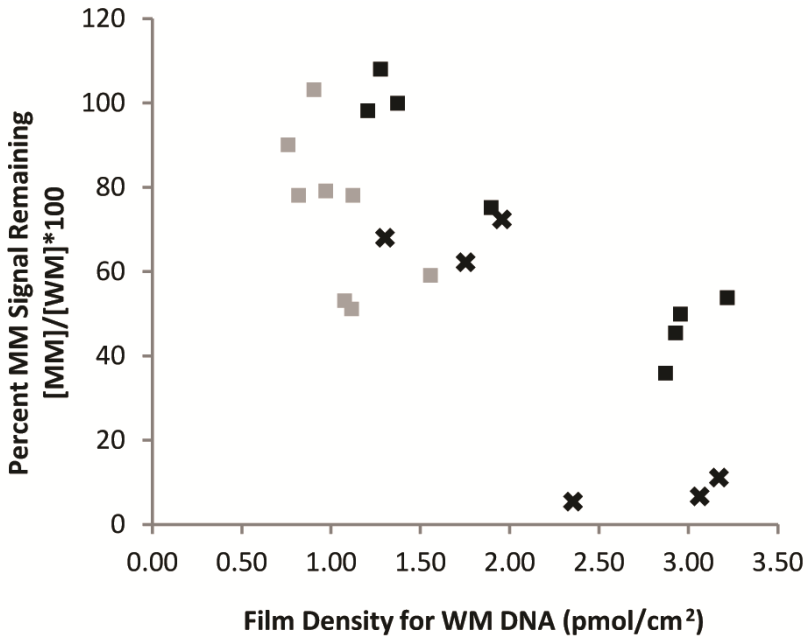

electrode surface. DNA assembled under low density conditions (without $MgCl_2$) has a higher surface accessibility compared to DNA assembled under high density conditions (with $MgCl_2$), thus increasing the possibility of direct surface reduction.

In order to gain further insight, the backfilling agent utilized was varied. Backfilling is used to decrease the background noise due to oxygen, and to minimize non-specific interactions between the DNA and the gold surface. 6-Mercaptohexanol (MCH) is the most common backfilling agent for DNA-modified electrodes. 6-mercaptohexanoic acid (MHA) offers an alternative backfilling agent with a more negative head group. The degree of signal attenuation obtained in spermidine buffer was compared between MCH and MHA for electrodes assembled with or without 100 mM $MgCl_2$. (Figure 2.8).

At either assembly concentration of $MgCl_2$, switching from MCH to MHA improves the signal attenuation observed due to mismatch incorporation. When electrodes were assembled with 100 mM $MgCl_2$ and scanned in spermidine buffer, the percent mismatch signal remaining improved from 52 ± 4 % to 36 ± 6 % by switching from MCH to MHA (Figure 2.8). Increasing the negative charge of the surface through backfilling with MHA increases the barrier between MB'-DNA and the electrode surface. The direct correlation between decreased surface accessibility and increased mismatch signal attenuation provides further evidence that, depending on assembly conditions, the signal observed from MB'-DNA may be generated by two different mechanisms: DNA CT and direct surface reduction.

Kinetics of MB'-DNA Reduction

The rates of electron transfer to the redox reporter for both MB'-DNA and NB-DNA were estimated under various assembly conditions, passivated with MCH, by measuring the scan rate dependence of the peak reduction potential and then applying the Laviron analysis (*45*). The Laviron analysis used to determine the rates of electron transfer has been

Figure 2.8. Dependence on assembly conditions of the percent mismatch signal remaining for MB'-DNA. Well-matched signal area (black) and the percent signal remaining (grey) were from 12 electrodes averaged across 3 chips. The backfilling agent (1 mM MCH or MHA) and concentration of $MgCl_2$ are indicated. Scans were acquired in spermidine buffer.

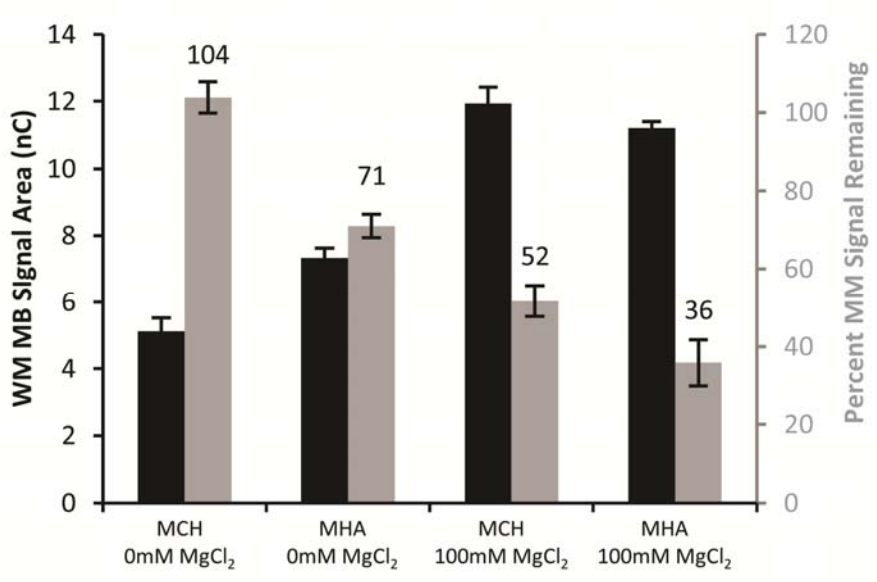

routinely employed for rate determinations in these systems (*12, 21*). Consistently we found for DNA-mediated electrochemistry that tunneling through the linker is rate-determining and the rate is slower than with direct reduction. The same method was applied to this system to compare reduction of the reporter by DNA CT to direct surface reduction. Electrodes assembled with only single stranded (ss) MB'-DNA and NB-DNA were used to estimate the rate of electron transfer by the direct surface reduction mechanism. In this case, the complementary thiol-modified strand was omitted during assembly, ensuring that there could be no DNA-mediated contribution to the observed signal; ssDNA does not efficiently conduct charge and has a high affinity for the gold surface. For comparison, the rates of electron transfer for the DNA-mediated reduction of MB'-DNA and NB-DNA were determined under conditions where the signal attenuation was maximal (double stranded (ds) DNA assembled with 100 mM $MgCl_2$), due to an incorporated mismatch.

It has been previously established that the rate for ssNB-DNA is 10-30 fold faster than the rate of electron transfer in dsNB-DNA, assembled with 100 mM $MgCl_2$ and acquired in spermidine buffer (*12*). The rate for dsDNA is limited by tunneling through the $(CH_2)_6$ - alkane linkage to the surface (*12*). This previous result for NB-DNA was reproduced in this study (Table 2.1). Furthermore, the rate of electron transfer for dsMB'-DNA, with 100 mM $MgCl_2$, is 20 fold slower than ssMB'-DNA in both spermidine and low salt buffers (Table 2.1). This result confirms that dsMB'-DNA is reduced via DNA CT when assembled with 100 mM $MgCl_2$.

The rates of electron transfer were then examined under conditions where DNA CT is not the sole mechanism for MB'-DNA reduction, evidenced by reduced signal attenuation from a CA mismatch (dsDNA without $MgCl_2$). At fast scan rates (5 V/s) for dsMB'-DNA, two reductive peaks are resolved with a 15 fold rate differential in both spermidine and low salt buffer (Figure 2.9 and Table 2.1). These data indicate that rates of electron transfer for these two modes of reduction correspond with direct surface reduction and DNA-mediated

Table 2.1. Electron-Transfer Rate Constants of NB-DNA ($k_{NB\text{-}DNA}$) and MB'-DNA ($k_{MB'\text{-}DNA}$) as Single-Stranded DNA(ssDNA) and Double-Stranded DNA (dsDNA) Under Different Running Conditions.

	ssDNA [c]	
	$log(k_{MB'\text{-}DNA}/s^{-1})$ [a]	$log(k_{NB\text{-}DNA}/s^{-1})$ [a]
Spermidine Buffer [b]	1.6	1.6
Low Salt Buffer [b]	1.2	1.6

	dsDNA [c] **0 mM $MgCl_2$**		**dsDNA** [c] **100 mM $MgCl_2$**	
	$log(k_{MB'\text{-}DNA}/s^{-1})$ [a]	$log(k_{NB\text{-}DNA}/s^{-1})$ [a]	$log(k_{MB'\text{-}DNA}/s^{-1})$ [a]	$log(k_{NB\text{-}DNA}/s^{-1})$ [a]
Spermidine Buffer [b]	0.5 & 1.6 [e]	0.3	0.5	0.6
Low Salt Buffer [b]	-0.2 & 1.6 [e]	N/A [d]	0.4	N/A [d]

a) The electron transfer rates were determined by applying Laviron analysis to CV data acquired at scan rates ranging from 50 mV/s to 13 V/s. The uncertainties are ~ 10 % of the log(k) values (*45*).

b) Low salt buffer is 5.0 mM phosphate, 50 mM NaCl, pH 7. Spermidine buffer is 5.0 mM phosphate, 50 mM NaCl, 4 mM $MgCl_2$, 4 mM spermidine, 50 µM EDTA, 10 % glycerol, pH 7.

c) Assembled overnight with 25 µM of ssDNA (probe strand lacking thiol complement) or dsDNA, with or without 100 mM $MgCl_2$.

d) The rate for double stranded NB-DNA could not be determined in low salt buffer as the signals were too small.

e) Two distinct reductive peaks were observed for MB'-DNA when assembled without $MgCl_2$ (Figure 2.9).

Figure 2.9. Top: Schematic illustration of reporter reduction mechanisms. Bottom: CV at 5 V/s (bottom) for NB-DNA (left) and MB'-DNA (center) assembled without $MgCl_2$ and MB'-DNA assembled with 100 mM $MgCl_2$ (right). Electrodes were backfilled with mercaptohexanol and scanned in spermidine buffer. The red arrows indicate the peaks quantified in order to determine the rate of the various processes for reporter reduction.

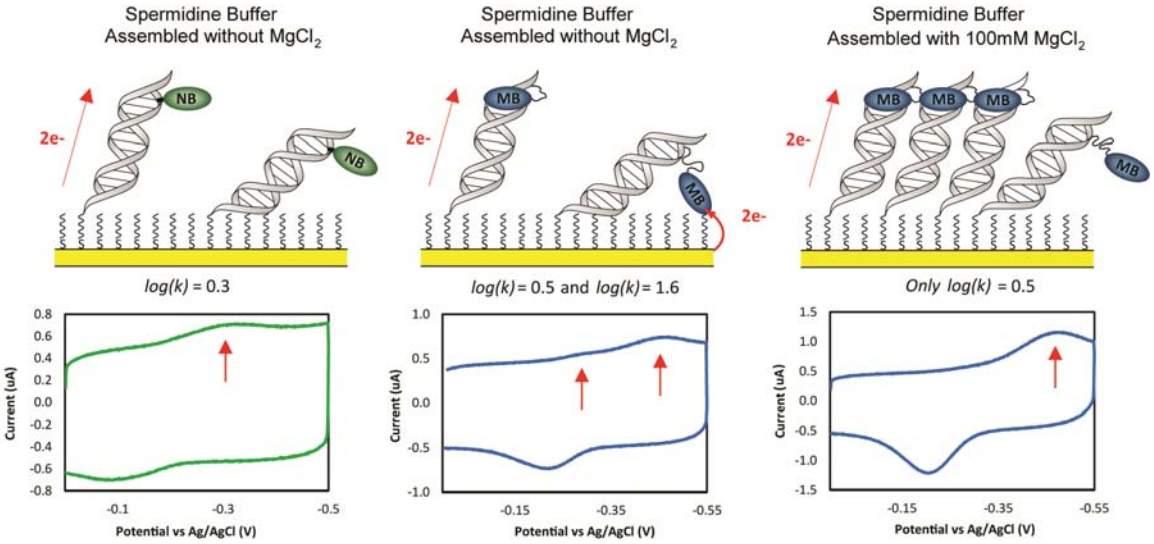

reduction of MB'-DNA. Well-matched and mismatched dsMB'-DNA were compared at 5 V/s, and signal attenuation due to mismatch incorporation was observed only in the peak with a slower rate of electron transfer, consistent with it being a DNA-mediated process (data not shown). Alternatively, for dsNB-DNA only a single peak is observed in spermidine buffer, with a rate that is 20 fold slower than ssNB-DNA. This observation suggests that while dsNB-DNA is only capable of being reduced via DNA CT, dsMB'-DNA may be reduced by either a DNA-mediated pathway or direct surface reduction. The ability of MB'-DNA to be reduced directly at the surface is likely due to the flexibility of the linkage through which MB' is covalently tethered (Figure 2.9).

Discussion

In this work, MB' is covalently tethered to DNA with a flexible C12 alkyl linkage to a modified uracil. MB'-DNA produces a reversible redox couple via DNA CT. Incorporation of a single CA mismatch within a 17-mer can attenuate the mismatch signal to 7 ± 2 % of the well-matched signal. The degree to which the mismatch signal is attenuated was found to be highly dependent on assembly conditions. Under conditions where DNA CT is the sole available mechanism for MB' reduction, a 10-fold improvement in the mismatch sensitivity is obtained, when compared to previously utilized non-amplified DNA-mediated platforms (*12, 19*). MB*'*-DNA was found also to be capable of being reduced directly by the surface of the electrode. The extent to which this mechanism contributes to the observed signal was found to be directly influenced by assembly conditions.

Therefore, MB'-DNA can both report on DNA CT through the intercalation of MB' into the base stack and report on the surface accessibility of the reporter through direct surface

reduction of MB'. We can discern which mechanism of MB' reduction is dominating under any given assembly condition by examining the signal sensitivity to π–stack perturbations or by examining the rate of electron transfer.

The fact that assembly conditions can alter which mechanism is dominant for MB' reduction has relevance in the further development of DNA-based biosensors. Sensors using direct surface reduction typically function through the formation of duplex DNA to attenuate the observed signal by increasing the separation between MB' and the electrode (*22-32*). Our work shows that upon duplex formation a new pathway for dsMB'-DNA reduction has been introduced, DNA CT, which can contribute to the residual observed signal.

Recent work performed to optimize these direct surface reduction-based platforms has demonstrated that, upon duplex formation, no signal suppression is observed at slow scan rates (100 mV/s) and the duplex signal yielded a rate of electron transfer slower than that of the non-duplex DNA structure (*23*). In order to optimize these devices, the scan rates were increased to minimize the contributions from the dsMB'-DNA (*23*). The trends observed in this work are consistent with the work presented here, and demonstrate that the DNA-mediated reduction of duplex MB'-DNA can significantly contribute to the observed signal.

It is clear that both direct reduction and DNA-mediated reduction need to be considered as important mechanisms in DNA-modified electrodes and that MB'-DNA is a viable reporter for both systems. Furthering our understanding of the underlying mechanism for the reduction of dsMB'-DNA is essential for exploiting both DNA CT and direct surface reduction based biosensors to their full extent. Only when both mechanisms are considered can the highest overall sensitivity be achieved.

REFERENCES

1. Murphy, C.J., Arkin, M. R., Jenkins, Y., Ghatlia, N. D., Bossmann, S. H., Turro, N. J., Barton, J. K. *Science* **1993**, *262*, 1025.

2. Holmlin, E. R., Dandliker P.J., Barton J.K. *Angew. Chem. Int. Ed.* **1997**, *36*, 2714.

3. Genereux, J.C., Boal, A.K., Barton, J.K. *J. Am. Chem. Soc.* **2010**, *132*, 891.

4. Long Range Charge Transfer in DNA II edited by Schuster, G.B,; Topics in Current Chemistry; Springer-Verlag, Berlin, Heidelberg,; 237, 103 (**2004**).

5. Charge Transfer in DNA:From Mechanism to Application edited by Wagenknecht, H.A. (Wiley-VCH Verlag GmbH & Co KGaA, Weiheim, **2005**).

6. Genereux, J.G., Barton, J.K. *Chem. Rev.* **2010**, *110*, 1642.

7. Hall, D.B., Holmlin, R.E., Barton, J.K. *Nature* **1996**, *382*, 731.

8. Kelley, S.O., Barton, J.K. *Science* **1999**, *283*, 375.

9. Delaney, S., Barton, J.K. *J. Org. Chem.,* **2003**, *68*, 6475.

10. Kelley, S.O., Holmlin R.E., Stemp, E.D.A., Barton, J.K. *J. Am. Chem. Soc.* **1997**, *119*, 9861.

11. Gorodetsky, A., Buzzeo, M.C., Barton, J.K. *Bioconjugate Chem.*, **2008**, *19*, 2285.

12. Slinker, J., Muren, N., Renfrew, S., Barton, J.K. *Nature Chemistry* **2011**, *3*, 228.

13. Kelley, S.O, Jackson, N.M., Hill, M.G., Barton, J.K. *Angew. Chem. Int. Ed.* **1999**, *38*, 941.

14. Boon, E.M., Salas, J.E., Barton, J.K. *Nature Biotechnology* **2002**, *20*, 282.

15. Kelley, S.O., Boon, E.M., Barton, J.K., Jackson, N.M., Hill, M.G. *Nucleic Acids Researc*h **1999**, *27*, 4830.

16. Boon, E.M., Ceres, D.M., Drummond, T.G., Hill, M.G., Barton, J.K. *Nature Biotechnology* **2000**, *18*, 1096.

17. Gorodetsky, A., Green, O., Yavin, E., Barton, J.K. *Bioconjugate Chem.* **2007**, *18*, 1434.

18. Kelley, S.O., Barton, J.K., Jackson, N., Hill M.G *Bioconjugate Chem.* **1997**, *8*, 31.

19. Slinker, J., Muren, N., Gorodetsky, A., Barton, J.K. *J. Am. Chem. Soc.* **2010**, *132*, 2769.

20. Boon, E., Jackson, N., Wightman, M., Kelley, S., Hill, M., Barton, J.K. *J. Phys. Chem. B.* **2003**, *107*, 11805.

21. Drummond, T.G., Hill, M.G., Barton, J.K. *J. Am. Chem. Soc.* **2004**, *126*, 15010.

22. Kang, D., Zuo, X., Yang, R., Xia, F., Plaxco, K., White, R. *Anal. Chem.* **2009**, *81*, 9109.

23. Yang, W., Lai, R.Y. *Langmuir* **2011**, *27*, 14669.

24. Xiang, Y., Qian, X., Chen, Y., Zhang, Y., Chai, Y., Yuan, R. *Chem. Commun.* **2011**, *47*, 2080.

25. Yang, W., Lai, R.Y. *Analyst* **2011**, *136*, 134.

26. Zhao, S., Yang, W., Lai, R.Y. *Biosensors and Bioelectronics* **2011**, *26*, 2442.

27. Yang, W., Lai, R.Y. *Electrochem. Commun.* **2011**, *13*, 989.

28. Farjami, E., Clima, L., Gothelf, K., Ferapontova, E.E. *Anal. Chem.* **2011**, *83*, 1594.

29. Xiao, Y., Lai, R., Plaxco, K. *Nature Protocols* **2007**, *2*, 2875.

30. Xiao, Y., Lou, X., Uzawa, T., Plakos, K., Plaxco, K., Soh, H.T. *J. Am. Chem. Soc.* **2009**, *131*, 15311.

31. Lubin, A., Vander Stoep Hunt, B., White, R., Plaxco, K. *Anal. Chem.* **2009**, *81*, 2150.

32. Cash, K., Heeger, A., Plaxco, K., Xiao, Y. *Anal. Chem.* **2009**, *81*, 656.

33. Ricci, F., Bonham, A., Mason, A., Reich, N., Plaxco, K. *Anal. Chem.* **2009**, *81*, 1608.

34. Zuo, W., Song, S., Zhang, J., Pan, D., Wang, L., Fan, C. *J. Am. Chem. Soc.* **2007**, *129*, 1042.

35. Di Giusto, D.A., Wlassoff, W. A., Giesebrecht, S., Gooding, J.J., King, G.C. *Angew. Chem. Int. Ed.* **2004**, *43*, 2809.

36. Di Giusto, D.A., Wlassoff, W. A., Giesebrecht, S., Gooding, J.J., King, G.C *J. Am. Chem. Soc.* **2004**, *126*, 4120.

37. Anne, A., Bouchardon, A., Moiroux J. *J. Am. Chem. Soc.* **2003**, *125*, 1112.

38. Boon, E.M., Barton, J.K., Bhaghat V., Nerissian M.,Wang W., Hill M.G. *Langmuir* **2003**, *19*, 9255.

39. Leng, F., Savkur, R., Fokt, I., Przewloka, T., RPiebe, W., Chaires, J.B. *J. Am. Chem. Soc.* **1996**, *118*, 4732.

40. Wang, A. H. J., Gao, Y.G., Liaw, Y.C., Li, Y.K. *Biochemistry* **1991**, *30*, 3812.

41. Wagner, S.J., Skripchenko, A., Robinette, D., Foley, J.W., Cincotta, L. *Photochemistry and Photobiology* **1998**, *67*, 343.

42. Chen, H., Herkstroeter, W.G., Perlstein, J., Law, K.Y., Whitten, D.G. *J. Phys. Chem.* **1994**, *98*, 5138.

43. Pedersen, D.S., Rosenbohm, C. *Synthesis* **2001**, *16*, 2431.

44. The reduction potential of NB is shifted positive by 200mV due to the direct conjugation of NB to the nucleobase.

45. Laviron, E. J. *J. Electroanal. Chem.* **1979**, *101*,19.

CHAPTER 3

Intraduplex DNA-mediated electrochemistry of covalently tethered redox-active reporters

Adapted from Pheeney, C.G. and Barton, J.K. (2013) *submitted.*

ABSTRACT

Intraduplex DNA-mediated reduction is established as a general mechanism for the reduction of distally bound redox-active species covalently tethered to DNA through flexible alkane linkages. Methylene Blue (MB), Nile Blue (NB), and Anthraquinone (AQ) were covalently tethered to DNA with three different covalent linkages. Using these reporters, DNA electrochemistry was shown to be both DNA-mediated and intra-, rather than inter-, duplex. The charge transport pathway occurring through the DNA π-stack was established by using an intervening AC mismatch to break this path. The fact that the DNA-mediated reduction of MB occurs primarily via intraduplex intercalation is established through varying the proximity and integrity of the neighboring duplex DNA.

INTRODUCTION

DNA-modified electrodes are extensively used in both the development of next generation diagnostic sensors (*1-6*) and the characterization of ground-state DNA-mediated electrochemistry (*7-15*). Many different electrochemical reporters have been developed for DNA-modified electrodes, including DNA binding compounds (*1, 5*), quantum dots (*4*), and metallization (*15, 16*). Two classes of DNA-based devices have since emerged using the same covalently tethered intercalative compounds but different mechanisms: DNA conformation (*3, 17-22*) and DNA-mediated charge transfer (DNA CT) (*6-14*).

The DNA-mediated reduction of both freely diffusing and covalently tethered redox-active reporters has long been established on these DNA-modified electrodes (*23-25*). The strategy of covalently tethering redox-active reporters to the DNA, as opposed to the use of freely diffusing reporters, has been adopted to significantly diminish non-specific signals (*11, 17*). Redox-active reporters covalently tethered to DNA have been shown to electronically couple to the π-stack by a variety of mechanisms: end capping (*13*), intercalation (*11, 12*), and direct conjugation (*14*). However, the recent characterization of covalently tethered Methylene Blue (MB), an extensively used reporter for DNA-conformation based assays, has spurred a new debate with regards to the mechanism of its reduction (*12*).

The capacity of these redox reporters to be reduced via an intraduplex DNA-mediated pathway has been brought into question with alternative mechanisms such as the duplex tilting to the surface, the charge traveling along the counter ions associated with the sugar phosphate backbone, or the reporter intercalating in a neighboring duplex (*19-21*). Here we demonstrate the generality of DNA-mediated reduction of covalently tethered reporters by varying both the redox-active species and the covalent linkage (Figure 3.1). Critical to these assays is the use of an intervening AC mismatch to establish that the

Figure 3.1. Schematic of DNA immobilized on an electrode modified with a variety of redox-active species by different covalent linkages. The structures of the three different redox-active species examined are presented on the right.

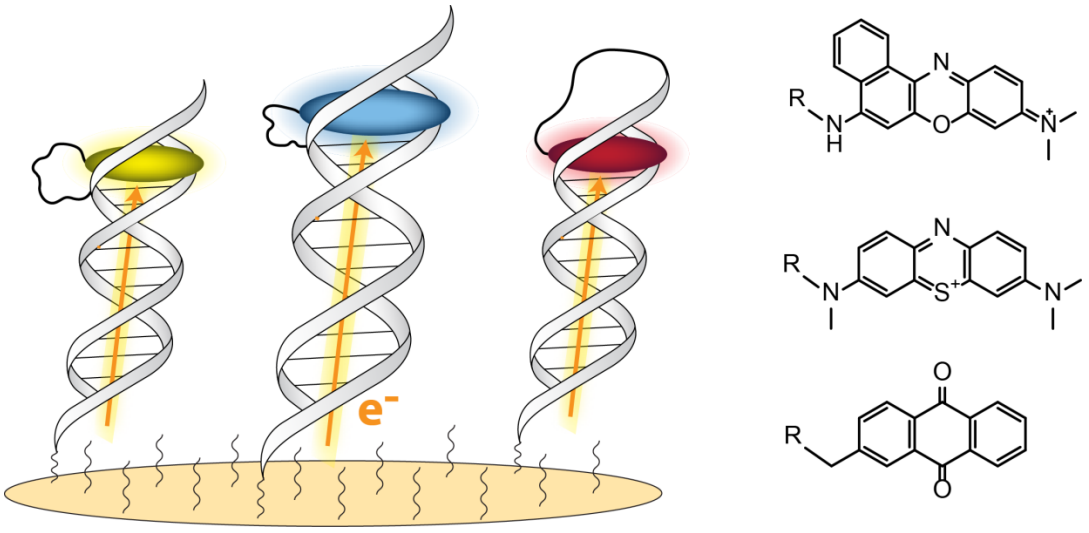

charge transport pathway is through the duplex base pair stack. Beyond demonstrating that the reduction is DNA-mediated, we also provide evidence supporting an intraduplex process by varying the identity and proximity of neighboring duplex DNA.

Materials and Methods

Chemicals and reagents used in the preparation of the activated redox-active reporters were purchased from Sigma and used without further purification. MB′ was prepared based on previously established protocols (*12*). All phosphoramidites and DNA synthesis reagents were purchased from Glen Research. Silicon wafers used for the fabrication of multiplexed chips were purchased from SiliconQuest.

Synthesis of proprionic acid modified Nile Blue (NB').

See Figure 3.2 for the synthetic strategy for the preparation of NB′.

*5-(Dimethylamino)-2-nitrosophenol (**1**) preparation.*

1 was prepared according to the procedure described by Moura (*26*) by dissolving 3-(dimethylamino)phenol (8.26 g, 50 mmol) in concentrated hydrochloric acid (25 mL) chilled to 0 ºC, followed by the slow addition of sodium nitrite (4.0 g, 58 mmol). The reaction mixture was maintained at 0 ºC and the addition of sodium nitrite was slowed if orange fumes were observed. The reaction was left to proceed for 30 min – 1 hr, until the contents solidified. The precipitate was isolated by vacuum filtration and washed with chilled diluted hydrochloric acid (1 N). The yellow-brown solid (5.6 g, 29 mmol, 57% yield) was confirmed as the desired product by ^{1}H NMR (300 MHz, DMSO-d_6): δ 7.66-7.24 (m, 1H), 7.24-6.78 (m, 2H), 3.36 (s, 6H) and ESI-MS in 7:3 $CHCl_3$:MeOH by the observed $[M+H]^+$ peak at 167.0 g/mol. **1** was dried and used in following reactions without further purification.

Figure 3.2. Synthetic strategy for the preparation of proprionic acid modified Nile Blue (NB′).

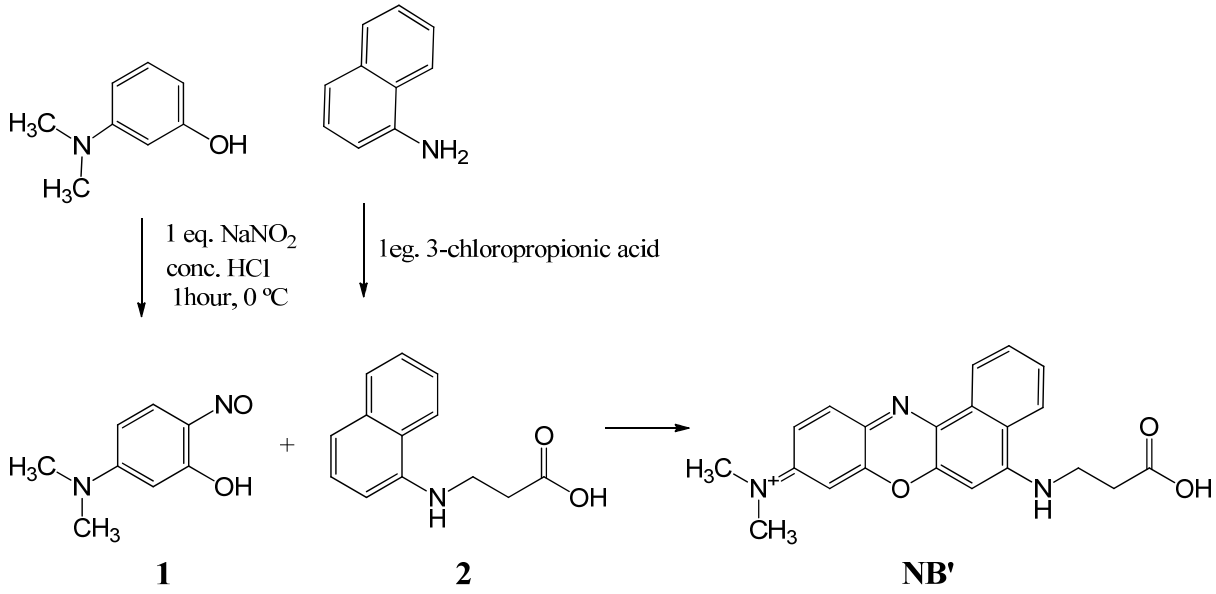

*3-(naphthalen-1-ylamino)propanoic acid (**2**) preparation.*

2 was prepared by dissolving naphthylamine (2.0 g, 14 mmol) in water (15 mL), followed by the addition of sodium hydroxide (6 M, 5.0 mL) and equimolar amounts of dissolved chloroproprionic acid (1.50 g, 15 mmol). The reaction was brought to a reflux and allowed to proceed for 12-24 hr. The excess solvent was removed under reduced pressure and the desired product was purified by silica chromatography ($CHCl_3$:MeOH 20:1) with an R_f of 0.5. The clear fraction was dried to yield a white solid product that was confirmed as the desired product (**2**) by ^{1}H NMR (300 MHz, CD_3OD): δ 80.5-7.87 (m, 1H), 7.85-7.62 (m, 1H), 7.53-7.23 (m, 3H), 7.18 (t, *J* = 8.4 Hz, 1H), 6.65 (t, *J* = 8.0 Hz, 1H), 3.59 (dt, *J* = 9.4, 7.0 Hz, 2H), 2.75 (t, 2H) and ESI-MS in 7:3 $CHCl_3$:MeOH by the observed $[M+H]^+$ peak at 216.1 g/mol.

Proprionic acid modified Nile Blue (NB′) preparation.

NB′ was prepared based on previously established procedures by Moura (*27*). Equimolar portions of **1** (0.17 g, 1.0 mmol) and **2** (0.22 g, 1.0 mmol) were combined and dissolved in dimethylformamide (DMF) (6 mL). The reaction mixture was heated to 70 ºC for 24 hr. The crude reaction mixture was dried under reduced pressure and purified by dry silica chromatography (*28*). Pure NB′ was eluted with 6:1 cholorform: methanol as a dark blue compound. The identity was verified by ESI-MS in MeOH:H_2O 5:1 based on the observed $[M]^+$ peak at 362.3 g/mol.

NHS-ester activation of carboxylic acid modified reporters

MB′, NB′, and anthraquinone-2-carboxylic acid (AQ′) were all activated to the NHS-esters immediately prior to coupling to amino-modified DNA to aid the yield of amide bond formation. The same procedure as previously used for the activation of MB′ was applied to

the activation of all three of these redox-active reporters (*12*). Briefly, the carboxylic acid modified reporter (0.022 mol) was stirred at room temperature in DMF with excess N,N′-dicyclohexylcarbodiimide (9.3 mg, 0.045 mmol) and N-hydroxysuccinimide (5.2 mg, 0.045 mmol) for 12-24 hr. The solvent was subsequently removed under reduced pressure and the reaction mixture was re-suspended in DMSO (20 μL per 1 mg activated).

Preparation of probe and thiol modified oligonucleotides

Thiol-modified and amino-modified DNA were synthesized and purified based on previously established protocols (*6, 12*). The procedure for DNA purification was unaltered across all three different amino modifiers utilized: dT-C6, dT-C4, and 5′-C6. The purified amino-modified DNA was covalently modified with NHS-ester activated MB′, NB′, and AQ′ using roughly 10-fold excess reporter in an aqueous basic solution (0.1 M $NaHCO_3$). The same thiol-modified complement stand was used for all duplex DNA, to negate variations caused by the thiol driven self-assembly of the DNA. Both well-matched and AC mismatched sequences were prepared of a CG-rich 17-mer duplex to investigate the effect due to π-stack perturbations (Table 3.1).

Electrochemistry of DNA-modified electrodes

Multiplexed chips, with sixteen individually addressable electrodes, were prepared and used based on previously established protocols (*10*). These sixteen-electrodes were divided into four isolated quadrants, each with four electrodes, allowing for four different typical of DNA or morphologies to be simultaneous compared without any variability introduced due to changing the underlying gold surface. Electrodes were exposed to duplex thiol-modified DNA (20 μL of 25 μM) in phosphate buffer (5.0 mM phosphate, 50 mM NaCl, pH 7) and allowed to self-assemble for 12-16 hr in a humid environment. $MgCl_2$ was added

Table 3.1. DNA sequences used for electrochemical measurements

Name	Sequence
Thiol-ssDNA	5'- HS - $(CH_2)_6$ – GAC TGA CCT CGG ACG CA -3'
Well-matched ssDNA (WM) [a, b]	5'-**T**G CGT CCG AGG TCA GTC -3'
AC-mismatched ssDNA (MM) [a, b]	5'-**T**G CGT CC*A* AGG TCA GTC -3'

[a] **T** is the site of the amino-modified nucleotide used to produce the dT-C6 and dT-C4 linkages.

[b] 5′-C6 linkage is produced by an additional 5′ phosphoramidite.

to solutions during DNA self-assembly, as indicated in the text, to alter the immobilization of the DNA. After DNA self-assembly, electrodes were washed with excess phosphate buffer and incubated with 6-mercaptohexanol (1 mM for 45 min) in phosphate buffer with 5% glycerol. Electrodes were washed again with excess phosphate buffer.

Electrochemical measurements were performed with a CHI620D Electrochemical Analyzer and a 16-channel multiplexer from CH Instruments. A three-electrode setup was used with a common Pt auxiliary and a quasi Ag/AgCl reference electrode (Cypress Systems) placed in the central well of the clamp. Cyclic voltammetry data were collected at 100 mV/s over a window of 0 mV to -0.6 mV versus Ag/AgCl unless otherwise indicated. The electrodes were exposed to the various running conditions in the following sequence: an initial background scan acquired in phosphate buffer (5.0 mM phosphate, 50 mM NaCl, pH 7), DNA quantification by $Ru(NH_3)_6^{3+}$ (1 μM in phosphate buffer), excess washing with phosphate buffer until $Ru(NH_3)_6^{3+}$ signal is no longer present, final scan in spermidine buffer (5.0 mM phosphate, 50 mM NaCl, 4 mM $MgCl_2$, 4 mM spermidine, 50 μM EDTA, 10% glycerol, and pH 7.0). Unless otherwise indicated, presented and quantified data for reporter signals is determined from CV in spermidine buffer. The signal averages and associated error are for a given data set (comparison of reporters vs. comparison of linkages) has many other factors that can alter the signal size including surface and self-assembly quality. To control for this, the data was acquired in distinct data sets such that results being directly compared are always from multiplexed chips running in close succession. Therefore, the data presented is either quadrant averages (4 electrodes) or an average of *n* quadrants (*n* x 4 electrodes) acquired within no more than a few days of each other and is indicated where applicable.

The Laviron analysis was used to determine the electron-transfer rate constant (*k*) for MB-modified DNA (*29, 30*). A plot of the peak shift ($E_{pc} - E^{o'}$, mV), where E_{pc} is the peak potential at a given scan rate and $E^{o'}$ is the midpoint potential determined at 50 mV, versus

the ln(scan rate), where the scan rate (*v*, mV/s) is varied from 50 mV/s to 13 V/s was constructed. The electron transfer rate can then be derived from the linear portion of this plot (ΔE vs ln(*v*), see Figure 3.9) based on Equation 3.1. However, the rates determined using this analysis are useful for comparisons and can only be assessed with confidence as order of magnitude estimates.

(Equation 3.1) $$E_{pc} = E^{o\prime} - \frac{RT}{\alpha nF} \ln\left(\frac{\alpha nFv}{RTk}\right)$$

Quantification of immobilized DNA

The quantity of immobilized DNA within a given DNA monolayer was quantified based off the area of reductive signal generated from the electrostatic binding of $Ru(NH_3)_6^{3+}$. The surface coverage of DNA (Γ) was calculated using equation 3.2 where *n* is the number of electrons per reduction event, *F* is the Faraday constant, *A* is the electrode area in cm^2 (2 cm^2), *z* is the charge on the $Ru(NH_3)_6^{3+}$, *m* is the number of base in the duplex DNA (17 mer), and finally *Q* is the reductive signal from $Ru(NH_3)_6^{3+}$ in phosphate buffer minus the redox reporter signal in spermidine buffer. As the contribution of reporter reduction could not be de-convoluted from the $Ru(NH_3)_6^{3+}$ signal it was subtracted, even though it was consistently negligible and less than 10% of the total $Ru(NH_3)_6^{3+}$ signal. Therefore the Q_{Ru} used for determining the surface coverage is obtained by taking the area of the $Q_{Ru + MB}$ and subtracting out the Q_{MB} (obtained after washing off the $Ru(NH_3)_6^{3+}$).

(Equation 3.2) $$\Gamma_{DNA} = \frac{Q_{Ru}}{n\,F\,A}\,\frac{z}{m}\,N_A$$

Results and Discussion

Electrochemistry of variation across redox-active reporters

The electronically coupling redox-active reporters that are covalently tethered through a long (dT-C12-DNA) flexible alkane linkage was demonstrated by coupling three different NHS-ester activated redox reporters (MB, Nile Blue (NB) and Anthraquinone (AQ)) to the same amine modified DNA (Figure 3.3). The reporter-modified DNA was annealed to a thiol-modified complement prior to the self-assembly on gold electrodes. Consistency between electrodes was ensured through the use of multiplexed chips containing sixteen individually addressable electrodes (*6*). The midpoint potentials of the signals generated from densely packed DNA monolayers (assembled at 25 μM in the presence of 100 mM $MgCl_2$) labeled with MB, NB, and AQ are -300 mV, -420 mV, and -500 mV, respectively (Figure 3.3). Interestingly, the oxidative signal sizes are 6.1 ± 0.3 nC (MB), 2.8 ± 0.2 nC (NB), and 2.2 ± 0.4 nC (AQ), which is not consistent across the reporters. This signal sizes, however, correlate with the binding affinity of reporters based on their ability to thermal stabilize the duplex DNA (Table 3.2). The quantity of immobilized DNA was determined using the electrostatic binding of $Ru(NH_3)_6^{3+}$ under saturation conditions (1 μM in 5.0 mM phosphate, 50 mM NaCl, pH 7.0) (Figure 3.4). Regardless of the redox reporter, the electrodes all were found to have surface coverages within error of each other, 5.2 ± 0.3 pmol/cm^2, consistent with that previously reported based on reporter reduction (*12*). This ensures that differences in signal sizes are not due to differences in the quantity of immobilized DNA.

Variation across covalent linkages

In addition to varying the redox-active species, both the length of the covalent linkage and the placement of the redox-active reporter were also probed (Figure 3.5). In

Figure 3.3. Variation of redox-active species. Structures (top) and cyclic voltammetry (scan rate = 100 mV/s)(bottom) of MB (blue), NB (purple), and AQ (orange) modified DNA covalently tethered via a C12 flexible alkane linkage on a modified thymine. DNA-monolayers were assembled in the presence of 100 mM $MgCl_2$, backfilled with 6-mercaptohexanol (1 mM for 45 min), and scanned in spermidine buffer.

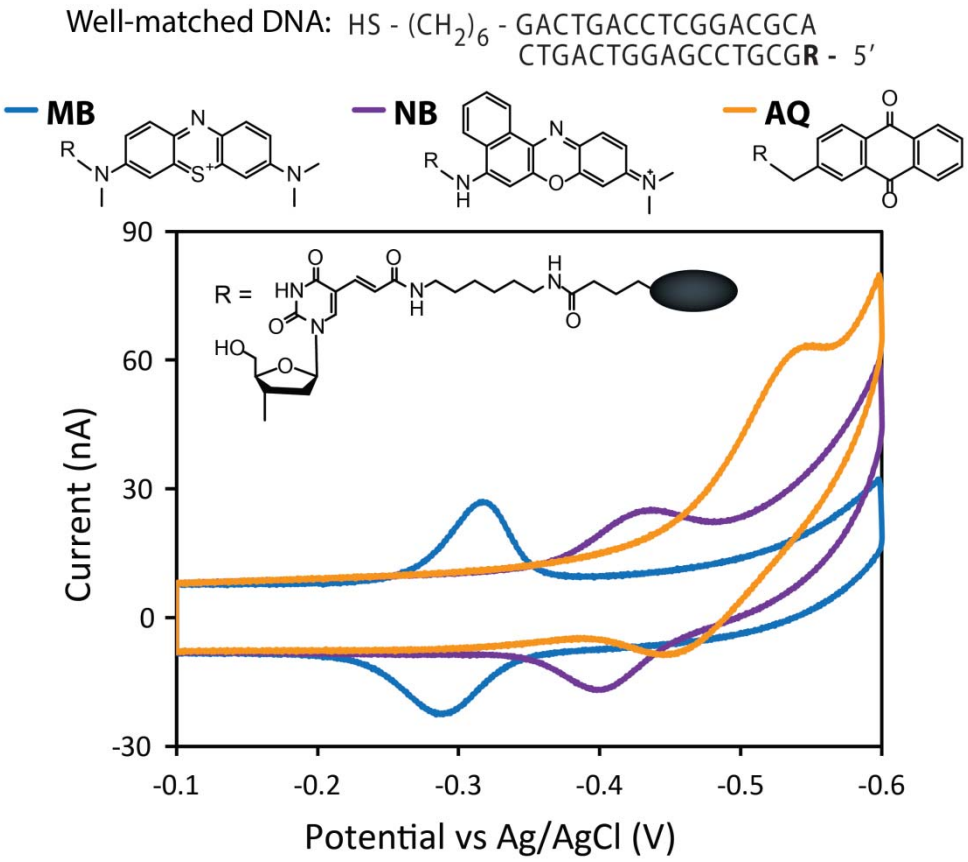

Table 3.2. Thermal Stability of Duplex DNA [a]

Redox-Active Species	T_M (°C)	Stabilization
Methylene Blue	63.7 °C	+ 1.6 °C
Nile Blue	63.1 °C	+ 1 °C
Anthraquinone	62.3 °C	+ 0.2 °C
None	62.1 °C	-

[a] Duplex DNA (1 μM) was incubated with the redox-active species (5 μM) in phosphate buffer (5.0 mM phosphate, 50 mM NaCl, pH 7.0) and the absorbance at 260 nm was monitored every 0.5 °C from 25 - 90 °C. The maximum of the derivative of the absorbance temperature trace was determined to extract the melting temperature under each condition.

Figure 3.4. Electrostatic binding of $Ru(NH_3)_6^{3+}$ to immobilized DNA. Representative cyclic voltammograms (scan rate = 100 mV/s) of MB-dT-C12-DNA-modified electrodes acquired after the addition of $Ru(NH_3)_6^{3+}$ (1 μM) in phosphate buffer (5.0 mM sodium phosphate, 50 mM NaCl, pH 7.0) are presented. The concentration of $MgCl_2$ present during DNA self-assembly was varied to alter the overall DNA morphology: without $MgCl_2$ (blue), with 1 mM $MgCl_2$ (red), and with 100 mM $MgCl_2$ (green). The representative traces for the three different DNA morphologies were obtained on a single multiplexed chip with a common $Ru(NH_3)_6^{3+}$ solution. The area of the total reductive signal minus the area of the reporter reductive signal, acquired after washing off the $Ru(NH_3)_6^{3+}$, was used to determine the surface coverage of DNA on the electrode as outlined above.

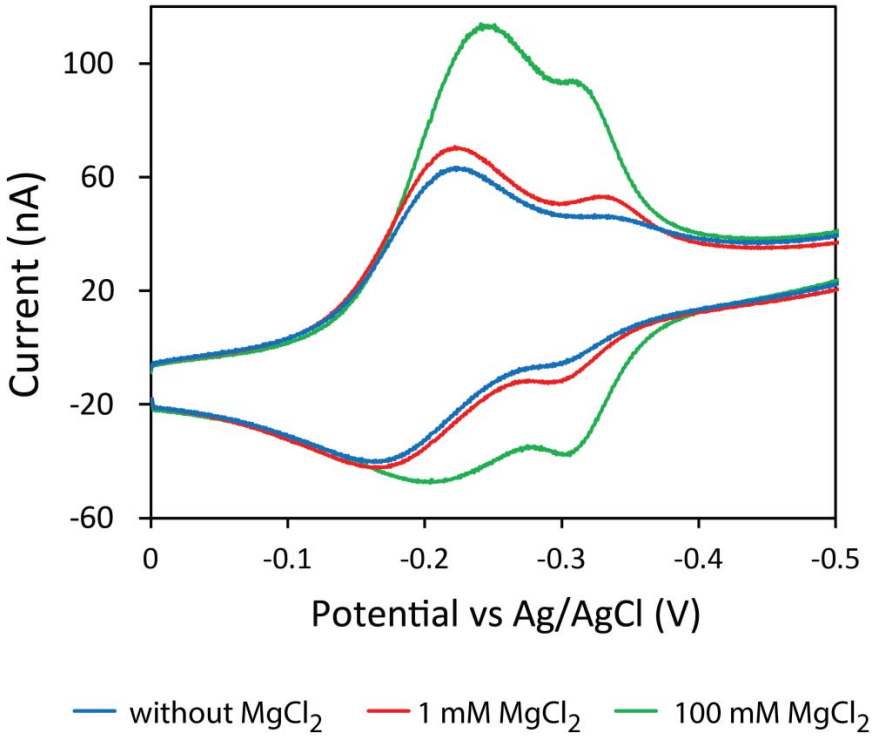

Figure 3.5. Variation of covalent linkage. Structures (top) and cyclic voltammetry (scan rate = 100 mV/s) (bottom) of MB covalently tethered to duplex DNA via three different linkages: 5′-C12 (red), dT-C12 (blue), and dT-C8 (green). The signals from well-matched (solid) and AC mismatched (dashed) 17-mer DNA are both presented, sequences available in (Table 3.1).

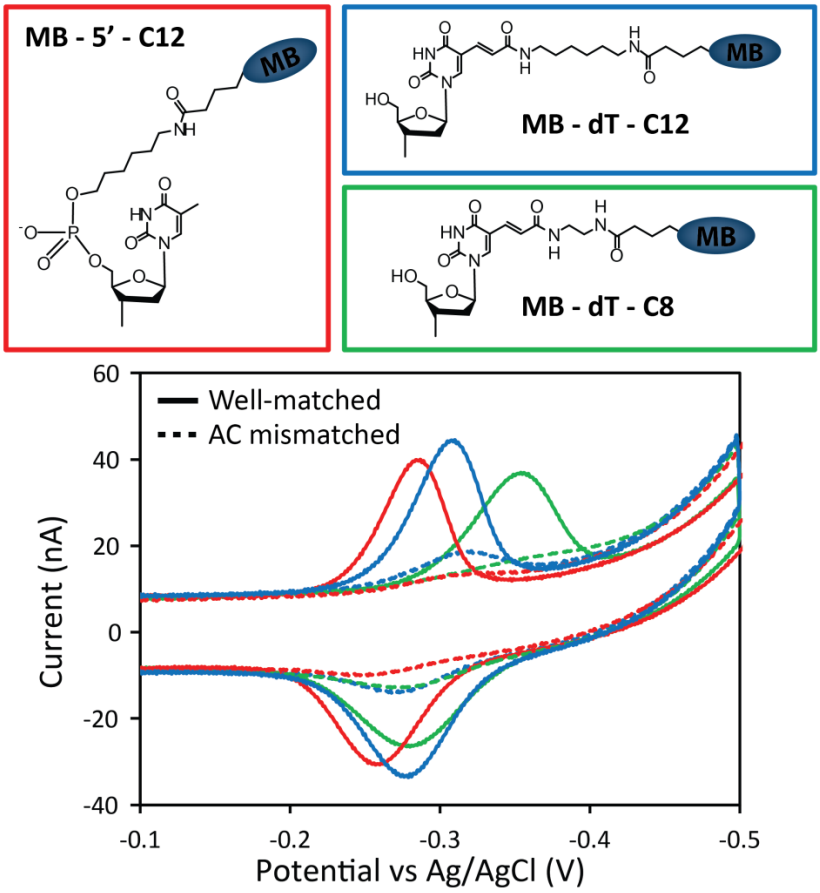

addition to the long C12 linkage appended off the thymine, two new linkages were prepared: a shortened C8 linkage appended off the modified thymine in the same manner and a C12 linkage instead appended off the 5′ hydroxyl (*31*). Densely packed monolayers were compared for MB (Figure 3.5) and NB (Figure 3.6) covalently tethered to the DNA through these three linkages. Taken together, the midpoint potential, peak splitting, and signal size create a distinct reproducible profile for each linkage (Table 3.3). Notably, differences are observed in the signals generated from MB covalently tethered via the same C12 linkages appended to the thymine and 5′ hydroxyl as well as between both the short and long linkages appended off the thymine. These distinct electrochemical profiles indicate that both the placement and length of the covalent tether play critical roles in dictating the coupling of the reporter with the base pair stack and therefore the kinetics of the redox signal. For example, the difference in midpoint potential between the dT-C12 and dT-C8 linkages is attributed to the truncated linkage, decreasing the binding affinity of the reporter; in fact, the midpoint potential shift results solely from a shift in the reduction peak, while the oxidative peak remains relatively constant. This differential behavior of the reductive and oxidative peaks can be understood based on the lowered binding affinity of the reporter in the reduced form (*32*). The shift in the midpoint potential of the 5’ hydroxyl linkage is attributed to binding via an end-capping mode as opposed to intercalation (*13*). Additionally, based on poorer coupling, NB consistently shows a decreased signal size (40% - 80%) compared to MB for all three linkages under all conditions examined.

DNA-mediated reduction based on mismatch sensitivity

The degree of DNA-mediated reduction for this family of redox reporters and linkages was assessed by introducing a single mismatched base pair intervening between the redox reporter and the gold electrode. This is an *essential* assay of DNA-mediation.

Figure 3.6. Variation of covalent linkage for NB-DNA. Cyclic voltammetry (scan rate = 100 mV/s), in spermidine buffer (5.0 mM phosphate, 50 mM NaCl, 4 mM MgCl2, 4 mM spermidine, 50 μM EDTA, 10% glycerol, and pH 7.0), of NB covalently tethered to duplex DNA via three different linkages: 5′-C12 (red), dT-C12 (blue), and dT-C8 (green). The monolayers of 17-mer well-matched DNA were assembled in the presence of 100 mM $MgCl_2$ to yield high density DNA films. See Table 3.1 for sequences and Figure 3.5 for structures of linkages.

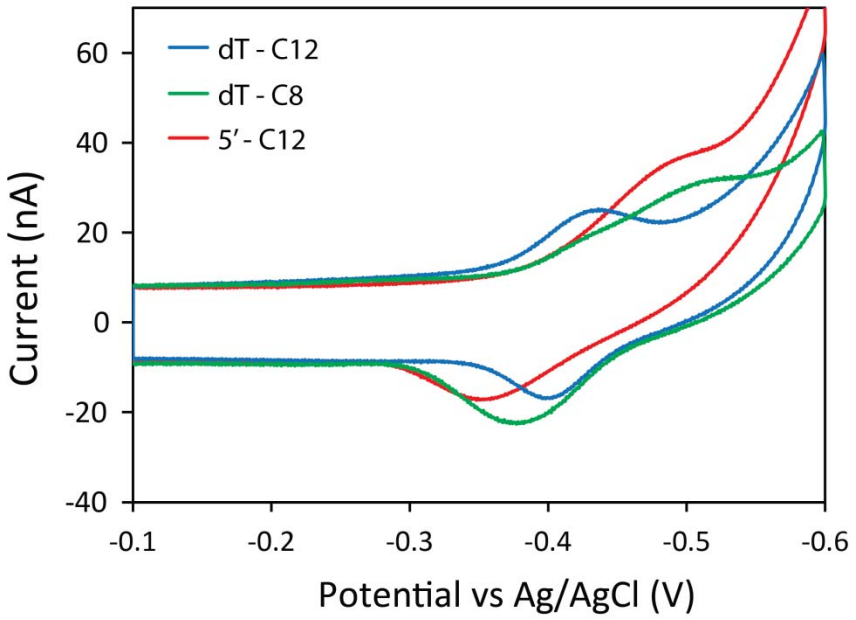

Table 3.3. Electrochemical parameters for MB signals

Linkage	Mid-point Potential (mV)	Peak Splitting (mV)	Signal Size (nC)
dT-C12	-300	35	9.1
dT-C8	-330	124	8.4
5′-C12	-280	26	10.2

DNA CT is known to be exquisitely sensitive to subtle perturbations to the π-stack; therefore the introduction of even a single intervening mismatched base pair (AC) significantly attenuates the overall yield of electrons reaching the distally bound reporter when the signals are generated via a DNA-mediated pathway (*7, 24*). This diminished yield of reporter reduction is seen to be associated with incorporation of a single base pair mismatch even in a 100-mer and over a wide range of temperatures (*9, 33*). Here, direct comparisons between fully well-matched and AC mismatched 17-mer DNA were performed on the same multiplexed surface to reduce effects caused by the assembly conditions and surface quality. The percent signal remaining with a single AC mismatch was determined relative to well-matched DNA for all linkages and for both MB and NB (Table 3.4). Although AQ appended by a C12 linkage to the terminal thymine was also shown to display significant signal attenuation upon introducing a single AC mismatch (Figure 3.7), its negative midpoint potential and oxygen- mediated electrocatalytic activity made signal quantification challenging. Overall, AQ poses the most challenges to quantification and is poorly coupled to the π-stack so it was not further investigated as an electrochemical reporter for DNA CT.

The degree of signal attenuation upon mismatch incorporation was characterized under both low and high density conditions. It has previously been established that the DNA-mediated reduction of MB-dT-C12-DNA is exceptionally sensitive to the assembly conditions of the electrode, yielding a greater DNA-mediated signal upon decreased surface accessibility of the reporter (*12*). All linkages attaching both MB and NB displayed significant signal attenuation upon incorporation of a single AC mismatch under high density conditions, validating that the predominant mechanism for reduction is a DNA-mediated pathway (Figure 3.5, Figure 3.6 and Table 3.4). The quantity of immobilized DNA was again verified by the addition of $Ru(NH_3)_6^{3+}$ (1 μM). DNA surface coverages were found to be within error of one another for well-matched or mismatched DNA for both film densities,

Table 3.4. Percent signal remaining for MB and NB modified DNA for all covalent linkages examined in high and low density DNA monolayers.

Covalent Tether	Percent Signal Remaining (MM/WM*100) [b,c]	
	MB-DNA	NB-DNA
High Density		
dT-C8	9	42
dT-C12	18	N/A[a]
5'-C12	6	15
Low Density		
dT-C8	65	66
dT-C12	89	N/A[a]
5'-C12	61	75

[a] Data was not acquired due to low yields of mismatched NB-dT-C12-DNA.

[b] Errors on all percent signal remaining are ± 1 %.

[c] WM is well-matched and MM is AC mismatched.

Figure 3.7. AQ-dT-C12-DNA response to π-stack perturbations. Cyclic voltammograms (scan rate = 100 mV/s) of AQ-dT-C12-DNA modified electrodes self-assembled in the presence of 100 mM $MgCl_2$ and acquired in de-oxygenated spermidine buffer (5.0 mM phosphate, 50 mM NaCl, 4 mM MgCl2, 4 mM spermidine, 50 μM EDTA, 10% glycerol, and pH 7.0). The sensitivity to the introduction of a single perturbation to the π-stack is demonstrated by the direct comparison of 17-mer well-matched (blue) and AC mismatched (red) DNA (see Table 3.1 for sequences). Despite de-oxygenation of the multiplexed chips, the extent of the background signals at the negative potentials of AQ allowed for only qualitative comparisons to be performed.

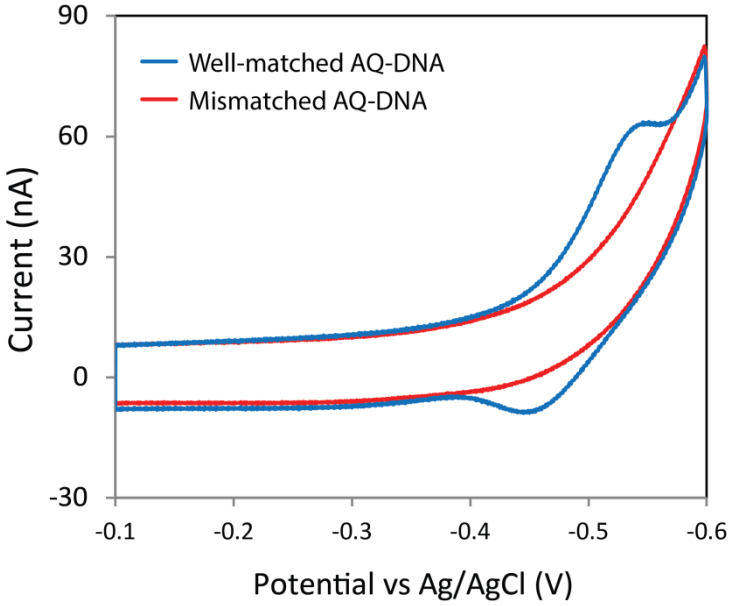

5.2 ± 0.3 pmol/cm^2 and 3.0 ± 0.3 pmol/cm^2 for high and low density respectively (Figure 3.8). This ensured that the observed differences in signal were not a result of altered hybridization efficiency caused by the incorporation of the AC mismatch. Finally, the scan rate was varied from 50 mV to 13 V to establish the rate of electron transfer for MB with both dT-C8 and dT-C12 linkages (Figure 3.9). Based on the Laviron analysis they displayed similar rates of electron transfer (2-4 s^{-1}), consistent with previously established results for a DNA-mediated mechanism where tunneling through the alkane-thiol is rate limiting (*8, 12*).

Under low density conditions, the percent signal remaining upon incorporation of a single AC mismatch ranged from 60% - 90%, compared to the high density conditions where it ranged from 10% - 40% across both reporters and all linkages (Table 3.4). The general nature of this dependence on film density speaks to the validity of our proposed mechanism, where surface accessibility dictates whether or not charge transport proceeds via DNA-mediated or surface-mediated pathways. Additionally, this demonstrates the utility of the truncated dT-C8 linkage as a means of decreasing the surface accessibility of the reporter as it retains the most DNA-mediated character under low density conditions.

Effect of neighboring duplex proximity

The proximity of the neighboring duplex DNA within the monolayer was again varied, this time including the additional assembly condition of 1 mM $MgCl_2$, to provide further support that DNA-mediated reduction is favored under conditions of high surface coverages and not simply because of the addition of $MgCl_2$ during assembly. The addition of $MgCl_2$ during monolayer formation has been used for over a decade to control the density of DNA monolayer packing (*2, 7*). As previously mentioned, 100 mM $MgCl_2$ has been used to produce dense DNA monolayers that physically extrude the reporter from directly accessing the electrode surface therefore enhancing DNA-mediated electrochemistry; however, it has

Figure 3.8. Consistency of $Ru(NH_3)_6^{3+}$ quantification across DNA sequences. Cyclic voltammograms (CVs) of the quantification of immobilized DNA by the electrostatic binding of $Ru(NH_3)_6^{3+}$ (1 μM) in phosphate buffer are presented for MB-dT-C8-DNA. CVs for high (left) and low (right) density DNA monolayers and both well-matched (blue) and AC mismatched (red) 17-mer DNA are presented. For each given condition 4 individual electrodes are presented to demonstrate the variability observed. Overall, the DNA sequence is shown to have no significant impact on the signal from $Ru(NH_3)_6^{3+}$ binding indicating that there is not significant dehybridization of the mismatched duplex at the surface of the electrode.

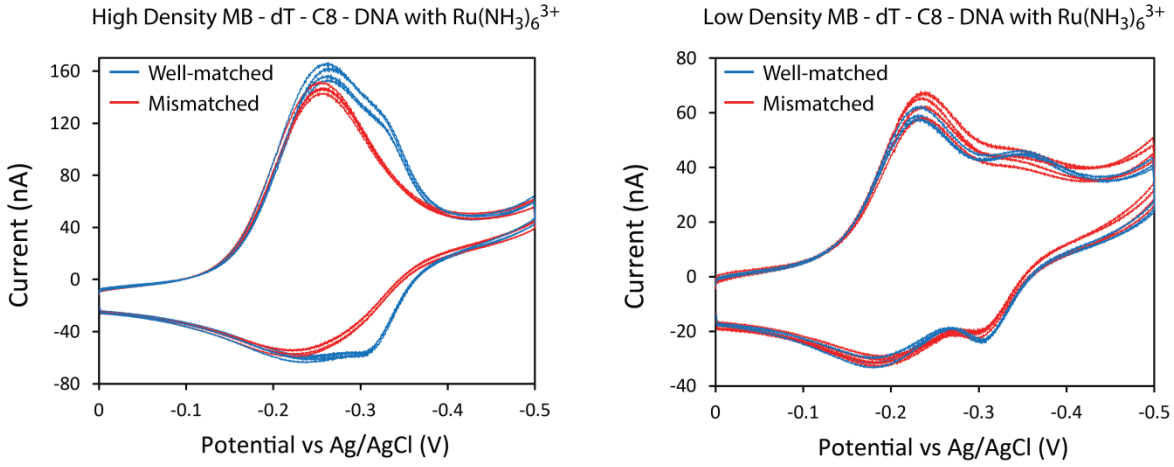

Figure 3.9. Scan rate dependence. The scan rate was varied from 50 mV to 13 V and the shift in the reduction potential was determined relative to 50 mV for MB covalently tether to DNA by both dT-C8 (blue) and dT-C12 linkages (red). Three different assembly conditions were also examined for each linkage: without $MgCl_2$ (triangle), with 1 mM $MgCl_2$ (square), and with 100 mM $MgCl_2$ (diamond). Cyclic voltammetry was acquired in spermidine buffer (5.0 mM phosphate, 50 mM NaCl, 4 mM MgCl2, 4 mM spermidine, 50 μM EDTA, 10% glycerol, and pH 7.0) with well-matched DNA. The rate of electron transfer was determined based on the Laviron analysis (*30*) and was found to be 2 - 4 s^{-1} for all conditions.

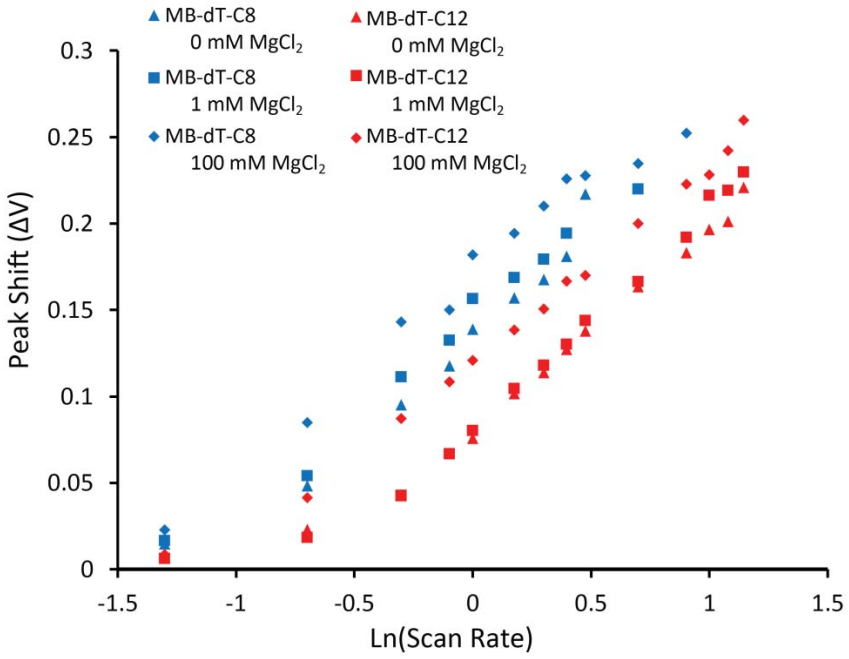

yet to be determined whether this effect results from simply the addition of $MgCl_2$ during assembly or from the increased surface coverages obtained at high $MgCl_2$ concentrations.

Signal attenuation upon introducing a single AC mismatch and the concentration of immobilized DNA, based on the electrostatic binding of $Ru(NH_3)_6^{3+}$, were quantified for MB covalently tethered by both dT-C8 and dT-C12 linkages at three different DNA monolayer conditions, incubation without $MgCl_2$, with 1 mM $MgCl_2$, and with 100 mM $MgCl_2$ (Figure 3.10). The observed signal attenuation upon incorporation of an AC mismatch and the DNA surface coverage in the 1 mM $MgCl_2$ film is not altered compared to signals for DNA monolayers assembled without MgCl2 (Figure 3.10). As the sensitivity to π-stack perturbations is only enhanced at higher DNA surface coverages, this result further supports the model where the extent of the exposed electrode surface dictates the mechanism of either DNA-mediated or surface-mediated reduction.

Effect of neighboring duplex π–stack integrity

The significance of the neighboring duplex integrity was investigated by introducing increasing fractions of unlabeled duplex DNA with a single AC mismatch. DNA-modified electrodes were assembled using a 50/50 mixture of well-matched MB-modified DNA and unlabeled DNA of varying compositions of well-matched and mismatched DNA. As the truncated dT-C8 linkage displays DNA-mediated character under both high and low density conditions it was used to establish whether inter- or intra- duplex intercalation is the predominant mode of reporter binding to the π-stack (Figure 3.11). Results for the dT-C12 linkage were included for completeness (Figure 3.12). As the fraction of well-matched MB-modified DNA remains constant, an attenuation of signal would only be expected in the presence of higher fractions of mismatched DNA if the reduction occurred through an interduplex pathway, as opposed to an intraduplex pathway where the signal is expected to remain unaltered. The predicted extent of signal attenuation for an interduplex pathway

Figure 3.10. Electrochemistry as a function of assembly conditions. The percent signal remaining (MM/WM*100) (red) and $Ru(NH_3)_6^{3+}$ signals (black) for MB modified DNA with both dT-C8 (dark) and dT-C12 (light) linkages were examined. DNA-modified electrodes were assembled without $MgCl_2$, with 1 mM $MgCl_2$, and with 100 mM $MgCl_2$. The error was determined from across three sets each containing four electrode replicates.

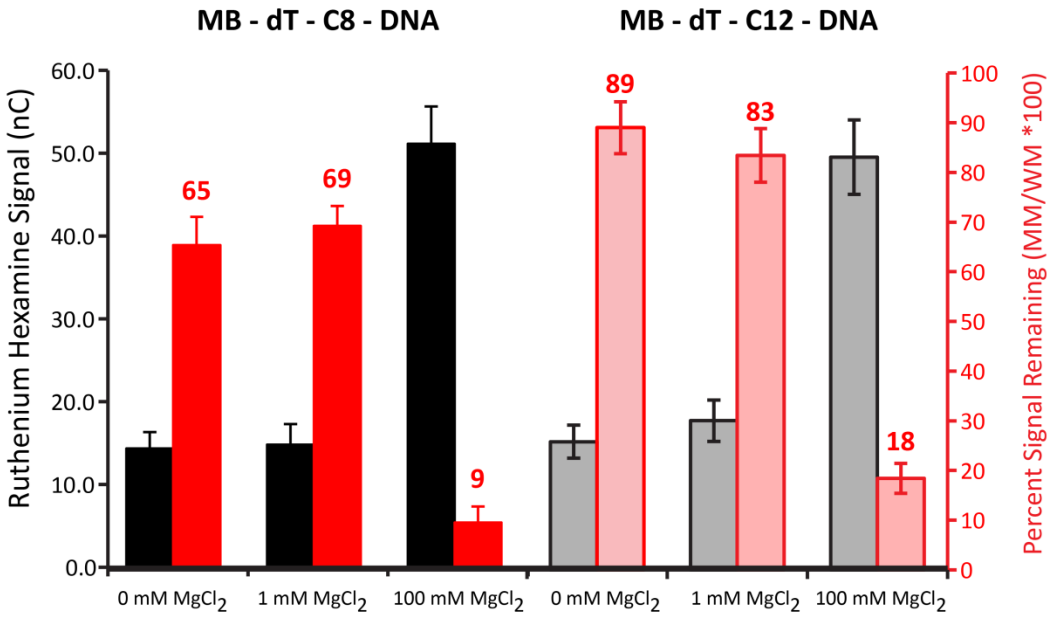

Figure 3.11. Effect of neighboring duplex integrity for MB-dT-C8-DNA. Electrodes assembled with MB-modified well-matched DNA and varied fractions of unlabeled well-matched and AC mismatched DNA. The experimental (blue) reductive signal areas were determined at each fraction of unlabeled mismatched DNA and normalized to the signal at 100% well-matched DNA. The predicted values were determined by the total fraction of mismatched DNA times by the percent signal attenuation for the given linkage and assembly conditions. Electrodes assembled in the presence (triangle) and absence (square) of 100 mM $MgCl_2$ are presented

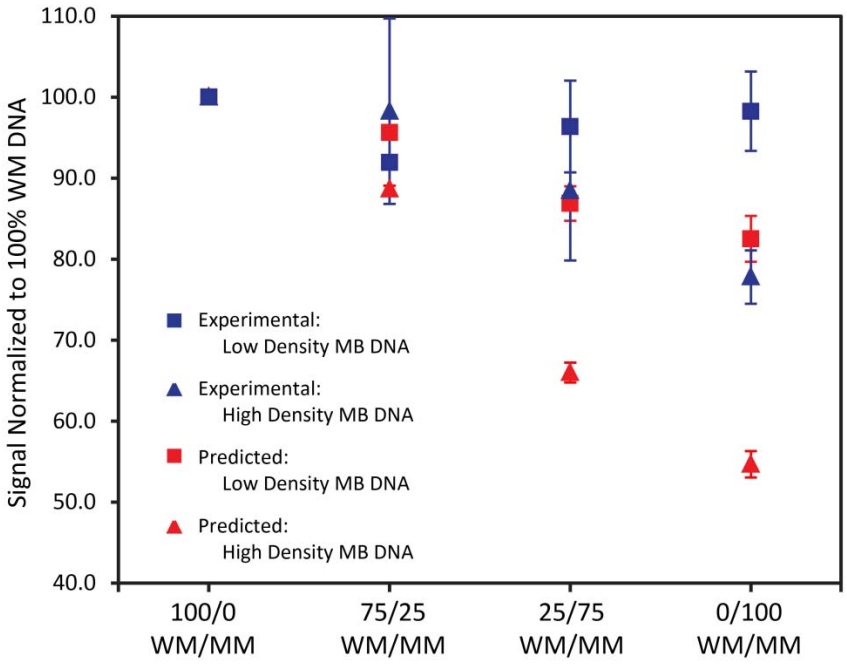

Figure 3.12. Effect of neighboring duplex integrity for MB-dT-C12-DNA. Electrodes assembled with MB-modified well-matched DNA and varied fractions of unlabeled well-matched and AC mismatched DNA. The experimental (blue) reductive signal areas were determined at each fraction of unlabeled mismatched DNA and normalized to the signal at 100% well-matched DNA. The predicted values were determined by the total fraction of mismatched DNA times by the percent signal attenuation for the given linkage and assembly conditions. Electrodes assembled in the presence (triangle) and absence (square) of 100 mM $MgCl_2$ are presented

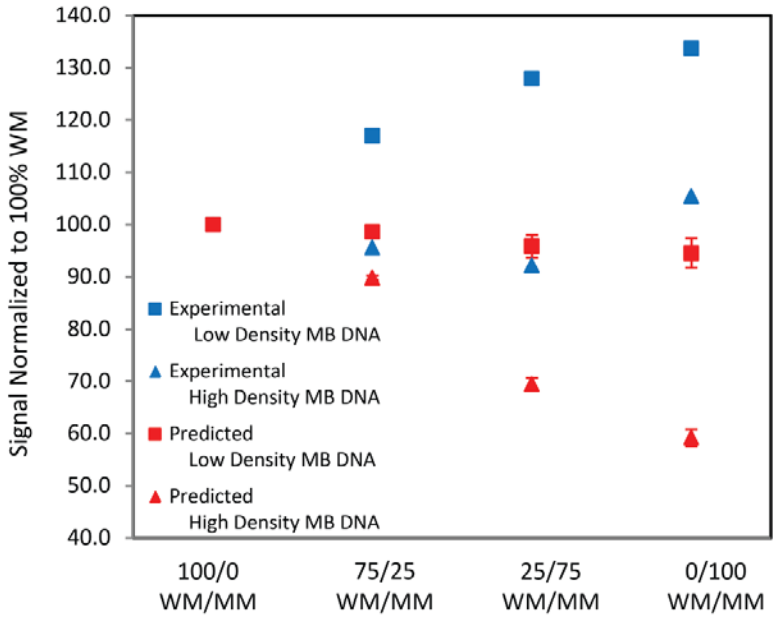

was calculated at each mismatch concentration based on the fraction of mismatched DNA in the film and the percent signal attenuation previously determined for a 100% mismatched DNA film for both assembly conditions (Table 3.4). In all cases, the experimental results of incorporating mismatched DNA showed significantly less signal attenuation than predicted, consistent with a predominantly intraduplex pathway (Figure 3.11). Most notably, for the case of the low density DNA films, the effect is less than 5% of that predicted, suggesting that 95% of the DNA-mediated signal is generated via an intraduplex pathway. Therefore, there is roughly 20-fold more intraduplex reduction occurring than interduplex reduction within these films. Even in the densely packed DNA monolayers where the decreased distance between duplexes would facilitate interduplex intercalation of the reporter, the observed attenuation was still only 25% of that predicted, indicating that intraduplex reduction is still 3-fold more favored than an interduplex pathway.

Conclusion

In conclusion, we have demonstrated that intraduplex DNA CT is a significant mechanism for the redox-activity of probe molecules that are covalently tethered to a DNA duplex. The extent of DNA-mediated electronic coupling depends not only on how tightly the redox-active species interacts with the π-stack, but also on the location and structure of the covalent tether. Finally, the possibility by which charge transport occurs through the counter ions associated with the sugar-phosphate backbone or the reporter intercalating into the neighboring duplex is not supported by our results. Instead we have observed reporter sensitivity to intervening π-stack perturbations and a tolerance to the integrity of the neighboring duplex DNA. These results fully support the intraduplex DNA-mediated reduction of these covalently tethered reporters. Ultimately, delineating the mechanisms of

electron transfer in DNA-modified electrodes is critical for their continued development as useful diagnostic tools.

REFERENCES

1. Lam, B., Fang, Z., Sargent, E.H., Kelley, S.O *Anal. Chem.* **2012**, *84*, 21.
2. Lapierre, M.A., O'Keefe, M., Taft, B.J., Kelley, S.O. *Anal Chem.* **2003**, *75*, 6327.
3. Zhao, S., Yang, W., Lai, R.Y. *Biosens. Bioelectron.* **2011**, *26*, 2442.
4. Kwon, S.J., Bard, A.J. *J. Am. Chem. Soc.* **2012**, *134*, 10777.
5. Pheeney, C.G., Guerra, L.F, Barton, J.K. *Proc. Natl. Acad. Sci.* **2012**, *109*, 11528.
6. Slinker, J.D, Muren, N.B., Gorodetsky, A.A., Barton, J.K. *J. Am. Chem. Soc.* **2010**, *132*, 2769.
7. Kelley, S.O., Jackson, N.M., Hill, M.G., Barton, J.K. *Angew. Chem. Int. Ed.* **1999**, *38*, 941.
8. Drummond, T.G., Hill, M.G., Barton, J.K. *J. Am. Chem. Soc.* **2004**, *126*, 15010.
9. Slinker, J.D., Muren, N.B., Renfrew, S.E., Barton, J.K. *Nat. Chem.* **2011**, *3*, 228.
10. Pheeney, C.G., Arnold, A.R., Grodick, M.A., Barton J.K. *J. Am. Chem. Soc.* **2013**, *135*, 11869.
11. Kelley, S. O., Barton, J. K., Jackson, N., Hill, M. G. *Bioconjugate Chem.* **1997**, *8*, 31.
12. Pheeney, C.G., Barton, J.K. *Langmuir* **2012**, *28*, 7063.
13. Boon, E., Jackson, N., Wightman, M., Kelley, S., Hill, M., Barton, J.K. *J. Phys. Chem. B* **2003**, *107*, 11805.
14. Gorodetsky, A., Green, O., Yavin, E., Barton, J.K. *Bioconjugate Chem.* **2007**, *18*, 1434.
15. Weizmann, Y., Chenoweth, D.M., Swager, T.M. *J. Am. Chem. Soc.* **2011**, *133*, 3228.
16. Wu, J, Chumbimuni-Torres, K.Y., Galik, M., Thammakhet, C., Haake, D.A., Wang, J. *Anal. Chem.* **2009**, *81*, 1007.
17. Plaxco, K.W., Soh, H.T. *Trends in Biotechnology* **2011**, *29*, 1.
18. Bonham, A.J., Hsieh, K., Ferguson, B.S., Vallee-Belisle, A., Ricci, F., Soh, H.T., Plaxco, K.W. *J. Am. Chem. Soc.* **2012**, *134*, 3346.
19. Abi, A., Ferapontova, E.E. *J. Am. Chem. Soc.* **2012**, *134*, 14499.
20. Farjami, E., Campos, R., Freapontova, E.E. *Langmuir* **2012**, *28*, 16218.

21. Yu, Z., Lai, R.Y. *Anal. Chem.* **2013**, *85*, 3340.

22. Wu, Y., Lai, R.Y. *Chem. Comm.* **2013**, *49*, 3422.

23. Charge Transfer in DNA:From Mechanism to Application edited by Wagenknecht, H.A. (Wiley-VCH Verlag GmbH & Co KGaA, Weiheim, 2005).

24. Genereux, J.C., Barton, J.K. *Chem. Rev.* **2010**, *110*, 1642.

25. Murphy, C.J., Arkin, M. R., Jenkins, Y., Ghatlia, N. D., Bossmann, S. H., Turro, N. J., Barton, J. K. *Science* **1993**, *262*, 1025.

26. Frade, V.H.J., Gonçalves, M.S.T., Moura, J.C.V.P. *Tetrahedron Letters* **2006**, *47*, 8567.

27. Frade, V.H.J., Gonçalves, M.S.T., Moura, J.C.V.P. *Tetrahedron Letters* **2005**, 46, 4949.

28. Pedersen, D.S., Rosenbohm, C. *Synthesis* **2001**, *16*, 2431.

29. Laviron, E. J. *J. Electroanal. Chem.* **1979**, *101*, 19.

30. Yu, H-Z., Luo, C-Y., Sankar, C.G., Sen, D. *Anal. Chem.* **2003**, *75*, 3902.

31. There is precedence for MB-modified DNA with all of the linkages used here: dT-C12 (12, 19), dT-C8 (5), and 5′-C12 (13, 20).

32. Boon, E.M.; Barton, J.K.; Bhaghat V.; Nerissian M.; Wang W.; Hill M.G. Langmuir 2003, 19, 9255.

33. Wohlgamuth, C.H; McWilliams, M.A.; Slinker, J.D. Anal. Chem. 2013, 85, 1462.

CHAPTER 4

DNA Sensing by Electrocatalysis with Hemoglobin

Adapted from Pheeney, C.G., Guerra, L.F., Barton, J.K. (2012) *Proceedings of the National Academies of* Sciences 109, 11528. L.F. Guerra was a Caltech undergrad working under the direction of C. G. Pheeney.

ABSTRACT

Electrocatalysis offers a means of electrochemical signal amplification, yet in DNA-based sensors, electrocatalysis has required high density DNA films and strict assembly and passivation conditions. Here we describe the use of hemoglobin as a robust and effective electron sink for electrocatalysis in DNA sensing on low density DNA films. Protein shielding of the heme redox center minimizes direct reduction at the electrode surface and permits assays on low density DNA films. Electrocatalysis with methylene blue that is covalently tethered to the DNA by a flexible alkyl chain linkage allows for efficient interactions with both the base stack and hemoglobin. Consistent suppression of the redox signal upon incorporation of single CA mismatch in the DNA oligomer demonstrates that both the unamplified and the electrocatalytically amplified redox signals are generated through DNA-mediated charge transport. Electrocatalysis with hemoglobin is robust: it is stable to pH and temperature variations. The utility and applicability of electrocatalysis with hemoglobin is demonstrated through restriction enzyme detection, and an enhancement in sensitivity permits femtomole DNA sampling.

INTRODUCTION

DNA-modified electrodes have been extensively studied in the development of sensitive DNA-based sensors using DNA-mediated charge transport (CT) chemistry (*1-18*). Sensors based on DNA-mediated CT are exquisitely sensitive to structural perturbations caused by single base mismatches, lesions, and DNA binding proteins (*2-4*). Due to the high specificity, robust nature, and low cost of these DNA-based electrochemical sensors they are being developed as new cancer diagnostics through the detection of transcription factors and low abundance microRNAs (*4,5,19,20*). Despite the intrinsic specificity of these devices, these DNA CT sensors currently lack the required sensitivity to detect biologically relevant levels of cancer markers. Therefore, a means to reliably and robustly amplify the DNA-mediated signal is essential for the application of these technologies to the rapid detection of cancer markers directly from cell lysates.

Different electrochemical strategies have been used to achieve higher sensitivities, including the use of gold nanoparticles, conducting polymers, and catalysis (*21-27*). Electrocatalysis, however, represents a preferred means of signal amplification in electrochemical sensors (*25-27*). The degree of electrocatalytic signal amplification depends upon the coupling of the catalysis with the electrode surface and the electrode sink (*28*). Additionally, robust reporting by electrocatalysis is dependent on the rigorous shielding of the electron sink from the electrode surface, which prevents direct reduction by the electrode and false positive outputs (27). In electrocatalysis, the redox reporter is coupled with a freely diffusing electron sink, typically ferricyanide. Methylene Blue (MB) is typically used as the redox reporter for DNA-mediated electrocatalysis, as it is well coupled to the base stack through intercalation (*26*). Reduction of the reporter leads to the reduction of the electron sink, returning the reporter back to its oxidized form and allowing for the repeated

interrogation of the base stack. To complete this catalytic cycle reporting on DNA-mediated changes, the reporter must interact with both the DNA film and the freely diffusing electron sink (*26*). Finally, in order for DNA-modified electrodes to be viable for the detection of DNA-binding proteins and the hybridization of oligonucleotides, the surface-bound DNA duplex must be sufficiently accessible (*29-32*). All three of these constraints must be met for electrocatalysis to be applied as a detection platform in DNA CT-based systems: dual reporter interactions, robust shielding of the electron sink from surface reduction, and DNA accessibility.

Initial electrocatalysis experiments were performed using non-covalently bound DNA reporters and high density DNA films (*2, 3, 25, 26*). The freely diffusing non-covalent reporter was able to readily interact with both the electron sink and the base stack, while the high density DNA films limited localization of the reporter to the distal end of the duplex. The high density films also imposed a strong kinetic barrier to the direct reduction of ferricyanide at the electrode surface (*2*). This platform demonstrated enhanced sensitivity due to electrocatalytic signal amplification, and allowed for efficient detection of single base mismatches (*2, 3, 25, 26*). The major limitation of this platform originated from the need for well-packed films to passivate the surface and ensure that the redox probe binds to the top of the DNA film. These high packing densities can be difficult to achieve reproducibly and lead to poor accessibility of the duplex DNA for analyte binding (*29-32*).

Low density DNA films are now the standard means for promoting efficient DNA binding and hybridization events, as they provide higher sensitivity and specificity. Low density DNA films, however, require covalent tethering of the reporter to the duplex to ensure placement of the reporter near the top of the surface. This covalent tethering of the reporter is furthermore essential for label-free assays of DNA or protein targets. However, low density films expose the electrode surface, as the negatively charged phosphate backbone of the immobilized DNA is insufficient to impose a kinetic barrier against the direct

reduction of positively charged species such as ferricyanide. A previous attempt at electrocatalysis with low density films utilized negatively charged functionalized mercaptoalkanes to shield ferricyanide, the electron sink, from the electrode (*27*). This platform has not been widely employed, due to the limited solution accessibility of the reporter and the difficulty imposing sufficient kinetic barriers to the reduction of ferricyanide to drive electrocatalysis. This platform did not address the poor interaction between the reporter and the electron sink imposed by the short, rigid covalent tether linking the reporter to the duplex (*27*). Therefore, a new means to promote efficient interactions between the reporter with the base stack and electron sink, as well as to robustly shield the electron sink from the electrode surface, must be developed for the application of electrocatalytic signal amplification with these low density DNA films.

Redox-active proteins may be useful as electron sinks for electrocatalysis. Enzymes such as horseradish peroxide and glucose oxidase have been shown to readily interact electronically with phenothiazine dyes such as MB, and have had wide application as recognition elements for molecular sensing (*33-42*). Detection platforms based on these enzymes are desirable due to their inherent catalytic activity. The application of a protein as an electron sink is also appealing because the protein shell itself can shield the redox core from the electrode surface (*34-41*). Hemoglobin exhibits this property and has been shown to couple with Nile Blue (*42*). Additionally, unlike many of the proteins typically employed for signal amplification, the reduction of hemoglobin does not generate any DNA damaging byproducts like peroxide.

Until now, no single DNA CT sensor has been compatible both with use of low density DNA films (required for hybridized DNA or protein targets) and robust electrocatalytic signal amplification (required for sufficient sensitivity). In this work, we report a DNA CT sensor that robustly and efficiently amplifies the signal from low density DNA films using electrocatalysis. This advancement is the result of a new flexible alkyl linkage between the

reporter and the duplex coupled with a novel electron sink. The new flexible linkage allows for the efficient shuttling of electrons between the duplex and the electron sink (*28*). The use of hemoglobin allows electronic interaction with MB while inherently being shielded from the electrode surface by the protein shell. No specialized backfilling agents or assembly conditions were required, demonstrating the general applicability of this system. This general technique, electrocatalysis of MB with hemoglobin, can therefore be utilized with current DNA detection strategies without imposing any new constraints to the platform. Most importantly, the enhanced sensitivity permits femtomole DNA sampling.

MATERIALS AND METHODS

Materials

All chemicals were purchased from Sigma Aldrich and used without further purification. All proteins were purchased from New England Biolabs. Oligonucleotides without unnatural modifications were purchased from IDT, while modified oligonucleotides were synthesized on a 3400 Applied Biosystems DNA synthesizer. Modified phosphoramidites were purchase from Glen Research. Hemoglobin was obtained from Sigma Aldrich as a lyophilized powder from bovine blood.

Oligonucleotides preparation

MB modified DNA was prepared by the synthesis of amino-modified DNA utilizing an Amino-$(CH_2)_2$-dT phosphoramidite (Figure 4.1). Amino-modified DNA, as well as thiol modified DNA, were purified through standard procedures as previously reported (*6*). MB modified with a terminal carboxylic acid was synthesized and coupled to the amino modified DNA (*43*). All single stranded DNA was purified by reverse-phase HPLC and characterized with MALDI-TOF mass spectrometry.

Figure 4.1. Structure of MB modified DNA with a flexible C8 linkage covalently tethering MB to the DNA.

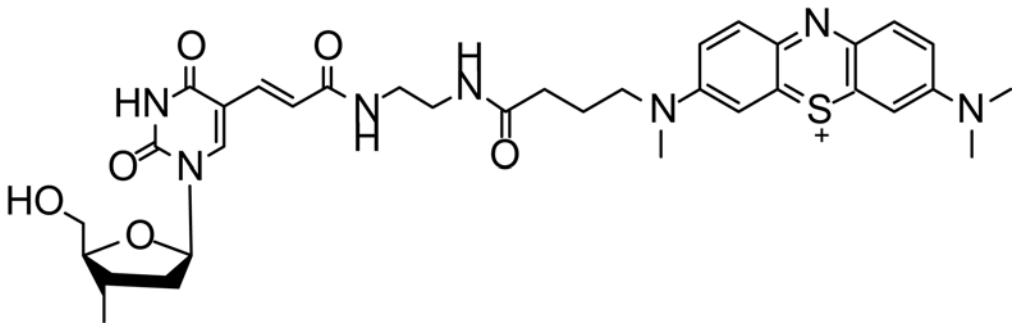

Single stranded DNA stock solutions were prepared in phosphate buffer (5.0 mM phosphate, 50 mM NaCl, pH 7) and quantified by UV-Vis spectroscopy based on their absorbance at 260 nm. The extinction coefficients for the single strand DNA were estimated using SciTools from IDT. The extinction coefficient for MB modified DNA at 260 nm was corrected for the contribution of MB to the absorbance by adding 10,300 $M^{-1}cm^{-1}$ to the IDT calculated extinction coefficient. All DNA solutions were thoroughly deoxygenated with argon prior to annealing. Equimolar amounts of single stranded stocks were combined and annealed by heating to 90 ºC and cooling to ambient temperature over 90 min.

DNA-modified electrodes

Multiplex chips were employed for the electrochemical experiments and were fabricated as previously reported (*6, Appendix III*). Chips consisted of 16 gold electrodes (2 mm^2 area) that were divided into four quadrants of four electrodes. Duplex DNA (25 µl of 25 µM, except for concentration dependence experiment) was assembled overnight (20-24 hr) in a humid environment allowing for monolayer formation. Low density films were assembled in the absence of $MgCl_2$, while high density films were assembled with the addition of 100 mM $MgCl_2$. Once DNA films were assembled and thoroughly washed with phosphate buffer, the electrodes were backfilled with 1 mM 6-mercaptohexanol (MCH) for 45 min in phosphate buffer with 5 % glycerol. The electrodes were scanned in a common running buffer (5.0 mM phosphate, 5 mM NaCl, 40 mM $MgCl_2$, 5 mM spermidine and pH 7). Electrocatalysis data was acquired following the addition of 25 µM hemoglobin (5 mM phosphate, 5 mM NaCl, 40 mM $MgCl_2$, 5 mM spermidine, and pH 7) to the central well.

Electrochemical measurements

Electrochemical measurements were performed with a CHI620D Electrochemical Analyzer and a 16-channel multiplexer from CH Instruments. A three-electrode setup was

used, with a common Ag/AgCl reference and a Pt wire auxiliary electrodes placed in the central buffer solution. Cyclic voltammetry data were collected at 100 mV/s unless otherwise indicated, and chronocoulometry data were acquired at an applied potential of -450 mV for an interval of 10 sec unless otherwise indicated. Non-electrocatalytic CV data were quantified by the area of the reduction peak for MB, while electrocatalytic chronocoulometry data were quantified by the accumulated charge after 10 sec. The surface coverage of the MB-DNA was based on the area of the reduction peak observed for the distally bound MB and calculated as previously reported (*6*). The catalytic turnover was calculated based on the ratio of the accumulated charge in the presence and absence of hemoglobin.

Temperature dependence

Temperature dependence experiments were performed by assembling the chip in a holder with a Peltier (thermoelectric) device (Melcor Corp.) placed underneath the chip. The temperature was measured using a digital probe placed in the central well containing the running buffer. Chronocoulometry data were repeatedly acquired at pulse widths of two seconds, while heating the chip at a rate of 0.5 ºC/min over a temperature range of 24-38 ºC.

Restriction enzyme detection

DNA-modified electrodes used for RsaI detection were incubated with Bovine Serum Albumin (BSA) (1 mM in 5.0 mM phosphate, 50 mM NaCl, 4.0 mM $MgCl_2$, 4.0 mM spermidine, 50 µM EDTA, 10% glycerol, and pH 7) for 1 hr to minimize any signal attenuation observed from non-specific protein binding. The electrodes were then washed and scanned in the running buffer (*8*). Half of the electrodes were then incubated for 2 hr with RsaI restriction enzyme (20 µL of 50 nM) in RsaI reaction buffer (10 mM Tris, 50 mM

NaCl, 4 mM spermidine, 10 mM $MgCl_2$, pH 7.9) and then washed and scanned in phosphate buffer.

RESULTS AND DISCUSSION

Electrocatalytic signal amplification of MB-modified DNA by hemoglobin

In this study, MB is covalently tethered to DNA with a flexible C8 linkage, such that upon reduction the tethered MB mimics the behavior of a non-covalent reporter (Figure 4.1). Hemoglobin is known to interact electrochemically with organic dyes such as MB and can function as an electronic sink for catalytically reduced MB (*42*). The general electrocatalytic cycle developed for this study utilizing MB-DNA and hemoglobin is presented in Figure 4.2. The two-electron reduction of MB to leucomethylene blue (LB) significantly decreases the binding affinity of the reporter, resulting in its dissociating from the duplex. LB proceeds to electrochemically interact with, and reduce, two equivalents of freely diffusing hemoglobin, returning the reporter to the oxidized form and completing the electrocatalytic cycle.

The low density MB-DNA films employed in this study were assembled without $MgCl_2$ and had typical surface coverages of 1.3 ± 0.2 pmol/cm^2. Prior to the addition of hemoglobin, the resulting cyclic voltammograms (CVs) demonstrate a reversible redox couple consistent with a signal generated from MB reduction via DNA-mediated CT: a midpoint potential of -340 mV, peak splitting of -50 mV, and a ratio of near unity for the cathodic and anodic peak areas (Figure 4.2). MB-DNA modified electrodes were then examined in the presence of freely diffusing hemoglobin (25 μM). The electrocatalytic signal amplification is apparent in the CV by the characteristic non-reversible signal, where the reductive peak is amplified and the oxidative peak is not observed. Hemoglobin was also added to DNA in the absence of MB, showing that hemoglobin alone has no effect on the

Figure 4.2. Electrocatalytic reduction of MB modified DNA by hemoglobin. Left: Schematic representation of the electrocatalytic cycle of MB-DNA. In this model, upon reduction of MB to leucomethylene blue (LB), the DNA binding affinity is significantly decreased, resulting in the dissociation of reporter from the duplex and its subsequent oxidation by freely diffusing hemoglobin. Center: Cyclic voltammetry (scan rate = 30 mV/s) of MB-DNA in the absence (black), DNA without MB in presence (gray) and MB-DNA in the presence (red) of 25 μM hemoglobin in phosphate buffer (5 mM phosphate, 5 mM NaCl, 40 mM $MgCl_2$, 5 mM spermidine and pH 7.0). Right: Corresponding chronocoulometry signal (V = -450 mV) acquired over 10 sec intervals.

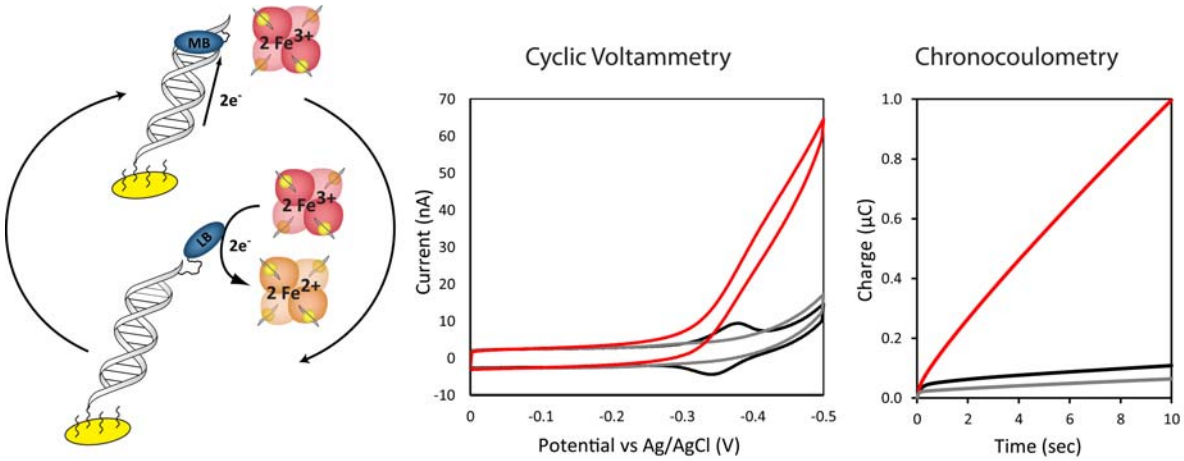

observed electrochemistry (Figure 4.2). Additionally, the electronic spectrum of hemoglobin showed no significant variation before and after electrocatalysis, indicating that protein integrity was retained (Figure 4.3).

In the absence of hemoglobin, chronocoulometry at -450 mV vs Ag/AgCl, a potential appropriate for reduction MB-DNA, showed a rapid initial accumulation of charge (0.04 μC over 0.3 sec), with minimal charge accumulation (0.1 μC) over the subsequent 10 sec (Figure 4.2). This modest accumulation of charge is consistent with the reduction of surface bound MB without an electron sink for catalytic cycling. In the presence of hemoglobin, there is the same rapid initial accumulation of charge as in the non-catalytic case, but over the subsequent 10 sec, a total of 0.99 ± 0.04 μC of charge is accumulated. A comparison of the accumulated charge as a function of the presence of hemoglobin yields insight into the catalytic behavior of MB. An accumulated charge of 0.99 ± 0.04 μC in the presence of freely diffusing hemoglobin correlates to roughly ten turnovers per MB-DNA. This electrocatalytic amplification of the accumulated charge due to MB-DNA reduction demonstrates that covalently tethering MB to DNA through a C8 linkage does not disrupt the ability of hemoglobin to electrochemically couple with MB.

Electrocatalytic amplification of MB-DNA with intervening mismatches

In order to demonstrate that the electrocatalytically amplified signal is generated via DNA-mediated CT, the signal suppression due to the incorporation of a single base mismatch was examined. Previously, the degree of signal attenuation upon incorporation of a single base mismatch indicated that MB covalently tethered to the DNA duplex through a flexible C12 linkage can be reduced by both DNA CT and direct surface reduction (*43*). Here we utilized a shorter C8 linkage to reduce contributions from the direct surface reduction of MB. Using this assembly, Figure 4.4 illustrates electrocatalysis with and without an intervening mismatch. CG-rich thiol modified DNA was annealed with

Figure 4.3. Absorbance spectrum of hemoglobin (5 μM) in phosphate buffer (5 mM phosphate, 5 mM NaCl, 40 mM $MgCl_2$, 5 mM spermidine, pH 7) before (solid) and after (dotted) electrocatalysis with MB-DNA.

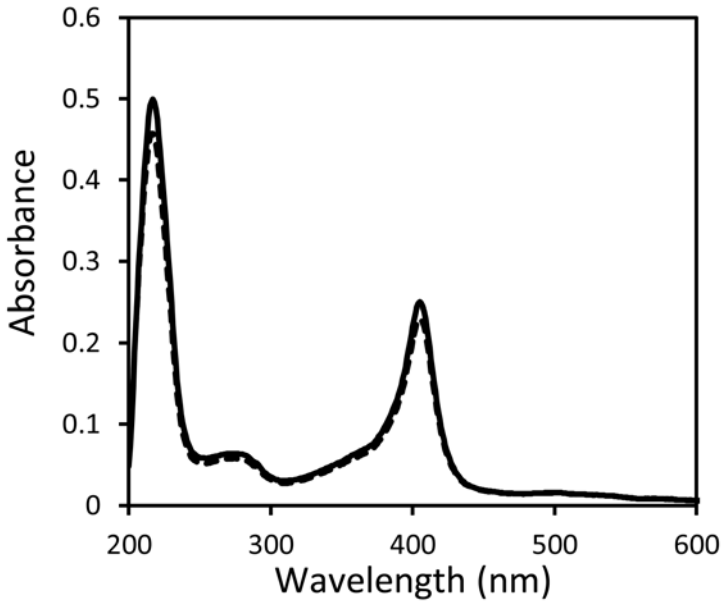

Figure 4.4. Signal suppression of MB-DNA due to incorporation of a single CA mismatch. Left: Low density MB-DNA films were assembled on multiplexed chips. Sequence for both well-matched MB-DNA (blue) and mismatched MB-DNA (red) are indicated. Center: In the absence of hemoglobin, CV scans (scan rate = 100 mV/s) were used to demonstrate the characteristic signal attenuation due to incorporation of a single CA mismatch. Right: chronocoulometry scans (V = -450 mV) were used for electrocatalytically amplified MB-DNA in the presence of 25 μM hemoglobin. All scans were acquired in phosphate buffer (5 mM phosphate, 5 mM NaCl, 40 mM $MgCl_2$, 5 mM spermidine and pH 7).

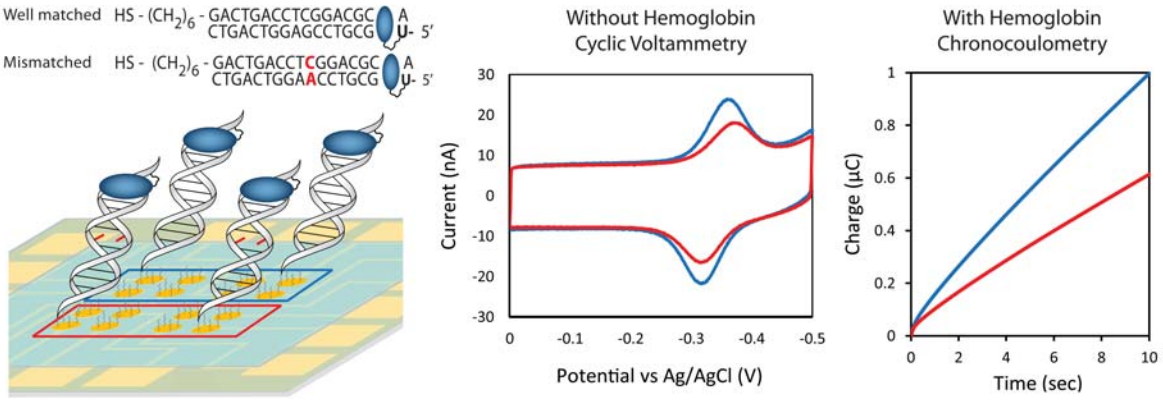

complementary well-matched DNA as well as a mismatched sequence containing a single CA mismatched base pair in the middle of the 17-mer duplex. Well-matched and mismatched CG-rich DNA were each assembled as low density DNA films on eight electrodes of a multiplexed chip. The use of equivalent thiol strands and multiplexed chips removes variability due surface quality and film formation.

As is evident in Figure 4.4, signal attenuation is observed in this system with an intervening mismatch. The average reductive peak area from the CVs for well-matched MB DNA is 5.0 ± 0.4 nC and that of mismatched MB-DNA is 3.2 ± 0.4 nC. This signal attenuation in the presence of a single base mismatch confirms that the signal observed is generated via DNA-mediated CT. Upon the addition of hemoglobin (25 μM) the MB-DNA signals are electrocatalytically amplified and the accumulated charge for well-matched and mismatched DNA were compared. The accumulated charge over 10 sec from the chronocoulometry data are 0.99 ± 0.04 μC and 0.62 ± 0.02 μC for well-matched and mismatched MB-DNA, respectively (Figure 4.4). The accumulated charge obtained for the mismatched MB-DNA was again only 62 % of the well-matched MB-DNA signal upon electrocatalytic amplification. The consistency in the signal suppression due to mismatch incorporation indicates that the catalytic reduction of MB-DNA occurs via DNA CT. Therefore, the sensitivity of the observed signal to subtle structural perturbations to the π–stack is still apparent with electrocatalytic amplification.

Variations in pH and temperature on amplification

DNA-modified electrodes are generally stable over the pH range of 5.5 to 8.5, where minimal damage occurs to DNA. The reduction peak area of MB-DNA, without amplification, is unaffected by changes in pH, while the peak potential is shifted positive with increasing acidity at a rate of 25 mV per pH unit (Figure 4.5). This is expected, as MB is protonated upon reduction. Previous work with enzyme-mediated electrocatalytic cascades has

Figure 4.5. Left: The MB-DNA peak reduction potential as a function of pH, ranging from 5.5 to 8.5 in the absence of hemoglobin measured from the cyclic voltammetry data (scan rate = 100mV/s). Right: The accumulated current for electrocatalytically amplified MB-DNA in phosphate buffer (5 mM phosphate, 5 mM NaCl, 40 mM $MgCl_2$, 5 mM spermidine) as a function of pH, ranging from 5.5 to 8.5, is presented. The accumulated current was determined from chronocoulometry (V = -450 mV for 10 sec) in the presence of 25 μM Hemoglobin.

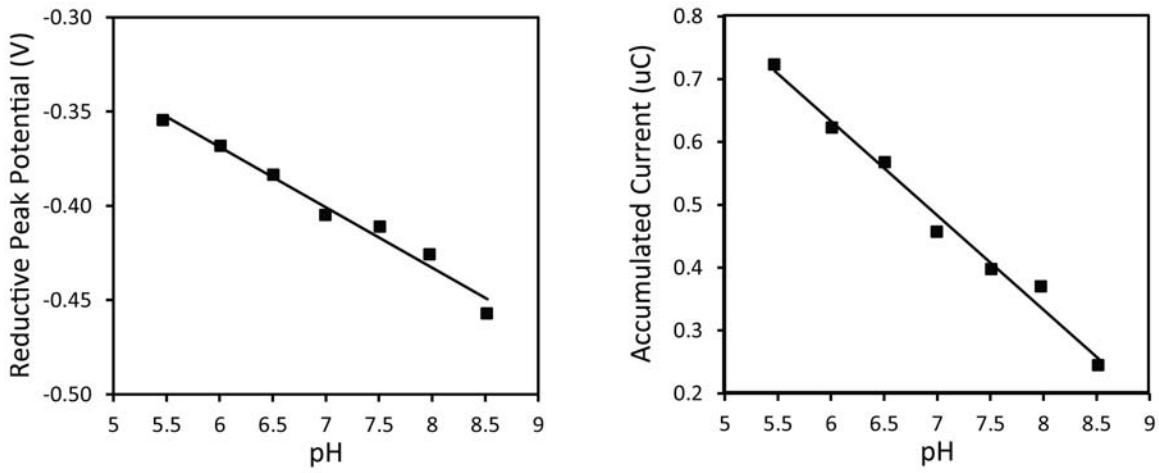

demonstrated a non-linear response to pH changes due to the pH dependence of the enzymatic activity (*34-42*). In these cases, where catalysis is limited by enzyme activity, constraints are imposed not only on the pH but also on other running conditions relevant to enzyme activity (*34-42*). In the system presented here, the electrocatalysis is not dependent on hemoglobin reactivity with oxygen, only the capability of hemoglobin to function as an electron sink. The electrocatalytic amplification of MB should therefore be optimal at a pH lower than the isoelectric point of hemoglobin (pI = 6.8) where hemoglobin will be less negatively charged (*42*). We demonstrated this to be true by examining the accumulated charge in the presence of hemoglobin at a range of pH values (5.5 to 8.5). All solutions were buffered and had the same salt and hemoglobin concentrations. Between pH 5.5 and 8.5, the accumulated charge increases linearly with increasing acidity at a rate of 0.15 μC per pH unit (Figure 4.5). This indicates that the electrocatalytic amplification obtained is not limited by hemoglobin activity and behaves as would be expected for a proton dependent electrocatalytic cycle. Therefore, hemoglobin activity does not impose new restrictions on the running conditions of DNA-modified electrodes compared to free iron, demonstrating the utility of hemoglobin as an electron sink in electrocatalysis.

The dependence of the total accumulated charge was also examined as a function of the temperature to demonstrate both the stability and necessity for protein activity. The temperature was systematically increased from 24 ºC to 38 ºC at a rate of 0.5 ºC/min. The accumulation of charge was found to increase at a rate of 20 μC/ºC in the range of 24 ºC to 32 ºC (Figure 4.6). Within this temperature range, mismatch discrimination was still observed in the catalytic signal. At increased temperatures ranging from 32 ºC to 40 ºC, the accumulated charge increased at a rate of 60 μC/ºC, roughly three times faster than at lower temperatures, and the discrimination due to mismatch incorporation was lost (Figure 4.6). While hemoglobin is stable under physiological conditions, the thermal denaturation of hemoglobin is highly pH and concentration-dependent. In the buffer used for this study, a

Figure 4.6. Temperature dependence of the electrocatalysis of MB-DNA. The temperature was increased at a rate of 0.5 ºC/min by a Peltier device placed beneath the multiplexed chip. The electrocatalytic amplification was monitored by chronocoulometry at 2 sec intervals. Left: The accumulated charge is plotted as a function of the measured solution temperature. Two different linear regimes can be discerned with rates of 20 µC/ºC and 60 µC/ºC at moderate (24 ºC to 32 ºC) and high (32 ºC to 40 ºC) temperatures respectively. Right: In each regime the effect on mismatch discrimination was examined by chronocoulometry; well-matched (blue) and mismatched (red) MB-DNA are shown at both 25 ºC (bottom) and 38 ºC (top). All scans were acquired in phosphate buffer (5 mM phosphate, 5 mM NaCl, 40 mM $MgCl_2$, 5 mM spermidine pH 7).

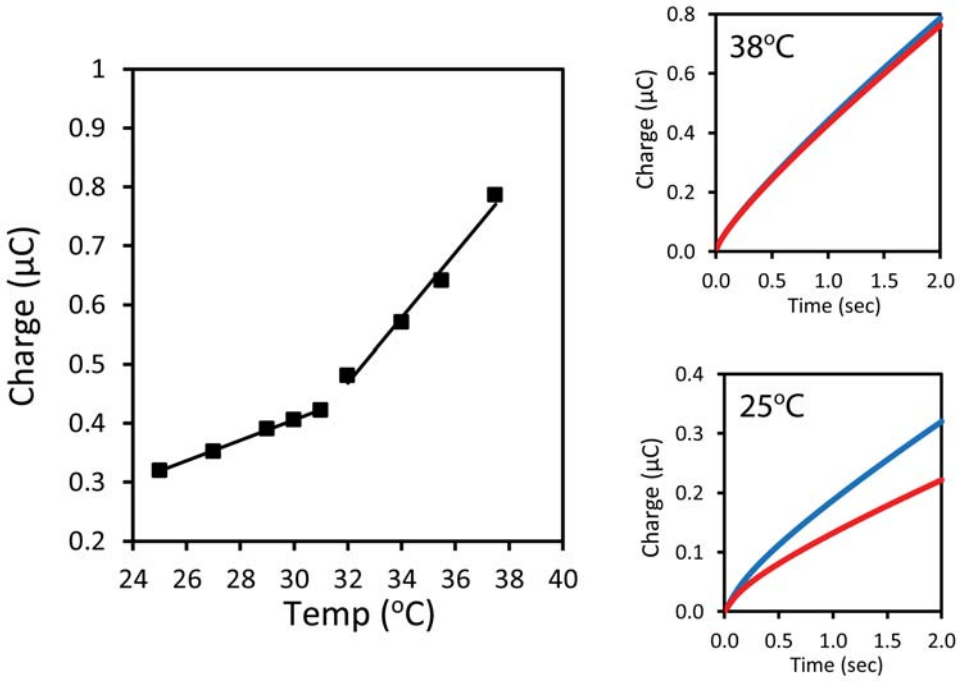

transition was observed by circular dichroism at 32-35 ºC (Figure 4.7). The accelerated charge accumulation and the loss in mismatch discrimination indicate that upon structural changes to hemoglobin the heme bound iron is no longer effectively shielded by the protein shell. These low density DNA films are not designed for passivation against the direct reduction of iron. This temperature profile demonstrates the necessity for intact hemoglobin to shield the iron from the electrode surface in order to observe the electrocatalytically amplified MB-DNA signal, and avoid false positives.

Detection of restriction enzyme activity

Having demonstrated that hemoglobin is an effective electron sink in DNA-mediated electrocatalysis, we can apply this electrocatalysis to the detection of DNA-binding proteins. The restriction enzyme RsaI sequence-specifically cuts duplex DNA that contains the binding site 5′-GTAC-3′ (*8*). RsaI activity was compared between DNA sequences with and without the binding site (Figure 4.8). Half the electrodes of a multiplex chip were treated with RsaI (20 μL of 50 nM) while the other half were left untreated. A comparison between the treated and untreated electrodes was made for each sequence in order to demonstrate the sequence-specificity of RsaI. Additionally, RsaI activity and electrocatalytic signal amplification was compared using both high density and low density DNA films to demonstrate the effect of duplex accessibility on the detection of DNA-binding proteins.

Low density films of the RsaI cutting sequence showed accumulated charges of 0.55 ± 0.02 μC for untreated samples and 0.32 ± 0.01 μC for samples treated with RsaI (Figure 4.8). With these low density DNA films, this corresponds to a 40 % signal attenuation due to treatment with RsaI. This signal attenuation was sequence-specific, as electrodes modified with low density DNA films of the control sequence showed no differential from those treated with RsaI (Figure 4.8).

Figure 4.7. Denaturation curve of hemoglobin (1 μM) measured by circular dichroism in phosphate buffer (5 mM phosphate, 5 mM NaCl, 40 mM $MgCl_2$, 5 mM spermidine, pH 7). The molar elipticity was measured at 225 nm as the temperature was varied from 20 ºC to 60 ºC. An initial transition can be observed from 32-35 ºC and a larger transition at 45-56 ºC corresponding to the denaturation of the alpha helices.

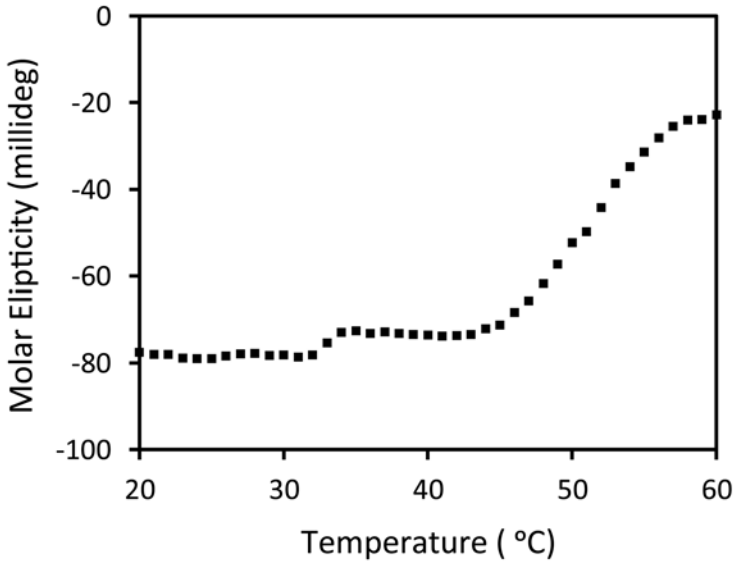

Figure 4.8. Electrocatalytic detection of sequence-specific restriction enzyme RsaI activity. Left: Sequences for the control and RsaI binding sequence are indicated. The binding site for RsaI is indicated in purple. All electrodes were incubated with BSA (1 mM for 1 hr to minimize any signal attenuation observed from non-specific protein binding). Electrodes were either left untreated (red) or treated (green) with RsaI (20 µL of 50 nM) for 2 hr. Right: The accumulated charge from the chronocoulometry data (V = -450 mV for 10 sec) of MB-DNA in the presence of 25 µM hemoglobin for the control sequence is plotted for both high density (dark) and low density (light) DNA films. High density films were formed by the addition of 100 mM $MgCl_2$ during DNA film self-assembly. The analogous data for the RsaI sequence is also presented.

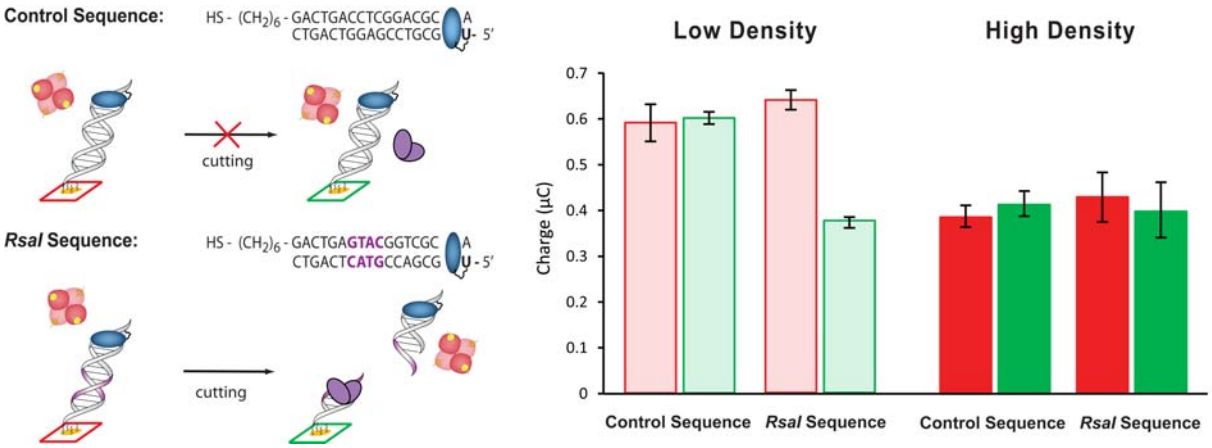

Using the traditionally implemented high density DNA films, no statistically relevant decrease could be discerned from either the RsaI sequence or the control sequence upon RsaI treatment. The RsaI sequence had accumulated charges of 0.36 ± 0.05 μC for untreated and 0.34 ± 0.08 μC for treatment with RsaI, while the control sequence had accumulated charges of 0.38 ± 0.02 μC for untreated and 0.41 ± 0.03 μC for treatment with RsaI (Figure 4.8). In addition to the lack of detectable RsaI activity with high density DNA films, there was significantly higher variability in the electrocatalytically amplified signal with high density films.

Overall, the low density DNA films had enhanced electrocatalytic activity and decreased variability compared to the high density films, which can be attributed to the enhanced accessibility of both RsaI and hemoglobin. Thus, electrocatalysis with hemoglobin clearly requires duplex accessibility.

Sensitivity of DNA detection

The sensitivity to the reduction of MB-DNA is compared with and without hemoglobin to demonstrate the enhanced sensitivity that is achieved with the overall signal gain of electrocatalysis. The reduction signal obtained from electrodes assembled with decreasing amounts of MB-DNA was compared with and without electrocatalysis. In this experiment, each set of four electrodes on a sixteen electrode multiplexed chip was assembled with 20 μL of MB-DNA of varying concentrations. The electrodes were exposed to MB-DNA ranging from 25 μM (500 pmol) down to 250 pM (5 fmol), and allowed to assemble overnight. Once thoroughly washed and backfilled with mercaptohexanol, the electrodes were examined by CV in the absence and chronocoulometry in the presence of electrocatalysis with hemoglobin (25 μM).

The area of the reduction signal from MB-DNA in CV measurements was found to decrease with decreasing amounts of MB-DNA from 500 pmol down to 500 fmol

(Figure 4.9). This represents a dynamic range of only three orders of magnitude; assembly with less than 500 fmol of MB-DNA results in no discernible peaks from MB-DNA reduction in the CV. Upon addition of hemoglobin, the accumulated charge after 10 sec measured by chronocoulometry was examined as a function of the amount of MB-DNA. Electrocatalytic signal amplification with hemoglobin resulted in a significantly enhanced dynamic range, where the decrease in the accumulated charge due to decreasing moles of MB-DNA during monolayer formation was discernible from 500 pmol down to 5 fmol, corresponding to an enhanced dynamic range of five orders of magnitude (Figure 4.9). This enhancement corresponds to a 100-fold improvement in the sensitivity of the device and a dynamic range down to femtomoles.

Implications

In this study, a new means to improve the sensitivity of DNA-modified electrodes by electrocatalysis is presented using the novel electron sink hemoglobin. The use of low density films is integral for current DNA-binding protein and oligonucleotide detection strategies, and electrocatalysis with hemoglobin is shown to be the first compatible means of enhancing the overall signal gain of these systems. Using a new flexible linkage between MB and the DNA, and hemoglobin as an electron sink, DNA-mediated CT in low density DNA films was electrocatalytically amplified. As an electron sink, hemoglobin is effective through physiologically relevant ranges of pH and temperature and, as a compact protein, does not carry out direct reduction at the surface, thus minimizing false positives. Restriction enzyme reaction can be readily detected with high sensitivity, given the duplex accessibility of the low density films and high efficiency of MB reaction with hemoglobin. Most importantly, the sensitivity for MB-DNA reduction was demonstrated to be improved ≥ 100-fold upon electrocatalytic signal amplification. This enhanced sensitivity, which allows a

Figure 4.9. Enhanced sensitivity for MB-DNA reduction upon electrocatalytic signal amplification. Electrodes were incubated with 20 µL of MB-DNA of varying concentrations ranging from 25 µM down to 250 pM, resulting in the electrodes being exposed to 500 pmol down to 5 fmol of MB-DNA during monolayer formation. The surfaces were thoroughly washed and backfilled with mercaptohexanol prior to measurement. Scans were performed in phosphate buffer (5 mM phosphate, 5 mM NaCl, 40 mM $MgCl_2$, 5 mM spermidine, pH 7) with and without hemoglobin (25 µM). The reduction of MB-DNA was quantified from the reductive peak area in the CV (black), without hemoglobin, and the accumulated charge after 10 sec in the chronocoulometry (red), with hemoglobin.

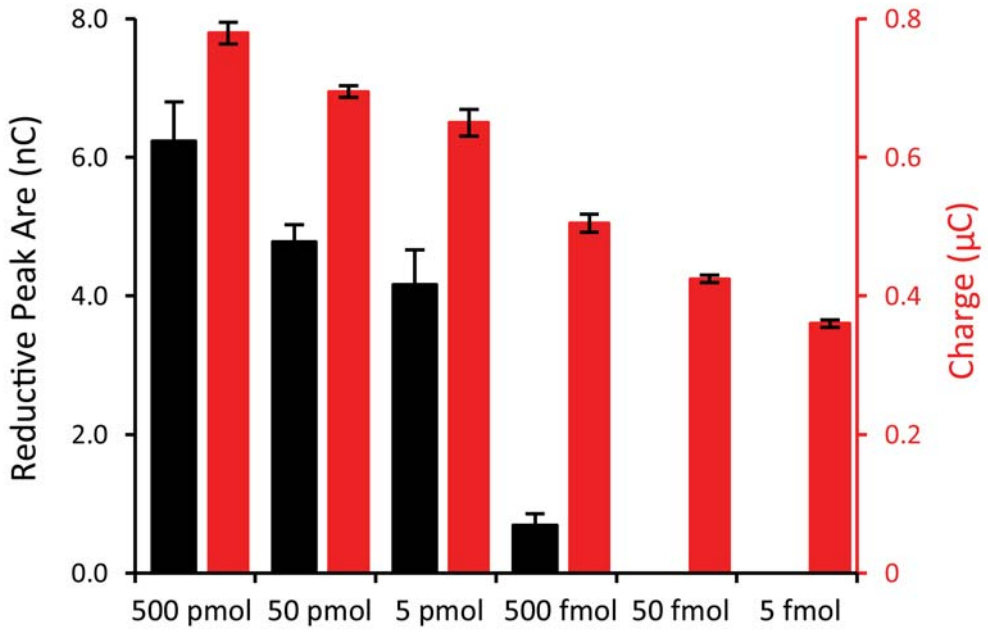

high signal-to-noise ratio from an electrode assembled with femtomoles of MB-DNA, should provide the response necessary to detect the unlabeled cellular markers, both DNA and protein targets, at low concentrations (*19,20*). As electrocatalytic signal amplification with hemoglobin is a general means of enhancing the sensitivity of current DNA-modified electrode technologies, it should be applicable to many DNA electrochemical strategies based on redox reporting of MB.

REFERENCES

1. Kelley, S. O., Barton, J. K. *Bioconjugate Chem.* **1997**, *8*, 31.

2. Kelley, S. O., Boon, E., Barton, J. K., Jackson, N., Hill, M. *Nucleic Acids Research* **1999**, *27*, 4830.

3. Boon, E., Ceres, D., Drummond, T., Hill, M., Barton, J. K. *Nature Biotechnology* **2000**, *18*, 1096.

4. Boon, E., Salas, J., Barton, J. K. *Nature Biotechnology* **2002**, *20*, 282.

5. Gorodetsky, A., Buzzeo, M. C., Barton, J. K. *Bioconj. Chem.* **2008**, *19*, 2285.

6. Slinker, J., Muren, N., Gorodetsky, A., Barton, J. K. *J. Am. Chem. Soc.* **2010**, *132*, 2769.

7. Kelley, S. O., Jackson, N. M., Hill, M. G., Barton, J. K. *Angew. Chem. Int. Ed.* **1999**, *38*, 941.

8. Slinker, J., Muren, N., Renfrew, S., Barton, J. K. *Nature Chemistry* **2011**, *3*, 230.

9. Murphy, C. J., Arkin, M. R., Jenkins, Y., Ghatlia, N. D., Bossmann, S. H., Turro, N. J., Barton, J. K. *Science* **1993**, *262*, 1025.

10. Long Range Charge Transfer in DNA II edited by Schuster, G.B,; Topics in Current Chemistry; Springer-Verlag, Berlin, Heidelberg,; **2004**, 237, 103.

11. Charge Transfer in DNA: From Mechanism to Application edited by Wagenknecht, H.A. (Wiley-VCH Verlag GmbH & Co KGaA, Weiheim, **2005**).

12. Holmlin, E. R., Dandliker, P. J., Barton, J. K. *Angew. Chem. Int. Ed.* **1997**, *36*, 2714.

13. Genereux, J. G., Barton, J. K. *Chem. Rev.* **2010**, *110*, 1642.

14. Hall, D. B., Holmlin, R. E., Barton, J. K. *Nature* **1996**, *382*, 731.

15. Kelley, S. O., Barton, J. K. *Science* **1999**, *283*, 375.

16. Kelley, S. O., Holmlin, R. E., Stemp, E. D. A., Barton, J. K. *J. Am. Chem. Soc.* **1997**, *119*, 9861.

17. Delaney, S., Barton, J. K. *J. Org. Chem.* **2003**, *68*, 6475.

18. Genereux, J. C., Boal, A. K., Barton, J. K. *J. Am. Chem. Soc.* **2010**, *132*, 891.

19. Husale, S., Persson, H., Ozgur, S. *Nature* **2009**, *462*, 1075.

20. Fang, Z. et. al *ACS Nano* **2009**, *3*, 3201.

21. Shao, Z., Liu, Y., Xiao H., Li G. *Electrochem. Commun.* **2008**, *10*, 1502.

22. Xia, F., et al. *J. Am. Chem. Soc.* **2010**, *132*, 14346.

23. Rowe, A., et al. *Anal. Chem.* **2011**, *83*, 9462.

24. Das, J., Yang, H. *J. Phys. Chem. C.* **2009**, *113*, 6093.

25. Boon, E., et al. *J. Angew. Chem. Int. Ed.* **2002**, *41*, 3402.

26. Boon, E., et al. *Langmuir* **2003**, *19*, 9255.

27. Gorodetsky, A., Hammond, W., Hill, M., Slowinski, K., Barton, J. K. *Langmuir* **2008**, *24*, 14282.

28. Anson, F. *J. Phys. Chem.* **1980**, *84*, 3336.

29. Zhang, J., Wang, L., Pan, D., Song, S., Fan, C. *Chem. Commun.* **2007**, *43*, 1154.

30. Lapierre, M., O'Keefe, M., Taft, B., Kelley, S.O. *Anal. Chem.* **2003**, *75*, 6327.

31. Lapierre-Devlin, M., et al. *Nano Letters* **2005**, *5*, 1051.

32. Biagiotti, V., et al *Anal. Bioanal. Chem.* **2012**, *402*,413.

33. Pelossof, G., Tel-Vered, R., Elbaz, J., Willner, I. *Anal. Chem.* **2010**, *82*, 4396.

34. Du, P., Zhou, B., Cai, C. *J. Electroanalytical Chem.* **2008**, *614*, 149.

35. Qian, J., Liu, Y., Liu, H., Yu, T., Deng, J. *Analytical Biochemistry* **1996**, *236*, 208.

36. Ni, F., Feng, H., Gorton, L., Cotton, T. *Langmuir* **1990**, *6*, 66.

37. Ju, H., Shen, C. *Electroanalysis* **2001**, *13*, 789.

38. Xu, J., Zhu, J., Wu, Q., Hu, Z., Chen, H. *Electroanalysis* **2003**, *15*, 219.

39. Liu, H., Lu, J., Zhang, M., Pang, D. *Analytical Sciences* **2002**, *18*, 1339.

40. Du, P., Wu, P., Cai, C. *J. Electroanalytical Chem.* **2008**, *624*, 21.

41. Evtugyn, G., Porfierva, Hianik, T., Cheburova, M., Budnikov, H. *Electroanalysis* **2008**, *20*, 1300.

42. Kuramitz H., et al *Analytical Sciences* **1999**, *15*, 589.

43. Pheeney, C.G., Barton, J. K. *Langmuir* **2012**, *28*, 7063.

CHAPTER 5

Multiplexed Electrochemistry of DNA-bound Metalloproteins

Adapted from Pheeney, C.G., Arnold, A.R., Grodick, M.A., Barton, J.K. (2013) *J. Am. Chem. Soc.* 135, 11869. Arnold, A.R. performed mutagenesis and protein purification for mutant EndoIII as well as circular dichroism. Grodick, M.A. performed protein purification of wild type EndoIII.

ABSTRACT

Here we describe a multiplexed electrochemical characterization of DNA-bound proteins containing [4Fe-4S] clusters. DNA-modified electrodes have become an essential tool for the characterization of the redox chemistry of DNA repair proteins containing redox cofactors, and multiplexing offers a means to probe different complex samples and substrates in parallel to elucidate this chemistry. Multiplexed analysis of EndonucleaseIII (EndoIII), a DNA repair protein containing a [4Fe-4S] cluster and known to be accessible via DNA-mediated charge transport, shows subtle differences in the electrochemical behavior as a function of DNA morphology. The peak splitting, signal broadness, sensitivity to π-stack perturbations, and kinetics were all characterized for the DNA-bound reduction of EndoIII on both closely and loosely packed DNA films. DNA-bound EndoIII is seen to have two different electron transfer pathways for reduction, either through the DNA base stack or through direct surface reduction; closely packed DNA films, where the protein has limited surface accessibility, produce electrochemical signals reflecting electron transfer that is DNA-mediated. Multiplexing furthermore permits the comparison of the electrochemistry of EndoIII mutants, including a new family of mutations altering the electrostatics surrounding the [4Fe-4S] cluster. While little change in the midpoint potential was found for this family of mutants, significant variations in the efficiency of DNA-mediated electron transfer were apparent. Based on the stability of these proteins, examined by circular dichroism, we propose that the electron transfer pathway can be perturbed not only by the removal of aromatic residues but also through changes in solvation near the cluster.

INTRODUCTION

Multiplexed electrodes are emerging as a powerful analytical tool, particularly in the development of electrochemical diagnostics for the detection of pathogens and cancer markers (*1-13*). Multiplexed DNA-modified electrodes have been developed to sense an extensive range of targets including small molecules (*4, 5, 11*), DNA (*6, 10, 11, 12*), RNA (*8, 9, 11*), and proteins (*3, 7, 11-13*). These devices all strive to achieve the same goals of enhanced sensitivity, faster detection times, and tolerance to cell lysates (*5, 9, 12*). Despite variety in the design of these multiplexed DNA-modified electrodes, they all possess the same intrinsic benefits of statistical comparisons and parallel experimentation; these advantages have proven to be essential for the electrochemical characterization of complex systems. Ultimately, these technologies possess ideal attributes for performing the next generation of fundamental electrochemical measurements, as they have been optimized for low variability, real-time monitoring, and complex substrates.

The utility of multiplexed analysis for the fundamental studies of macromolecules was demonstrated in the characterization of charge transport through DNA (*12-14*). One such case is the measurement of ground state DNA-mediated charge transport (DNA CT) through exceptionally long DNA distances up to 34 nm (*14*). DNA CT is the process through which charge is conducted through the π-stack of the DNA base pairs (*15-17*). Both the exquisite sensitivity of even a subtle perturbation in DNA stacking (*18,19*) and the shallow distance dependence (*14,15*) of DNA CT have been characterized using DNA-modified electrodes affixed with a redox-active moiety at the distal end of the duplex. Multiplexing these DNA-modified electrodes onto a single device was crucial in establishing that the electrochemical signal was generated via DNA CT over such long molecular distances and

that the π-stack of the DNA was well stacked and in a biologically relevant conformation (*14*).

Here we utilize multiplexed technology to investigate the electrochemistry of DNA repair proteins containing [4Fe-4S] clusters (Figure 5.1). DNA-modified electrodes have become a necessary tool to investigate the electrochemistry of the iron-sulfur cofactor of many DNA repair proteins, including EndonucleaseIII (EndoIII), MutY, UDG, SoxR, and XPD, towards identifying the *in vivo* relevance for this redox activity (*20-24*). Upon DNA-binding of EndoIII, the $3^+/2^+$ redox couple of its [4Fe-4S] cluster has been shown to shift negative ~ 200 mV compared to freely diffusing protein, to approximately 80 mV versus NHE (*25*). Thus binding of the DNA polyanion brings the $3^+/2^+$ redox potential of the [4Fe-4S] cluster into a physiologically relevant range. Moreover, disease related mutants show deficiencies in DNA CT through their weaker electrochemical signals. Interestingly, DNA–binding proteins involved in genome maintenance have increasingly been found to contain [4Fe-4S] clusters (*26-29*). We have proposed that the redox chemistry of these [4Fe-4S] clusters are critical as a first step in the search mechanism used by DNA repair proteins to redistribute to the vicinity of DNA damage (*21, 30*). The proposed model hinges on the ability of these [4Fe-4S] cluster proteins to electronically couple to the π-stack of DNA in order to perform efficient searching of the genome facilitated by DNA CT. This efficient DNA-mediated CT between repair proteins seems to depend on the similar reduction potentials of their clusters. The consistent DNA-bound midpoint potential of these various proteins containing [4Fe-4S] clusters has been of particular interest. In this work, we investigate how the electrostatics of the protein fold, in addition to binding of the DNA polyanion, may tune the reduction potential of the cluster. Thus it becomes important to characterize the DNA-bound electrochemistry of these proteins containing [4Fe-4S] clusters in a quantitative manner that allows for direct side-by-side comparison of potentials and couplings through multiplexing.

Figure 5.1. Schematic depicting the versatility of multiplexed analysis for the investigation of metalloprotein electrochemistry. Our multiplexed devices are composed of sixteen electrodes that are divisible into four separate quadrants of four electrodes, having the capability of producing four distinct experimental conditions on a single Au surface. This assembly allows for facile comparisons of the electrochemical signal from various DNA-bound proteins across varying DNA substrates and morphologies.

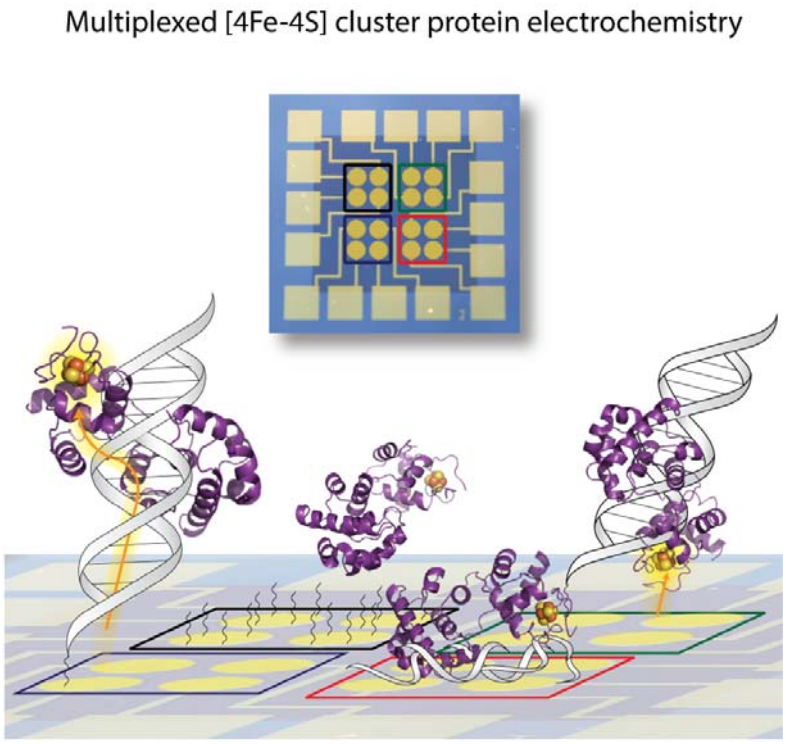

MATERIALS AND METHODS

Oligonucleotide preparation

All DNA substrates were synthesized on a 3400 Applied Biosystems DNA synthesizer with all phosphoramidites and reagents purchased from Glen Research. The sequences of the DNA substrates used were 5′ - HS –$(CH_2)_6$– AGT ACA GTC ATC GCG - 3′ for the thiol strand and 3′ - TCA TGT CAG TAG CGC - 5′ for the complement strand. Additional complements were prepared that yielded either a TC mismatch or an abasic site at the position of the underlined adenine. Both the complement and thiol-modified DNA were purified through standard procedures as previously reported (*13*). All single-stranded DNA was purified by high pressure liquid chromatography (HPLC) using a reverse phase PLRP-S column, purchased from Agilent. The identity of the oligonucleotides was confirmed by matrix-assisted laser-desorption ionization – time of flight (MALDI-TOF) mass spectrometry. The thiol-modified single stranded DNA was reduced with 100 mM dithiothreitol (Sigma) in Tris buffer (50 mM Tris HCl, 50 mM NaCl, pH 8.4) for 40 min and purified by size exclusion chromatography (Nap5 Sephadex G-25, GE Healthcare) as well as reverse phase HPLC. Single-stranded DNA stocks were then desalted by precipitation in ethanol and re-suspended in phosphate buffer (5.0 mM phosphate, 50 mM NaCl, pH 7.0). Equimolar amounts of single-stranded stocks were combined based on quantification by UV-Visible spectroscopy. The extinction coefficients at 260 nm from the IDT SciTools were used for the quantification of the single-stranded DNA stocks. All DNA solutions were then thoroughly deoxygenated with argon and annealed by heating to 90 ºC followed by a slow cooling to ambient temperature over 90 min.

Site-Directed Mutagenesis

E200K, Y205H and K208E EndoIII mutants were prepared using a pET11 vector containing the *nth* gene with N-terminal ubiquitin and hexahistidine tags (*22*) and a Quikchange II-E Site-Directed Mutagenesis Kit (Stratagene). Y82A EndoIII was prepared previously (*22*). Primers were purchased from Integrated DNA Technologies and primer sequences are provided in Table 5.1. All mutagenized plasmids were sequenced (Laragen) to confirm the desired sequences.

Protein Overexpression and Purification

A stock of BL21star-(DE3)pLysS containing a pET11-ubiquitin-His6-*nth* construct was used to inoculate a 100 mL culture of LB containing 100 μg/mL of ampicillin and 35 μg/mL of chloramphenicol. This culture was grown overnight at 37 °C with shaking. Then, 1 mL of the overnight culture was used to inoculate each of four 1 L cultures of LB containing the same amount of ampicillin and chloramphenicol as the overnight culture. The 1 L cultures were shaken at 37 °C until the OD_{600} reached ~0.6 - 0.8. Enough isopropyl β-D-1-thiogalactopyranoside (IPTG) was then added to bring the total concentration of IPTG to 300 μM. The cultures were subsequently shaken at 150 rpm for ~ 3.5 hr at 30° C. The cells were collected by centrifugation at 5,500 rpm for 15 min, flash-frozen, and stored at - 80 ºC. All subsequent steps were carried out at 4 °C or on ice. On the day of the purification the pellet was re-suspended in 250 mL of Buffer A (20 mM sodium phosphate, pH 7.4, 250 mM NaCl, 5 mM DTT, 5 % glycerol, DNase (Roche), RNase (Roche), and EDTA-free protease inhibitor cocktail tablets (Roche)). The re-suspended cells were lysed via microfluidization. The cell lysate was clarified by centrifugation at 17,000 g for 30 min. Enough NaCl was added to the resulting supernatant to bring the NaCl concentration to 500 mM. The supernatant was then loaded onto a Histrap HP column (GE Healthcare) that had been equilibrated with buffer B (20 mM sodium phosphate, pH 7.4, 500 mM NaCl, 1 mM DTT).

Table 5.1. Primer Sequences for Site-Directed Mutagenesis.

Mutation	Primer
Y205H	5'- TGT GAA CAC AAA GAG AAA GTT GAC ATC TGA GGA TCC GGC TGC TAA C -3' (Forward) 5'- GTT AGC AGC CGG ATC CTC AGA TGT CAA CTT TCT CTT TGT GTT CAC A -3' (Reverse)
E200K	5'- GCC CCG CTG TGG CTC TTG TAT TAT TAA AGA TCT TTG TGA ATA C -3' (Forward) 5'- GTA TTC ACA AAG ATC TTT AAT AAT ACA AGA GCC ACA GCG GGG C -3' (Reverse)
K208E	5'- GTG AAT ACA AAG AGG AAG TTG ACA TCT GAG GAT CCG GCT GCT AAC -3' (Forward) 5'- GTT AGC AGC CGG ATC CTC AGA TGT CAA CTT CCT CTT TGT ATT CAC -3' (Reverse)

After washing with buffer B, EndoIII was eluted using a gradient from 0-100 % buffer C (20 mM sodium phosphate, pH 7.4, 500 mM NaCl, 500 mM imidazole, 1 mM DTT) over 20 column volumes. A yellow band that eluted at ~ 100 mM imidazole was collected. This imidazole-containing buffer was then immediately exchanged into buffer D (20 mM sodium phosphate, pH 7.4, 500 mM NaCl, 0.5 mM EDTA, and 20 % glycerol) using a HiPrep 26/10 desalting column (GE Healthcare). The protein solution, now in buffer D, was concentrated down to ~ 5 mL using 10,000 MWCO Amicon Ultra-15 centrifugation filter units (Millipore) and was loaded onto a HiLoad Superdex 16/600 75 pg size exclusion column (GE Healthcare) that had been equilibrated with the protein storage buffer (20 mM sodium phosphate, pH 7.4, 100 mM NaCl, 0.5 mM EDTA, 20 % glycerol). A clean peak that eluted after approximately 50 - 55 mL of buffer had passed through the column was collected and concentrated to achieve a final concentration of ~ 100 μM as quantified using an ε_{410} of 17,000 $M^{-1}cm^{-1}$ (*30*). The protein was then aliquoted, flash-frozen in liquid nitrogen, and stored at - 80 °C. The approximate yield was 6 mg/L. The purity of the protein was determined to be > 95% as analyzed by SDS-PAGE (data not shown).

Enzymatic assay for Glycosylase Activity.

Glycosylase activity was determined for each mutant (Y205H, K208E, and E200K) compared to wild type EndoIII based on previously established methods (*22*). Protein samples (1 μM) were incubated for 15 min at 37 ºC with 5′ radiolabeled 35-mer duplex DNA modified with a 5-hydroxy-uracil. Reactions were quenched by adding 1 M NaOH to a final concentration of 100 mM NaOH. The glycosylase activity was determined as the fraction of 14-mer product observed relative to the total quantity of DNA and the percent activity compared to WT (Figure 5.2).

Figure 5.2 Enzymatic assay for EndoIII glycosylase activity. Glycosylase activity was determined for each mutant (Y205H, K208E, and E200K) compared to wild type EndoIII based on previously established methods (*22*). For this assay, protein samples (1 μM) were incubated for 15 min at 37 ºC with 5′-32P-radiolabeled 35-mer duplex DNA (100 nM) modified with 5-hydroxy uracil, a substrate for EndoIII, in 10 mM Tris HCl, 1 mM EDTA, 50 mM NaCl, pH 7.6. Reactions were then quenched by adding 1 M NaOH to a final concentration of 100 mM NaOH, which was dried, and electrophoresed through 20% denaturing PAGE at 90 W for 1.5 hr. Glycosylase activity of EndoIII results in the appearance of the 14-mer cleavage product in the denaturing gel. The glycosylase activity was determined as the fraction of 14-mer product observed relative to the total quantity of DNA and the percent activity compared to WT (purple) was then calculated for Y205H (green), K208E (blue), and E200K (red). Two control lanes containing the 35-mer duplexed DNA, yet lacking the enzymatic protein, were either untreated or treated with the 1 M NaOH.

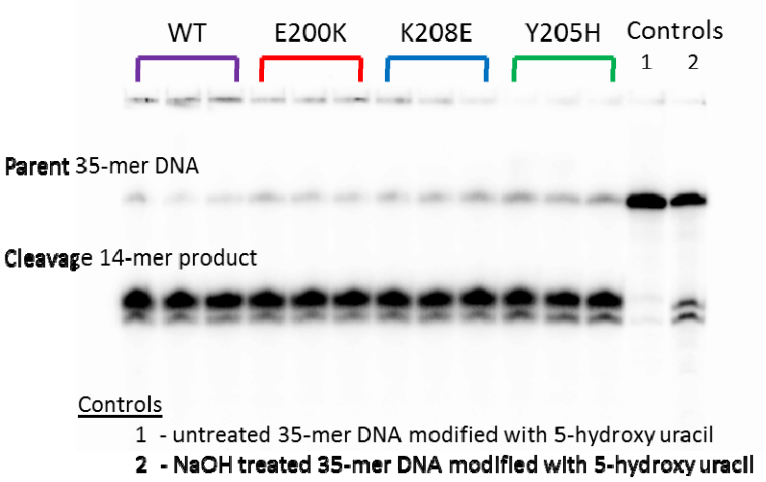

Mutant	% Activity Compared to WT
E200K	98.0 ± 1.5
K208E	95.8 ± 1.8
Y205H	91.6 ± 2.1

Multiplexed Chip Fabrication

Multiplexed chips consisting of sixteen gold electrodes were prepared using standard photolithography techniques as adapted from previously established protocols (*13, see Appendix III for further details*). Photoresist was used to pattern nine 1-inch-by-1-inch chips on 525 μm thick silicon wafers (SiliconQuest) that had a thermal oxide layer grown to a thickness of roughly 4,000 Å to insulate the wafer. A titanium adhesion layer (3 nm) followed by a gold layer (100 nm) was deposited using an electron beam evaporator without breaking the vacuum between depositions. The metal lift-off was performed directly after metal deposition using Remover PG (MicroChem) heated to 60 °C for 1 hr. The wafers were then dehydrated by baking at 180 °C for at least 2 hr and an insulating SU8 layer (3 μm) was coated on the wafer. This SU8 layer was patterned such that the working electrodes and contact pads were left exposed, yet the connective wires were covered to define a controlled working electrode area (2 mm^2). The SU8 was cured with a final hard bake at 150 °C for 15 min. The wafer was then cleaved into individual chips (Dynatex Scriber/Braker) to prevent any scratching of the exposed working electrode surfaces.

DNA-modified Electrode Assembly

Single electrode experiments were performed with a low-volume constrained Au(111) on mica surface (Molecular Imaging), as previously established (*20*). Multiplexed electrode experiments were performed with the sixteen-electrode chips divided into four quadrants of four electrodes each (*13*). Multiplexed chips were cleaned in acetone and isopropanol as well as ozone-cleaned for 5 min at 20 mW immediately prior to the assembly into a holder and the exposure to thiol-modified DNA. The cleaned chip was then assembled in a polycarbonate holder used to position the chip. A rubber gasket and acrylic clamp was used to define the four quadrants and create a common central well. The rubber

Buna N gasket (0.020″ thick, unless otherwise indicated) and clamp are manufactured by SAS Industries and Xcentric, respectively. A fresh gasket and clamp was used for each experiment to prevent any cross contamination between experiments.

Duplex DNA (20 µl of 25 µM) was placed in each quadrant of a multiplexed chip and left to self-assemble overnight (16 - 24 hr) in a humid environment. To ensure efficient monolayer formation, thiol-modified DNA was used within two weeks of the dithiothreitol reduction. Loosely packed DNA films were assembled in the absence of $MgCl_2$ while closely packed DNA films were assembled with the addition of 100 mM $MgCl_2$. Once DNA films were assembled and thoroughly washed with phosphate buffer, the electrodes were backfilled with 1 mM 6-mercaptohexanol (MCH) for 45 min in phosphate buffer with 5 % glycerol. Background scans were acquired with common running buffers exposed to the electrodes. An initial background scan is acquired in phosphate buffer (5 mM phosphate, 50 mM NaCl, pH 7.0) followed by a subsequent scan in spermidine buffer (5 mM phosphate, 50 mM NaCl, 40 mM $MgCl_2$, 5 mM spermidine, pH 7.0).

Protein Electrochemical Measurements

Electrochemical measurements were performed with a CHI620D Electrochemical Analyzer and a 16-channel multiplexer from CH Instruments. A three-electrode setup was used with a common Pt auxiliary and a quasi Ag/AgCl reference electrode (Cypress Systems) placed in the central well of the clamp. Cyclic voltammetry data were collected at 100 mV/s over a window of 0.1 mV to -0.4 mV versus Ag/AgCl unless otherwise indicated. After background scans, EndoIII samples in phosphate buffer (20 mM sodium phosphate, 100 mM NaCl, 0.5 mM EDTA, 20 % glycerol, pH 7.4) were added to the central well or separated quadrants (120 µL total for the four quadrants), ranging in concentrations from 30 – 90 µM quantified using the absorbance of the [4Fe-4S] cluster at 410 nm (ε = 17,000 $M^{-1}cm^{-1}$) (*30*). EndoIII was allowed to incubate on the multiplexed chip for up to

12 hr and monitored over time. The chip was stored in a humid environment between subsequent scans to prevent solution evaporation and concentration consistency over time.

Circular Dichroism Thermal Denaturation

For protein samples (5 μM), the ellipticity at 223 nm (the largest difference between native and denatured protein) was measured as a function of increasing temperature (20 °C to 60 °C) using a Model 62A DS circular dichroism spectrometer (AVIV). All data shown are the average of at least duplicate measurements. Measured ellipticity was converted to fractional change in ellipticity by assigning the native protein a value of 0 and the fully denatured protein a value of 1. In order to extract melting temperature values, data were fit using a non-linear least-squares regression to a simple two-state unfolding model using the Equation 5.1 (*32*). Reported errors in the thermal denaturation values are derived from this fitting.

RESULTS

Multiplexed electrochemistry of EndoIII

The electrochemical behavior of the [4Fe-4S] cluster of EndoIII incubated on loosely packed DNA films, assembled in the absence of $MgCl_2$, was first compared between individual and multiplexed electrode assemblies. A reversible signal for the [4Fe-4S]-cluster of EndoIII, with the ratio of the reduction and oxidation currents being near unity, at a mid-point potential of 80 ± 3 mV vs. NHE was observed on both single electrode and multiplexed assemblies (Figure 5.3). The signal size for the redox couple of EndoIII depended on incubation time and concentration on both assemblies; this behavior, as well as the mid-point potential, is consistent with previously established results for EndoIII on DNA-modified electrodes (*22*). The consistency across all sixteen multiplexed electrodes was comparable

Equation 5.1. Circular dichroism (CD) thermal denaturation data was fit using a non-linear least-squares regression to a simple two-state unfolding model (*32*), where Y is the fractional ellipticity, T is the temperature in Celsius, ΔH_m is the enthalpy at the unfolding transition, T_m is the melting temperature (°C), R is the ideal gas constant, while m_n and y_n describe the pre-transition (native protein) slope and y-intercept and m_d and y_d describe the equivalent values post-transition (denatured protein). Reported errors in T_m values are derived from this fitting.

$$Y = \frac{(y_n + m_n T) + (y_d + m_d T)\exp\left(\frac{\Delta H_m}{R}\left(\frac{1}{T_m} - \frac{1}{T}\right)\right)}{1 + \exp\left(\frac{\Delta H_m}{R}\left(\frac{1}{T_m} - \frac{1}{T}\right)\right)}$$

Figure 5.3. (*Left*) The signals generated after incubation of loosely packed DNA-modified electrodes with EndoIII (30 μM) in phosphate buffer (20 mM sodium phosphate, 100 mM NaCl, 0.5 mM EDTA, 20% glycerol, pH 7.4) were used to directly compared the single- (solid) and multiplexed (dashed) electrochemical assemblies. The cyclic voltammetry (scan rate = 100 mV/s) was normalized, based on the capacitance at 0.3 mV vs NHE, so relative signal sizes could be compared across platforms. (*Right*) The variability of the EndoIII signal, under the same conditions, across all sixteen electrodes (light solid line) of a single multiplexed device was within 3.5% of the average CV for the device (dark dashed line).

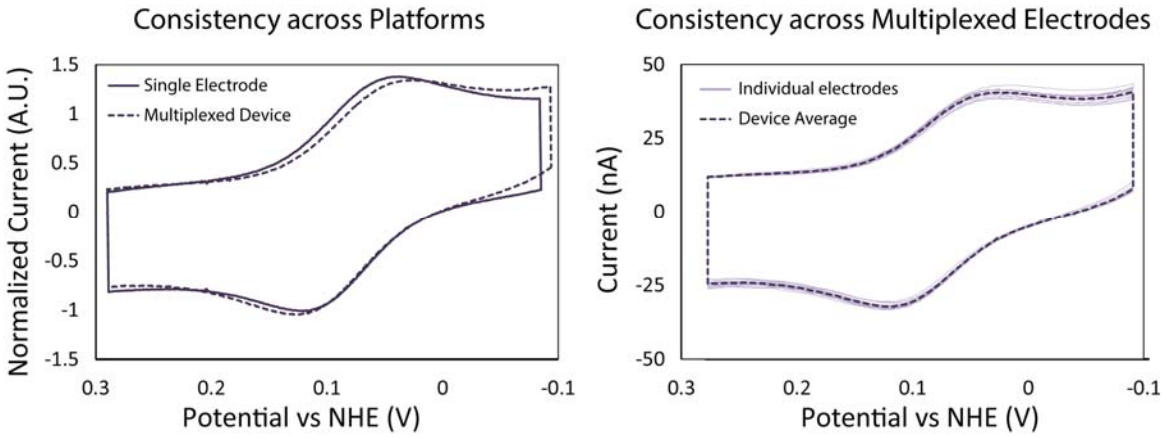

to that seen with previous multiplexed DNA-modified electrodes and showed at most a 3.5 % deviation in signal size (Figure 5.3) (*13*). The analogous experiment run on individual single electrodes would yield dramatically higher variability on the order of 20 - 40 % (*22*).

Due to the modular nature of the multiplexed electrode assembly, the thickness of the rubber gasket used to seal the central well was varied to increase accessibility to the electrodes. Background scans and EndoIII signal sizes were compared for gaskets 0.064″, 0.032″, and 0.020″ thick. Oxygen contributions in the background scans, likely caused by trapped oxygen in close proximity to the electrode surface, were decreased drastically with the use of the thinner gaskets, yielding much more uniform CVs and increased EndoIII signal size (Figure 5.4). Overall, the most exposed electrodes produced a featureless background scan, resulting in a 0.020″ thick Buna N gasket being utilized for all subsequent experiments.

EndoIII on differing DNA monolayers.

The effect of DNA substrates and film morphology on the EndoIII signal was next investigated. Allowing the self-assembly of DNA monolayers to form in the presence of $MgCl_2$ dramatically affects the film packing and ultimately the density of the DNA monolayer formed (*33*). In the presence of $MgCl_2$, the negative charge of the DNA phosphate backbone is screened, allowing neighboring duplexes to more closely associate and self-assemble into a tightly packed DNA monolayer.

Incubation of EndoIII on DNA-modified electrodes assembled with duplex DNA (dsDNA) was found to produce a redox couple with the same mid-point potential as previously described (80 ± 3 mV vs. NHE) regardless of DNA film morphology, while single-stranded DNA (ssDNA) monolayers showed cyclic voltammograms that were relatively featureless compared to background scans, even after 8 hr of protein incubation (Figure 5.5). As both the underlying gold surface and the protein solution were common

Figure 5.4. Cyclic voltammetry (scan rate = 100 mV/s) of EndoIII (30 μM) incubated on closely packed well-matched duplex DNA monolayers acquired in phosphate buffer (20 mM sodium phosphate, 100 mM NaCl, 0.5 mM EDTA, 20 % glycerol, pH 7.4) are presented. Three different thicknesses for the Buna N gasket, utilized during the multiplexed chip assembly, were tested: 0.064″ (green), 0.032″ (red), and 0.020″ (red). With decreasing gasket thickness the signal generated from EndoIII is shown to increase while the background contributions decrease. Inset: Background signals acquired prior to the addition of EndoIII in spermidine buffer (5 mM phosphate, 50 mM NaCl, 40 mM $MgCl_2$, 5 mM spermidine, pH 7.0).

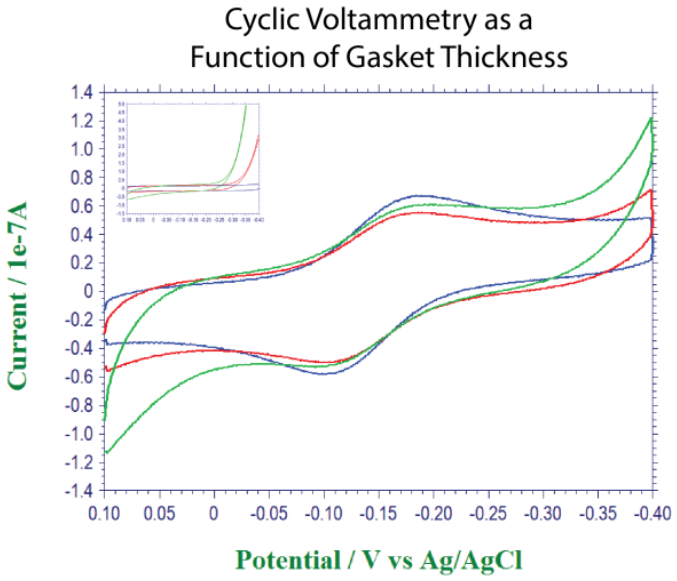

Figure 5.5. The electrochemistry of EndoIII on DNA-modified electrodes was determined as a function of the underlying DNA film morphology. DNA monolayers were allowed to self-assemble over 16 - 24 hr either with or without 100 mM $MgCl_2$ to form either closely (purple) or loosely (blue) packed DNA monolayers. All morphologies were directly compared on the same multiplexed device so the differences in the EndoIII (60 μM) redox signal could be resolved. Cyclic voltammetry scans (scan rate = 100 mV/s) were compared in phosphate buffer (20 mM sodium phosphate, 100 mM NaCl, 0.5 mM EDTA, 20% glycerol, pH 7.4) and the peak splitting and signal size were both quantified. Single-stranded DNA monolayers (grey) were prepared and shown to not produce a DNA-bound EndoIII signal.

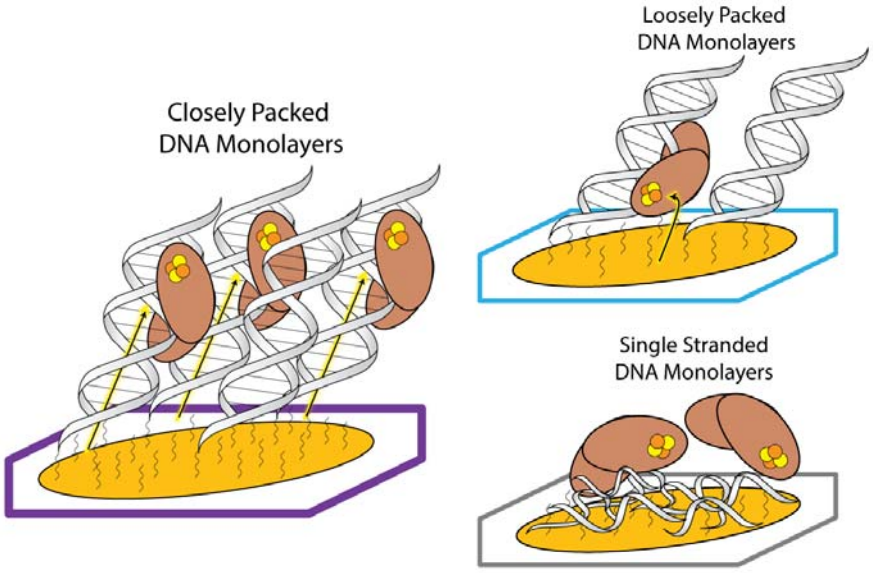

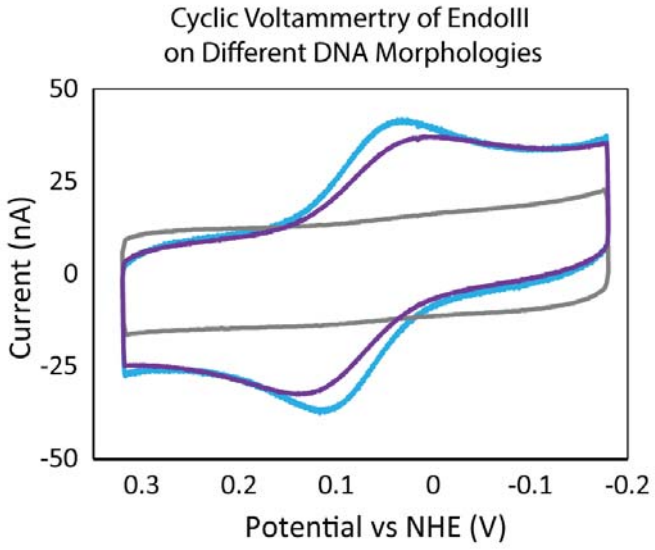

across all electrodes, this appearance of a reversible redox couple from EndoIII on the dsDNA monolayers but not on the ssDNA films indicates that the signal generated from EndoIII is dependent on binding to duplex DNA. Moreover, since the DNA-bound redox potential for EndoIII is not observed on these ssDNA-modified electrodes, these ssDNA-modified electrodes provide a useful control against surface contaminants.

The DNA-bound signal of EndoIII was then compared on DNA-modified electrodes assembled with different morphologies. The peak splitting for the $3^+/2^+$ redox couple of the [4Fe-4S] cluster of EndoIII was found to be dependent on monolayer morphology, while the mid-point potential remained unaltered. The consistency of the mid-point potential between the surface morphologies indicates that EndoIII is in the same electrostatic environment, bound to duplex DNA, regardless of the monolayer morphology. The closely and loosely packed DNA monolayers show peak splittings of 88 ± 4 mV and 64 ± 2 mV respectively (Figure 5.5). In addition to the increase in peak splitting, there is also a broadening of the signal observed upon switching to the more closely packed DNA films. Increases in the peak splitting and broadening of the redox couple are both indicative of decreases in the rate of electron transfer and the homogeneity of the electrochemical process (*34*). These two characteristics, an increase in peak splitting and heterogeneity, have previously been seen as characteristics of a redox-active moiety on DNA-modified electrodes being reduced by DNA CT (*35*).

DNA-mediated electrochemistry of EndoIII

The mechanism of electron transfer to the [4Fe-4S] cluster in EndoIII was next investigated on both loosely and closely packed dsDNA-modified electrodes. DNA-mediated reduction is exceptionally sensitive to even subtle perturbations to the intervening π-stack (*18, 19*). Therefore the yield of [4Fe-4S] cluster reduction was examined after introducing a single perturbation site into the DNA duplexes self-assembled on the electrodes. Either a

single thymine-cytosine mismatch (TC) or an abasic site (Ab) were incorporated into thiol-modified dsDNA near the electrode surface to prevent EndoIII binding to the π-stack below the perturbation site, as EndoIII binds non-specifically to non-substrate DNA. The dsDNA stocks for the well-matched (WM), TC, and Ab sequences were all quantified and annealed using the same thiol-modified ssDNA stock. This consistency of the thiol strand avoids any variability caused by the efficiency of monolayer formation due to the reactivity of the thiol-modifier. These dsDNA sequences, as well as a ssDNA control, were then assembled on a multiplexed chip.

The reduction signal for the [4Fe-4S] cluster of EndoIII was characterized across these different DNA substrates on both loosely and closely packed films (Figure 5.6). When these DNA substrates were assembled in the presence of $MgCl_2$, producing closely packed DNA monolayers, the reduction signal of EndoIII was attenuated upon introducing single base pair lesions. The WM, TC, and Ab dsDNA monolayers gave signal sizes of 56 ± 1 nA, 42 ± 1 nA, and 41 ± 4 nA respectively after EndoIII incubation (60 μM for 8 hr), resulting in an average signal attenuation of 24 ± 1% and 26 ± 2% upon incorporating a TC mismatch or an abasic site, respectively (Figure 5.6). This attenuation in the reduction signal due to the incorporation of perturbations to the π-stack support the assignment of the electrochemical signal from EndoIII observed on closely packed DNA films being mediated by DNA CT. Conversely, when the same set of DNA substrates was compared using loosely packed DNA monolayers, there was no significant difference in the reduction signal observed with the introduction of these perturbations. The loosely packed DNA monolayers of WM, TC mismatched, and Ab DNA produced signal sizes of 45 ± 0.3 nA, 42 ± 1 nA, and 44 ± 1 nA respectively, which yield a p-value > 0.05 when compared using a one-tailed t-test, do not display statistically significant signal attenuation as compared to EndoIII bound to the closely packed DNA monolayer. This lack of signal attenuation with the incorporation of perturbation to the π-stack indicates that the DNA-bound signal of EndoIII is not mediated

Figure 5.6. The degree of signal attenuation, induced by a single perturbation to the π-stack, for both closely and loosely packed DNA monolayers was investigated. (*Left*) Schematic of multiplexed devices prepared with well-matched (blue), TC mismatched (red), and abasic site (green) duplexed DNA, and a single-stranded control (black).The sequences are indicated above. (*Right*) The reductive signals from DNA-bound EndoIII in phosphate buffer (20 mM sodium phosphate, 100 mM NaCl, 0.5 mM EDTA, 20% glycerol, pH 7.4) were quantified for DNA monolayers assembled in both the presence (dark) and absence (light) of 100 mM $MgCl_2$ yielding closely and loosely packed DNA, respectively. The percent signal attenuations of the TC mismatch and abasic site were determined based on the average signal size, across all four electrodes in a quadrant, compared to that of well-matched DNA. The signals generated from closely packed DNA-films displayed distinct attenuation upon introducing either a mismatch or abasic site, while the signals from loosely packed DNA-films did not display this sequence dependence.

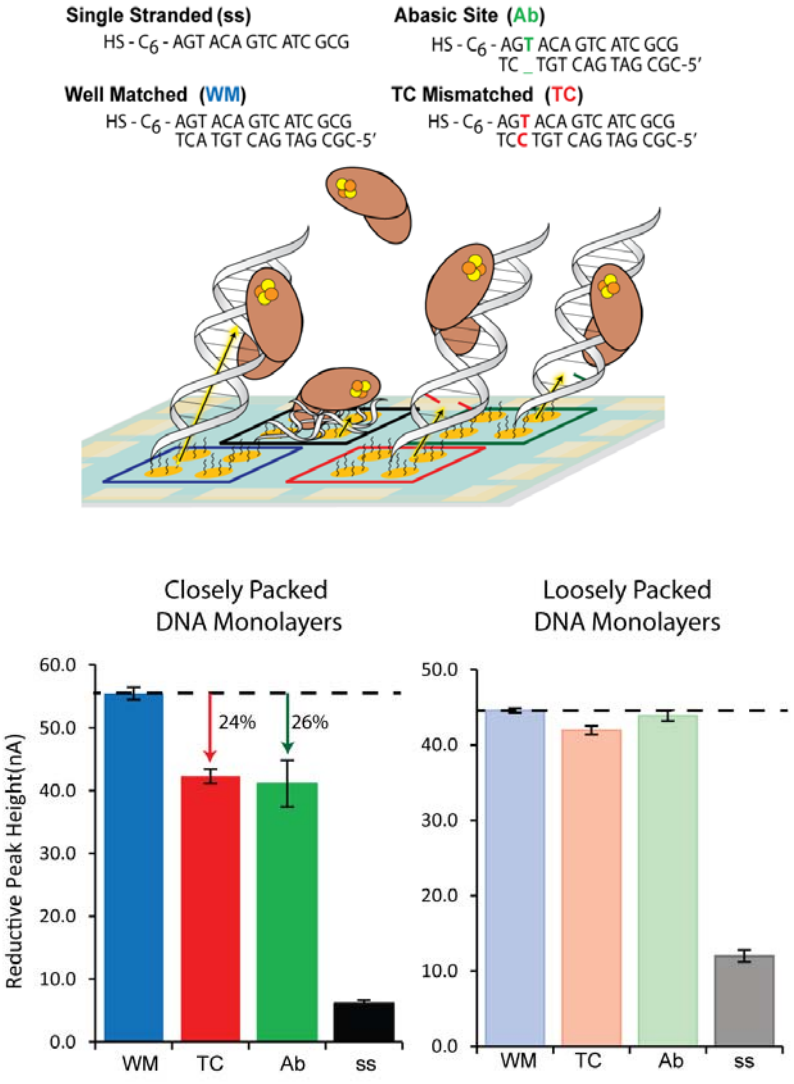

by electron transfer through the π-stack in loosely packed DNA monolayers.

Kinetics of EndoIII reduction

The kinetics of EndoIII reduction was assessed on these two different dsDNA morphologies to explore further the mechanistic differences in the electron transfer pathways. In addition to the peak splitting, the EndoIII reduction on loosely and closely packed DNA monolayers was found to differ in the signal accumulation, both as a function of scan rate as well as incubation time. For a diffusion rate-limited process this signal accumulation increased linearly as a function of the square root of the scan rate (*34*). The [4Fe-4S] cluster signal of EndoIII was measured over ten different scan rates, ranging from 10 mV/s to 200 mV/s, on both loosely and closely packed dsDNA films and plotted as a function of the square root of the scan rate, $v^{1/2}$ (Figure 5.7). In the case of loosely packed dsDNA films, the current was found to be linear with respect to $v^{1/2}$, as previously established for the diffusion rate-limited reduction of DNA-bound [4Fe-4S] cluster proteins on this dsDNA film morphology (*24*). The same protein solution on the same multiplexed chip displayed nonlinear behavior on closely packed dsDNA films. More quantitative approaches for determining the rate of electron transfer, such as the Laviron analysis, were not possible due to the degree of heterogeneity of the observed electrochemical signals. However, the total signal accumulation for the reduction of EndoIII as a function of time on both these dsDNA film morphologies displayed the same trend; loosely versus closely packed dsDNA films accumulated signal linearly and nonlinearly respectively, over time (Figure 5.8). This further supports the finding that only the signal observed on the loosely packed dsDNA films is limited by diffusion.

Multiplexed characterization of DNA CT proficiency

Since the electrochemical signal for the [4Fe-4S] cluster of EndoIII is generated

Figure 5.7. Kinetic analysis of the signal generated from EndoIII on differing DNA film morphologies is indicated. Cyclic voltammetry (scan rates ranging from 10 mV/s to 200 mV/s) of EndoIII were obtained in phosphate buffer (20 mM sodium phosphate, 100 mM NaCl, 0.5 mM EDTA, 20% glycerol, pH 7.4) for both closely (solid) and loosely (outlined) packed DNA monolayers. The reductive peak height for both morphologies on the same multiplexed device was quantified and plotted as a function of the square root of the scan rate, $v^{1/2}$. The non-linearity of the signal from closely packed DNA films indicates that the signal is not diffusion rate limited.

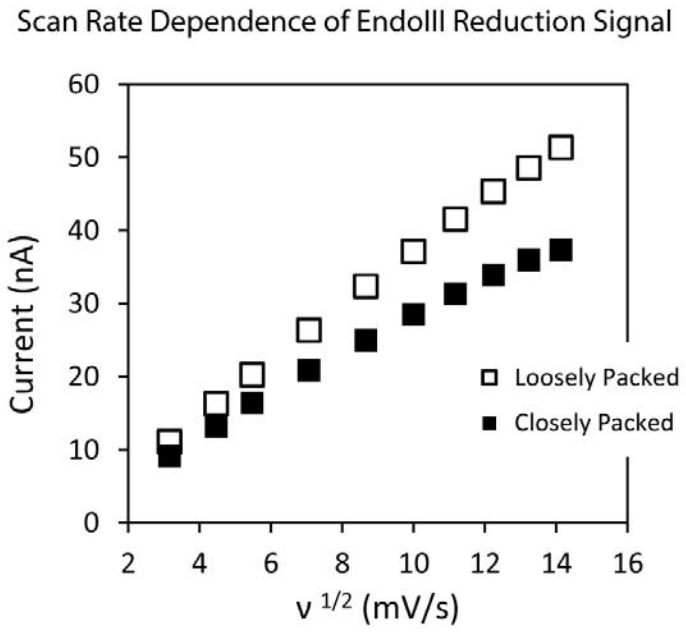

Figure 5.8. Signal accumulation of EndoIII as a function of time at various concentrations on both closely and loosely packed dsDNA monolayers formed in the presence and absence of 100 mM $MgCl_2$ during assembly, respectively. The peak signal current was quantified based on the reductive signal of EndoIII in the cyclic voltammaogram (scan rate = 100 mV/s) acquired in phosphate buffer (20 mM sodium phosphate, 100 mM NaCl, 0.5 mM EDTA, 20% glycerol, pH 7.4).

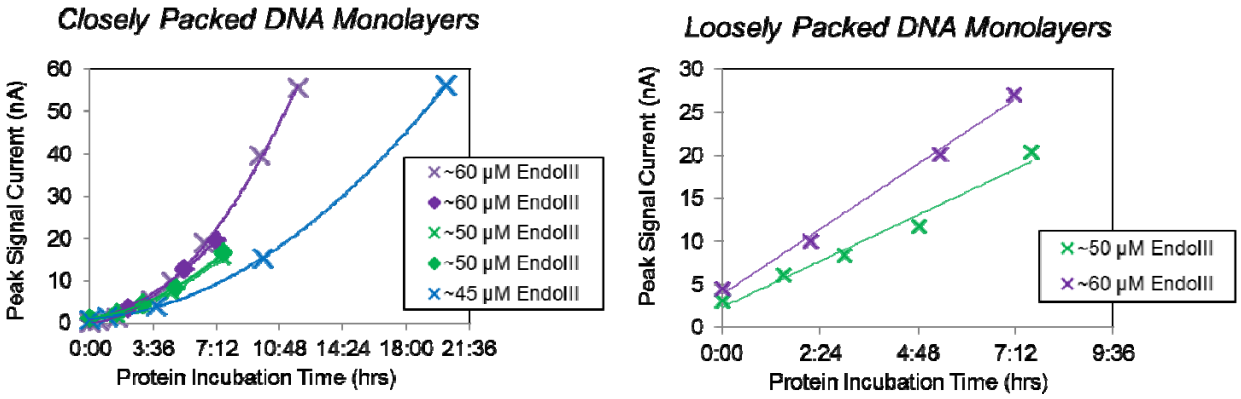

primarily via DNA CT on closely packed dsDNA films, the DNA CT proficiency of a known disease-related mutant, Y82A, was compared to that of wild type EndoIII using this morphology. The Y82A mutant of EndoIII has previously been shown to be DNA CT deficient compared to wild type EndoIII using individual DNA-modified electrodes (*21, 22*). The DNA CT deficiency has been attributed to disruptions in the electron transport pathway from the DNA π–stack to the [4Fe-4S] cluster due to mutation of the aromatic tyrosine residue, located in close proximity to the π–stack based on the crystal structure of the wild type protein bound to DNA (*36*). The quantification of the extent of DNA CT proficiency for [4Fe-4S] cluster proteins has proven to be challenging due to the variability between individual DNA-modified electrodes.

Multiplexed characterization of the wild type (WT) and Y82A mutant EndoIII allows for a more quantitative comparison of the extent of coupling with the DNA-modified electrode. Multiplexed chips were assembled with half well-matched and half TC-mismatched closely packed dsDNA films. Orthogonally, WT and Y82A EndoIII were added to two quadrants each, such that each protein was incubated on both well-matched and TC-mismatch DNA-modified electrodes (Figure 5.9). Samples of equal protein concentration were prepared based on the absorption at 410 nm, reflecting the [4Fe-4S] cluster concentration for each protein (~ 70 μM). Using this multiplexed configuration, the reduction of the [4Fe-4S] cluster in both WT and Y82A mutant EndoIII was confirmed to have been generated via DNA CT, since both proteins displayed signal attenuation (23 ± 3 %) upon introducing a TC mismatch. Furthermore, the signal from Y82A was 72 ± 5 % attenuated compared to that of wild type EndoIII. Taken together with the attenuation upon mismatch incorporation, the observation of decreased DNA-mediated signal intensity verifies that the Y82A mutation results in a deficiency in DNA CT. Circular dichroism (CD) thermal denaturation confirmed that the stability of the protein fold was relatively unaltered upon introducing the Y82A mutation (Figure 5.9). Upon fitting the thermal denaturation curves to

Figure 5.9. Comparison of the electrochemical properties and stability of wild type EndoIII and a Y82A mutant. (*A*) Multiplexed electrode assembly schematic where electrodes are assembled with 100 mM $MgCl_2$, with either well-matched (blue) or TC mismatched (red) duplexed DNA, and then incubated with either wild type (purple) or Y82A (orange) EndoIII (90 μM, based on absorbance at 410 nm). (*B*) Cyclic voltammetry (scan rate = 100 mV/s) in phosphate buffer (20 mM sodium phosphate, 100 mM NaCl, 0.5 mM EDTA, 20% glycerol, pH 7.4) are indicated for both wild type and Y82A EndoIII on closely packed, well-matched DNA monolayers. (*C*) The reductive signal upon introducing a TC mismatch (red) compared to well-matched (blue) validates the mechanism of reduction to be DNA-mediated for both proteins. (*D*) Circular dichroism thermal denaturation (5 μM protein) validates that the Y82A mutation does not significantly alter the stability of the protein.

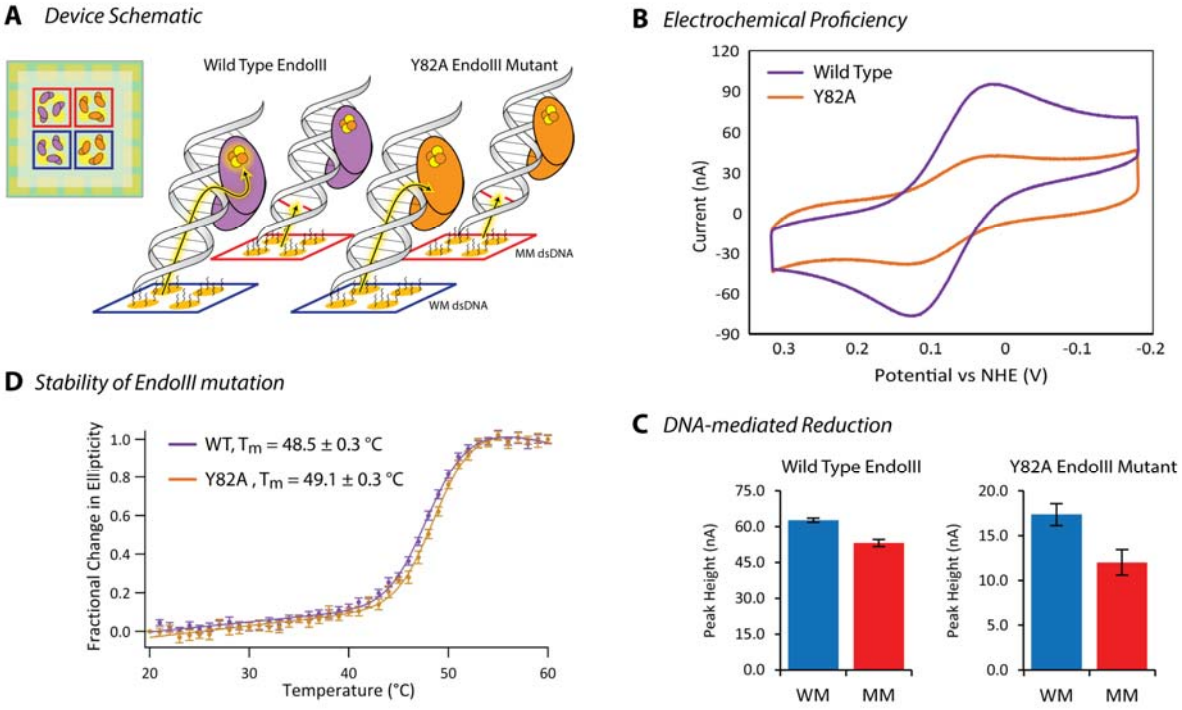

a 2-state unfolding model (*32*), melting temperatures for Y82A and WT EndoIII were found to be 49.2 ± 0.3 °C and 48.5 ± 0.3 °C respectively.

Direct comparison of electrostatic EndoIII mutants

Finally, the multiplexed DNA-modified electrodes were harnessed for the characterization of a new family of EndoIII mutants relative to wild type protein. In designing this new family of EndoIII mutants, only residues that were unlikely to cause significant changes in the DNA-binding affinity of EndoIII were chosen (*37*). The glycosylase activity of these mutants was verified to be within error of wild type protein (Figure 5.2), so that the observed electrochemical differences could not be attributed to deficiencies in DNA binding. The Y205H, K208E and E200K EndoIII mutations investigated were originally designed to explore a possible shift in the mid-point potential of the [4Fe-4S] cluster, since these mutations alter the electrostatics surrounding the cluster. However, as can be seen in Figure 5.10, when compared in parallel on a single multiplexed chip on a closely packed dsDNA film, the mid-point potential of all the mutants is not found to be statistically different, ± 10 mV of the WT protein (Figure 5.10). Likely, the electrostatic effects of the DNA polyanion, along with the associated counter ions, mitigate any effects of local electrostatic changes of nearby peptides.

Interestingly, despite the lack of difference in mid-point potential, large differences in signal intensity between the mutants relative to WT were observed when the electrochemistry of the proteins was assayed at equivalent concentrations based on the absorbance of the [4Fe-4S] cluster at 410 nm, which are statistically significant with 95% confidence based on a two-tailed t-test. E200K yields a reductive current of 14.8 ± 0.3 nA in the cyclic voltammaogram, and is seen to be CT-deficient relative to WT EndoIII which displays a current intensity of 24.4 ± 0.8 nA. In contrast, K208E and Y205H exhibit

Figure 5.10. Electrochemical and stability comparison of a new family of electrostatic EndoIII mutations, Y205H (green), K208E (blue), and E200K (red), with wild type EndoIII (purple). (*Left*) Cyclic voltammetry (scan rate = 100 mV/s) in phosphate buffer (20 mM sodium phosphate, 100 mM NaCl, 0.5 mM EDTA, 20% glycerol, pH 7.4) is displayed for all four proteins on closely packed, (assembled with 100 mM Mg Cl_2) well-matched DNA monolayers. Protein samples have equivalent concentrations of [4Fe-4S] (70 μM based on the 410 nm absorbance). (*Right*) Circular dichroism thermal denaturation (5 μM protein) was performed to correlate the altered electronic coupling of these mutations in close proximity of the [4Fe-4S] cluster with the altered stability of the protein.

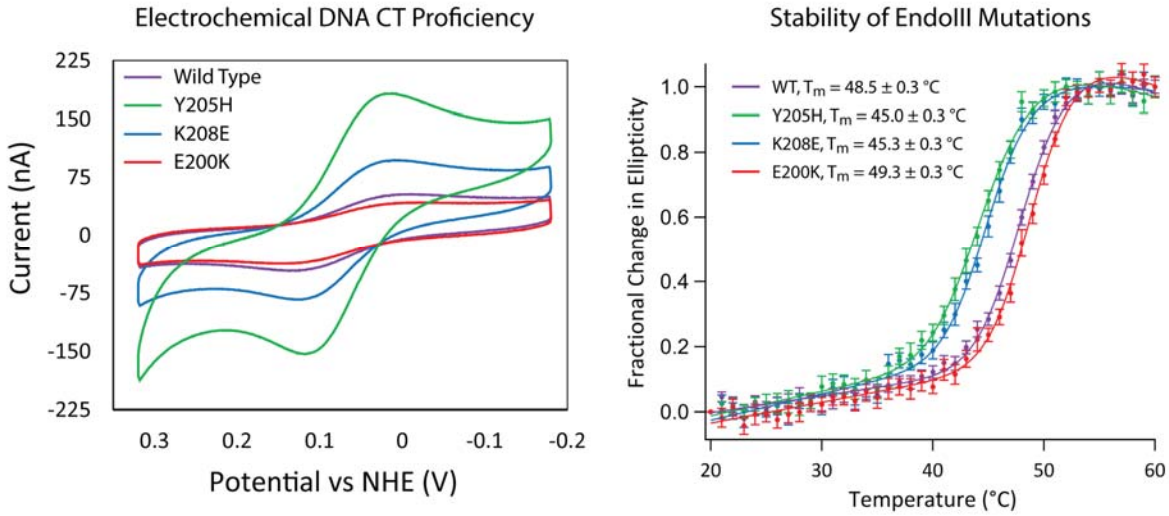

significantly larger signals, 56.5 ± 2 nA and 118 ± 6 nA, respectively, relative to the WT protein.

To explore these significant differences, CD thermal denaturation experiments were performed. The melting temperature for the Y205H, K208E and E200K EndoIII, as well as wild type protein (5 μM) are 45.0 ± 0.3 °C, 45.3 ± 0.3°C, 49.3 ± 0.3 °C, and 48.5 ± 0.3°C respectively (Figure 5.10). The denaturation temperature of these EndoIII mutants correlates with the electrochemical signal size. Those that show a thermal stability that is reduced relative to the wild type protein show a significantly higher signal size electrochemically. Conversely, E200K is slightly stabilized relative to the wild type protein, and displays an attenuated electrochemical signal. For all proteins, the signal initially grows with time and subsequently diminishes over extended incubation times. This signal decrease with time correlates with the thermal stability of the proteins; those proteins that are thermal destabilized diminish faster, while the signal persists for more stable proteins (Figure 5.11). Notably, the Y205H mutation, which is involved in hydrogen bonding to the [4Fe-4S] cluster, is found to be the most proficient in DNA CT, with a 5-fold larger signal than wild type, and the least stable mutant by both electrochemical measurements and CD thermal denaturation.

DISCUSSION

Multiplexed electrochemical analysis of EndoIII

In this study, the redox activity of the [4Fe-4S] cluster of EndoIII upon DNA binding was investigated using multiplexed DNA-modified electrodes. The utility of multiplexed analysis has previously been illustrated in using DNA-modified electrodes for the detection of biomarkers (*3-11*), as well as in performing sensitive measurements of DNA CT on long DNA duplexes (*14*). As there is growing interest in understanding the redox properties of

Figure 5.11. Electrochemical stability of EndoIII mutants. (*Left*) Protein concentrations were normalized for electrochemistry coupling to yield approximately equivalent signal sizes at early time points (~ 4 hr). Cyclic voltammetry (scan rate =100 mV/s) acquired in phosphate buffer (20 mM sodium phosphate, 100 mM NaCl, 0.5 mM EDTA, 20 % glycerol, pH 7.4) for wild type (purple), Y205H (green), K208E (blue), and E200K (red) EndoIII are presented. (*Right*) After extended incubation (~20 hr) on the multiplexed chip, the electrochemical signal from the electrostatic EndoIII mutants and wild type protein diminished based on their CVs. The degree of signal loss directly correlates with the stability and DNA CT proficiency of the proteins, with the remaining signal size decreasing in the following order: E200K (red), wild type (purple), K208E (blue), and finally Y205H (green), which had no discernible signal remaining.

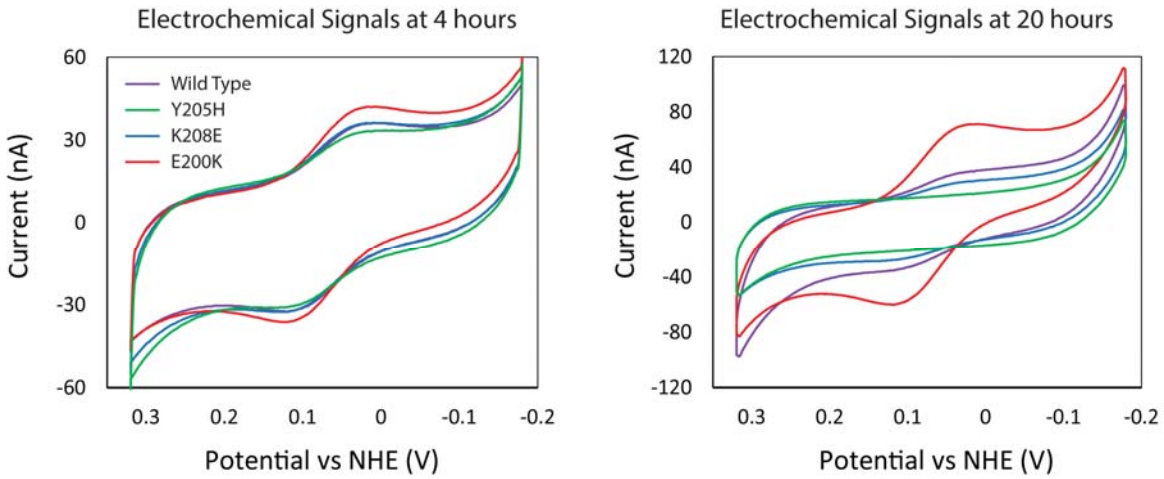

proteins containing [4Fe-4S] clusters that are involved in genome maintenance, the extension of multiplexed analysis has become essential to investigating these complex proteins and their subtle differences in redox behavior.

The electrochemical signal of EndoIII obtained using multiplexed DNA-modified electrodes was shown to be comparable to that seen using individual DNA-modified electrodes (*20-22*). Differences in peak potential and signal size are difficult to compare on individual electrodes, given the variability in DNA-modified surfaces among experiments. The complexity of protein samples further amplifies this variability. Multiplexing removes the variability associated with protein preparation and surface modification. Specifically, multiplexing allows, with confidence, for a given protein to be examined in parallel across different DNA substrates or for many proteins to be compared on a given DNA-substrate. Thus, by harnessing this ability to probe in parallel for subtle differences in the electrochemical signal of EndoIII, effects of DNA substrate and morphology can be elucidated.

Mechanistic insights into EndoIII electrochemistry

Multiplexed analysis of the $3^{+}/2^{+}$ redox couple of EndoIII on differing DNA morphologies show subtle differences in the DNA-bound electrochemical signals. These differences in electrochemistry result from differences in electron transfer pathways between the electrode and DNA-bound EndoIII that vary as a function of DNA film morphology. DNA-modified electrodes with single-stranded DNA are found to function as an ideal control. Since EndoIII does not bind single-stranded DNA with high affinity, the single-stranded DNA does not serve as a means to increase the local concentration of EndoIII at the electrode surface. Moreover it appears that the negatively charged signal-stranded DNA serves as an effective passivation layer, preventing protein denaturation on the gold surface, a common

occurrence for protein electrochemistry (*38*). Instead EndoIII appears to be electrochemically silent on these electrodes modified with single stranded DNA.

Secondly, the duplex DNA film morphology, established during electrode assembly, is demonstrated to be critical in dictating the predominant electron transfer pathway between the electrode surface and the [4Fe-4S] cluster of DNA-bound EndoIII. Differing electron transfer pathways to a single DNA-bound redox active moiety were previously characterized using DNA-modified electrodes with covalent redox active reporters (*14, 35*). In the case of a DNA-bound redox-active reporter, such as DNA-tethered methylene blue, it has been shown that the accessibility of the redox-active moiety to the electrode surface determines whether the predominant reduction mechanism is DNA CT or direct reduction by the surface of the electrode (*35*). In the case of DNA-mediated reduction, we have established that the rate limiting step for the DNA-mediated reduction of distally bound redox active species is not DNA CT itself, but the tunneling through the alkane thiol linkage to the electrode (*39*). The lateral charge diffusion through these DNA-modified films has also been established to be quite slow, negating the possibility of cross-talk throughout these films (*40*). The redox activity of EndoIII on DNA-modified electrodes assembled with closely packed DNA monolayers, with limited surface accessibility, displays all the previously established hallmarks of a DNA-mediated reduction pathway, including increased peak splitting, signal broadening, sensitivity to perturbations, and non-diffusion rate limited kinetics. Conversely, the DNA-bound electrochemical signal from EndoIII on loosely packed DNA films, which have enhanced surface accessibility, displays the opposite electrochemical behaviors that are characteristic of an electron transfer pathway that is not DNA-mediated. As both these signals involve reduction of *DNA-bound* EndoIII, the signals display only subtle differences. Only by using multiplexed analysis to investigate the electrochemistry of a single protein solution in parallel across differing DNA-modified electrodes are these two different electron transfer pathways cleanly distinguishable.

Electron transfer in EndoIII mutants

Multiplexed analysis was demonstrated to be useful not only in the characterization of different electron transfer pathways from the electrode surface to the DNA-bound EndoIII, but also in comparing directly the electron transfer efficiencies of different EndoIII mutants. As proof-of-principle, the DNA CT proficiency of a known disease-related EndoIII mutant, Y82A, was electrochemically compared to wild type EndoIII. It has previously been established that introducing the Y82A mutation into EndoIII yields a functionally active protein that is DNA CT-deficient (*21*). Due to the proximity of this aromatic tyrosine residue to the DNA π-stack, the deficiencies in the electrochemical signal have been attributed to disrupting the electron transfer pathway between the DNA and [4Fe-4S] cluster (*21*). Our multiplexed experiment allowed for the validation of this result along with a more quantitative assessment of CT deficiency.

The mechanism of reduction for both wild type and Y82A EndoIII was shown to be DNA-mediated on the closely packed DNA films, since both proteins display the characteristic sensitivity to single base pair perturbations. The inherent DNA CT-deficiency of Y82A was characterized in parallel so that the difference in electrochemical efficiency of Y82A bound to DNA compared to wild type can be conclusively attributed to decreased DNA CT proficiency. The degree of DNA CT deficiency quantified for this mutant was found to be twice as pronounced compared to previous measurements, given the overall decreased variability of the DNA-modified electrodes and, importantly, the decreased contributions from surface reduction of the [4Fe-4S] cluster due to the optimized DNA morphology.

Moreover, this multiplexed technology is sufficiently reliable to permit characterization of the effects on the electron transfer pathway of a new family of EndoIII mutations. This family was found to show significant differences in DNA CT efficiency, while displaying very similar DNA-bound reduction potentials for the $3^{+}/2^{+}$ redox couple of the

[4Fe-4S]. Key to conclusively attributing differences, or lack thereof, observed in the mutant electrochemistry to changes in the electron transfer pathway through EndoIII was the ability to perform this comparison on identical gold surfaces, allowing for the geometry of electron transfer between the electrode and EndoIII to be held constant.

Previous work by Burgess and co-workers that focused on changing the electrostatics in *Azotobacter vinelandii* ferredoxin I resulted in large potential shifts; a single phenylalanine to histidine mutation caused a shift of over 200 mV for the [4Fe-4S] cluster while leaving overall protein structure unaffected (*41*). With the same aims, EndoIII mutations were prepared that invert the electrostatics of three residues within 4 Å of the [4Fe-4S] cluster that are oriented on the opposite face of the cluster relative to the DNA. Multiplexed analysis of these three different EndoIII mutants allowed for their simultaneous comparison to wild type EndoIII. The lack of distinguishable differences of the DNA-bound midpoint potentials for these electrostatic EndoIII mutants likely reflects the overwhelming contribution of polyanionic DNA, as DNA binding already negatively shifts the reduction potential of EndoIII by approximately 200 mV (*25*). The strict consistency of the measured DNA-bound midpoint potentials likely further derives from the screening effect of counter-ions associated with the DNA, as well as from the broad, heterogeneous nature of the observed DNA-mediated signals.

As mentioned above, we have proposed a model where DNA repair proteins containing [4Fe-4S] clusters utilize DNA CT as a first step to localize to the vicinity of DNA damage (*21*). All of the proteins that we have investigated thus far have similar DNA-bound reduction potentials of approximately 80 mV vs. NHE (*20*). These results suggest that DNA-binding could be a mechanism that standardizes the reduction potentials of iron-sulfur cluster-containing DNA repair proteins once bound to DNA, allowing for efficient DNA-mediated electron self-exchange between repair proteins.

Unlike the Y82A mutation, these mutations were specifically designed to affect residues in close proximity to the [4Fe-4S] cluster, but presumably without affecting the pathway for DNA-mediated electron transfer (Figure 5.12). Nonetheless, as seen in Figure 5.10, these changes unambiguously result in significant changes in the DNA CT efficiency. Multiplexed electrochemical characterization in conjunction with thermal denaturation circular dichroism experiments indicates that the differences in DNA CT efficiencies of these mutants are most likely caused by changes in the stability and solvent accessibility of the [4Fe-4S] cluster. Those proteins with decreased thermal stability show increased DNA CT yield compared to WT. Structured water molecules have been proposed to mediate efficient biological electron transfer in several intra- (*42, 43*) and intermolecular protein systems (*44-46*), generally by forming robust hydrogen-bonding pathways that increase electronic coupling between the donor and acceptor (*47*). We hypothesize that the destabilization we observed in Y205H and K208E EndoIII may result in the formation of a water pocket in EndoIII that would facilitate ET, as we have suggested previously for other destabilizing EndoIII mutations (*22*). In the case of E200K, which is slightly stabilized relative to wild type, substitution for a larger lysine residue along the face of the cluster may instead screen the cluster from solvent and contribute to the observed CT deficiency. While the Y82A mutant is marginally stabilized compared to WT EndoIII, it is more significantly defective in DNA CT proficiency compared to E200K. Therefore, the extent the DNA CT deficiency of Y82A cannot be fully attributed to the change in stability and is thought to originate from directly disrupting the electron transfer pathway. Overall, it appears that differences in DNA CT proficiency can be caused both by altering the electron transfer pathway by removing aromatics, and by more indirectly modulating the electronic coupling of the cluster by changing protein stability and presumably solvent accessibility.

Figure 5.12. Crystal structure of EndoIII with the location of mutants shown relative to the DNA (cyan) and [4Fe-4S] cluster: Y205 (green), K208 (blue), E200 (red), and Y82 (orange). PDB: 2ABK with DNA from 1ORN.

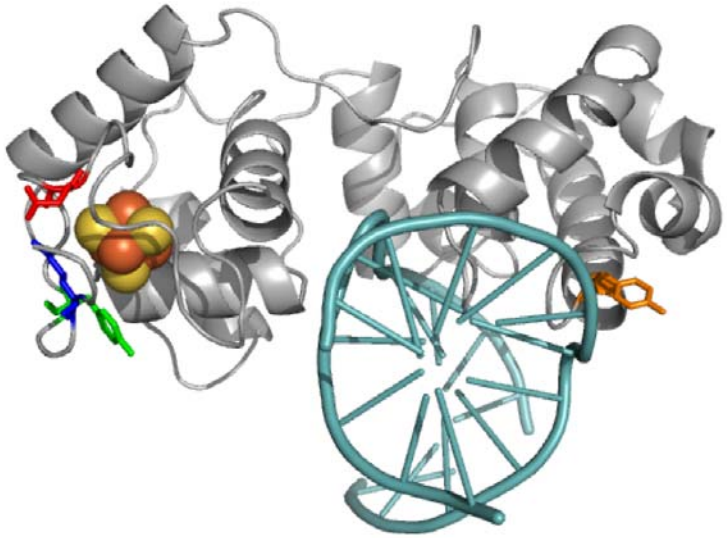

CONCLUSION

Multiplexed characterization of the DNA repair protein EndoIII bound to DNA provides new insights into the DNA-mediated reduction of this metalloprotein and the resolution of subtle electrochemical variations associated with DNA substrate and surface morphology. Multiplexed analysis leads to more reliable statistics as well as decreased surface variability and background contribution. The reduction of EndoIII is seen to be DNA-dependent, yet once bound to duplex DNA, there are two different pathways through which the electron transfer proceeds. The predominant mechanism for the reduction of the [4Fe-4S] cluster of EndoIII is shown to correlate with the surface accessibility of the protein, resulting in DNA-mediated reduction being observed only with closely packed DNA films. In addition to the electron transfer pathway between the electrode surface and EndoIII being characterized, the use of multiplexed analysis also allowed for the direct comparison of electron transfer pathways through the protein itself. The electrochemistry and stability of various EndoIII mutants was characterized, including a new family of mutations introducing electrostatic changes in close proximity to the [4Fe-4S] cluster. The stability of a given mutation was shown to correlate with the electrochemical yield, leading to the hypothesis that mutations not directly on the electron transfer pathway through the protein can alter the rate of electron transfer by affecting the solvation surrounding the [4Fe-4S] cluster. Most interestingly, this side-by-side quantitative comparison of varying electrostatics in the protein fold provides a demonstration of the dominance that DNA-binding elicits on the reduction potential of DNA repair proteins.

These multiplexed chips provide the needed flexibility and robustness to characterize the redox activity of emerging [4Fe-4S]-containing proteins that bind DNA. Multiplexed

analysis will be integral in relating the function and redox activity of these DNA-binding proteins in order to establish roles for these critical redox active co-factors *in vivo*.

REFERENCES

1. Zheng, G., Patolsky, F., Cui, Y., Wang, U. W., Lieber, C. M. *Nature Biotechnol*. **2005**, *23*, 1294.

2. Morrow, T. J., Li, M., Kim, J., Mayer, T. S., Keating, C. D. *Science* **2009**, *323*, 352.

3. Swensen, J.S., Xiao, Y., Ferguson, B.S., Lubin, A.A., Lai, R.Y., Heeger, A.J., Plaxco, K.W., Soh, H.T. *J. Am. Chem. Soc.* **2009**, *131*, 4262.

4. Plaxco, K.W., Soh, H.T. *Trends in Biotechnology* **2011**, *29*, 1.

5. Bonham, A.J., Hsieh, K., Ferguson, B.S, Vallee-Belisle, A., Ricci, F., Soh, H.T., Plaxco, K.W. *J. Am. Chem. Soc.* **2012**, *134*, 3346.

6. White, R.J., Kallewaard, H.M., Hsieh, W., Patterson, A.S., Kasehagen, J.B., Cash, K.J., Uzawa, T., Soh, H.T., Plaxco, K.W. *Anal. Chem.* **2012**, *84*, 1098.

7. Hsieh, K., Patterson, A.S., Ferguson, B.S, Plaxco, K.W., Soh, H.T. *Angew. Chem. Int. Ed.* **2012**, *51*, 4896.

8. Fang, Z., Soleymani, L., Pampalakis, G., Yoshimoto, M., Squire, J.A., Sargent, E.H., Kelley, S.O. *ACS Nano* **2009**, *10*, 3207.

9. Vasilyeva, E., Lam, B., Fang, Z., Minden, M.D., Sargent, E.H., Kelley, S.O. Angew. *Chem. Int. Ed.* **2011**, *50*, 4137.

10. Lam, B., Fang, Z., Sargent, E.H., Kelley, S.O *Anal. Chem.* **2012**, *84*, 21.

11. Das, J., Cederquist, K.B., Zaragoza, A.A., Lee, P.E., Sargent, E.H. and Kelley, S.O. *Nat. Chem.* **2012**, *4*, 642.

12. Pheeney, C.G., Guerra, L.F, Barton, J.K. *Proc. Natl. Acad. Sci.* **2012**, *109*, 11528.

13. Slinker, J.D, Muren, N.B., Gorodetsky, A.A., Barton, J.K. *J. Am. Chem. Soc.* **2010**, *132*, 2769.

14. Slinker, J.D., Muren, N.B., Renfrew, S.E., Barton, J.K. *Nat. Chem.* **2011**, *3*, 228.

15. Genereux, J.C., Barton, J.K. *Chem. Rev.* **2010**, *110*, 1642.

16. Murphy, C.J., Arkin, M. R., Jenkins, Y., Ghatlia, N. D., Bossmann, S. H., Turro, N. J., Barton, J. K. *Science* **1993**, *262*, 1025.

17. Charge Transfer in DNA:From Mechanism to Application edited by Wagenknecht, H.A. (Wiley-VCH Verlag GmbH & Co KGaA, Weiheim, 2005).

18. Boon, E. M., Ceres, D. M., Drummond, T. G., Hill, M. G., Barton, J. K. *Nat. Biotechnol.* **2000**, *18*, 1096.

19. Boal, A. K., Barton, J. K. *Bioconjugate Chem.* **2005**, *16*, 312.

20. Boal, A. K., Yavin, E., Lukianova, O. A., O'Shea, V. L., David, S. S., Barton, J. K. *Biochemistry* **2005**, *44*, 8397.

21. Boal, A. K.,Genereux, J. C., Sontz, P. A.,Gralnick, J. A.,Newman, D. K., Barton, J. K. *Proc. Natl. Acad. Sci. U.S.A*. **2009**, *106*, 15237.

22. Romano, C. A, Sontz, P. A., Barton, J. K. *Biochemistry* **2011**, *50*, 6133.

23. Lee, P.E., Demple, B., Barton, J.K. *Proc. Natl. Acad. Sci.* **2009**, *106*, 13164.

24. Mui, T.P, Fuss, J.O, Ishida, J.P., Tainer, J.A., Barton, J.K. *J. Am. Chem. Soc.* **2011**, *133*, 16378.

25. Gorodetsky, A. A., Boal, A. K., Barton, J. K. *J. Am. Chem. Soc.* **2006**, *128*, 12082.

26. Wu, Y., Suhasini, A. N., Brosh, R. M., Jr. *Cell. Mol. Life Sci.* **2009**, *66*, 1209.

27. Vaithiyalingam, S., Warren, E. M., Eichman, B. F., Chazin, W. J. *Proc. Natl. Acad. Sci. U.S.A.* **2010**, *107*, 13684.

28. White, M.F., Dillingham, M.S. *Current Opinion in Structural Biol.* **2012**, *22*, 94.

29. Wu, Y., Brosh Jr., R.M. *Nucleic Acids Research* **2012**, *10*, 1.

30. Sontz, P.A., Mui, T.P., Fuss, J.O., Tainer, J.A., Barton, J.K. *Proc. Natl. Acad. Sci.* **2012**, *109*, 1856.

31. Cunningham, R. P., Asahara, H., Bank, J. F., Scholes, C. P., Salerno, J. C., Surerus, K., Münck, E., McCracken, J., Peisach, J., Emptage, M. H. *Biochemistry* **1989**, *28*, 4450.

32. Koepf, E.K., Petrassi, H.M., Sudol, M., Kelly, J.W. *Protein Sci.* **1999**, *8*, 841.

33. Lapierre, M.A., O'Keefe, M., Taft, B.J., Kelley, S.O. *Anal. Chem.* **2003**, *75*, 6327.

34. Bard, A. J., Faulkner, L. R. Electrochemical Methods—Fundamental and Application, 2nd ed., John Wiley&Sons: New York, 2000, pp 580-631.

35. Pheeney, C.G., Barton, J.K. *Langmuir* **2012**, *28*, 7063.

36. Fromme, J.C.; Verdine, G.L. *EMBO J.* **2003**, *22*, 3461.

37. No residues in the conserved DNA-binding FCL motif, residues Thr186 – Cys194, were mutated (Thayer, M.M., Ahern, H., Xing, D., Cunningham, R.P., Tainer, J.A. *EMBO J.* **1995**, *14*, 4108).

38. Zhang, J., Chi, Q., Hansen, A.G., Jensen, P.S., Salvatore, P., Ulstrup, J. *FEBS Letters* **2012**, *586*, 526.

39. Drummond, T.G., Hill, M.G., Barton, J.K. *J. Am. Chem. Soc.* **2004**, *126*, 15010.

40. Kelley, S.O., Jackson, N.M., Hill, M.G., Barton, J.K. *Angew. Chem. Int. Ed.* **1999**, *38*, 941.

41. Chen, K., Bonagura, C.A., Tilley, G.J., McEvoy, J.P., Jung, Y.S., Armstrong, F.A., Stout, C.D., Burgess, B.K. *Nature Struct. Biol.* **2002**, *9*, 188.

42. Francisco, W. A., Wille, G., Smith, A. J., Merkler, D. J., Klinman, J. P. *J. Am. Chem. Soc.* **2004**, *126*, 13168.

43. Casimiro, D. R., Richards, J. H., Winkler, J. R., Gray, H. B. *J. Phys. Chem.***1993**, *97*, 13073.

44. Tezcan ,F. A., Crane, B. R., Winkler, J. R., Gray, H. B. *Proc. Natl. Acad. Sci. U.S.A.* **2001**, *98*, 5002.

45. van Amsterdam, I. M. C., Ubbink, M., Einsle, O., Messerschmidt, A., Merli, A., Cavazzini, D., Rossi, G. L., Canters, G. W. *Nat. Struct. Biol.* **2002**, *9*, 48.

46. Miyashita, O., Okamura, M. Y., Onuchic, J. N. *Proc. Natl. Acad.Sci. U.S.A.* **2005**, *102*, 3558.

47. Lin, J., Balabin, I. A., Beratan, D. N. *Science* **2005**, *310*, 1311.

APPENDIX I

NHS-ester modified Methylene Blue Synthesis

INTRODUCTION

The procedures here are modified (*1, 2*) and augmented (*3*) from previously published work. See Figure A1.1 for overall synthesis strategy for butanoic acid-modified Methylene Blue (MB′).

MATERIALS AND METHODS

Materials

All reagents and solvents were purchased from Sigma Aldrich and used without further purification.

Synthetic procedure for 2-amino-5-dimethylaminophenylthiosulfonic acid (1, 3).

Table A1.1. Reagents for the synthesis of 2-amino-5-dimethylaminophenylthiosulfonic acid.

	Reagents	**Molecular Weight (g/mol)**	**Moles (mmol)**	**Mass (g)**	**Dissolve in H_2O (mL)**
1	N,N-dimethylphenylene diamine	136.19	73	10	----
2	$Al_2(SO_4)_3 \cdot 18H_2O$	666.42	65	43.6	100
3	$Na_2S_2O_3 \cdot 5H_2O$	248.18	140	22.0	80
4	$ZnCl_2$	136.28	63	8.8	12
5	$K_2Cr_2O_7$	294.19	17	5.0	30

1. Add reagent **1** to a 500 mL round bottom flask.
2. Dissolve individually reagents **2** through **5** in indicated volumes of DI Water.
3. Add **2** to flask followed by **3** and then **4**.
4. Cool reaction mixture down to O °C with an ice bath.

Figure A1.1. Synthetic Scheme for butanoic acid modified MB

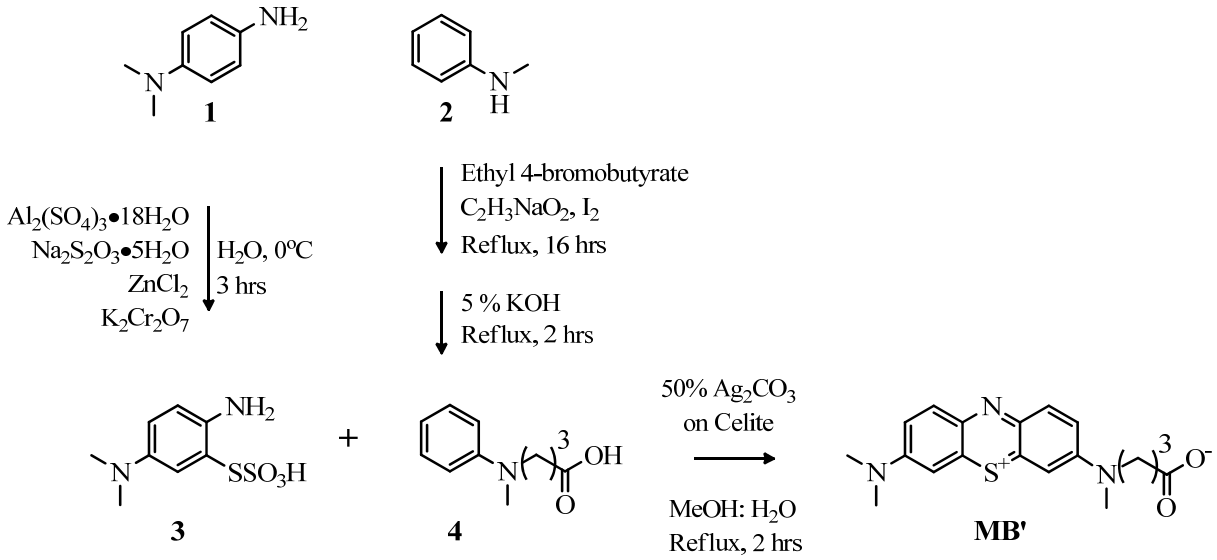

5. Slow step-wise addition of **5** to chilled flask over the course of 15 min.
    a. Maintain the reaction at O °C throughout addition of **5**, slow down addition if temperature rises.
6. Let reaction proceed for 3 hr.
    a. **Important:** Reaction is exothermic therefore perform in fume hood and monitor regularly.
7. Remove from ice bath and let the reaction warm to room temperature.
8. Isolate precipitate by vacuum filtration, using a large Buchner funnel and an aspirator.
    a. Wash precipitate with water, acetone, ethanol:diethyl ether (1:1).
    b. Note, excessive washing will cause loss of product.
9. Collect pink solid without further purification and place under vacuum to dry solid.

Characterization

Yield ~50%.

ESI-MS in ACN: 247.02 g/mol $[M-H]^+$.

Synthetic procedure for N-methyl-N-ethyl-4-butanoate aniline (2, 3).

Table A1.2. Reagents for the synthesis of N-methyl-N-ethyl-4-butanoate aniline.

	Reagents	**Molecular Weight (g/mol)**	**Density**	**Boiling Point**	**Moles (mmols)**	**Mass/ Volume**
1	N-methyl Aniline	107.15	0.989	15 at 0.2 mm Hg	140	15.17 mL
2	Ethyl 4-bromobutanoate	195.05	1.363	46 at 0.2 mm Hg	140	20.0 mL
3	Sodium Acetate	82.03			140	11.9 g
4	Iodine	253.81			0.4	0.12 g

1. Combine equimolar amounts of **1** and **2** into a 100 mL round bottom flask.
2. Stir reaction and add **3** followed by a catalytic amount of **4**.

3. Reflux the reaction in an oil bath (~ 110 °C) for 16 hr.
4. Let reaction mixture cool to room temperature.
5. Check reaction by TLC and visualize under UV.
    a. Run in 95 % Chloroform & 5 % Methanol.
6. Dissolve reaction in H_2O (15 mL) and transfer to a separation funnel.
7. Make aqueous layer basic with 1 N NaOH, test by pH paper.
    a. At pH > 7 the product is deprotonated and is in the organic layer.
8. Extract organics with ether (15 mL x 3 times).
    a. Reagents **1** & **2** and desired product will be in the organic layer.
9. Dry ether by adding $MgSO_4$ (~30 g) to the ether collection flask.
10. Gravity filter ether, removing drying agent.
11. Purify by vacuum distillation: starting material should come off around 20 – 30 °C at 0.2 mm Hg while product is at 110 °C at 0.2 mm Hg.
    a. Ensure adequate vacuum pressure.
    b. Clean, grease, and assemble simple vacuum distillation glassware. Fractionating distillation column is not necessary.
    c. Place reaction vessel over a hot plate.
    d. Heat reaction mixture to 50 °C and collect everything in first round bottom.
    e. Heat to 120 °C, collect first 10 % in first round bottom and the rest into the second round bottom, this will be your clean product (clear/yellowish). **Important**: Do not leave oil bath unattended at these temperatures.

Characterization

Yield ~60%.

^{1}H NMR (500 MHz, $CDCl_3$): δ 7.34-7.08 (m, 2H), 6.87-6.54 (m, 3H), 4.17 (qt, J=7.1, 1.0Hz, 2H), 3.48-3.27 (m, 2H), 2.96 (s, 3H), 2.38 (t, J=7.2 Hz, 2H), 2.02-1.81 (m, 2H), 1.29 (tt, J=7.1, 1.0 Hz, 3H).

^{13}C NMR (126 MHz, $CDCl_3$): δ 173.27, 149.27, 129.20, 116.24, 112.23, 60.41, 51.94, 38.30, 31.61, 22.20, 14.27.

ESI-MS in ACN:H_2O:HAc: 221.3 g/mol $[M]^+$.

Synthetic procedure for N-methyl-N-(carboxypropyl)aniline (2, 3).

Table A1.3. Reagents for the synthesis of N-methyl-N-(carboxypropyl)aniline.

	Reagents	**Molecular Weight (g/mol)**	**Moles (mmol)**	**Mass (g)**
1	Ethyl 4-(methyl(phenyl)amino)butanoate	221.30	45	10

1. Add reagent 1 to a 250 mL round bottom flask.
2. Dissolve in 150 mL 5 % by weigh KOH.
3. Reflux for 2 hr (~105 °C).
    a. Carboxylic acid is soluble in aqueous solvent; therefore reaction can be monitored by increased solubility.
4. Cool reaction and transfer to a separation funnel.
5. Wash with ether (2 x 70 mL).
    a. Carboxylic acid product is deprotonated under these basic conditions and is in the aqueous layer. Ether is top layer, so between each washing collect both the aqueous and organic layer. Clean separation funnel and re-add the aqueous layer for next washing.
6. Adjust pH of aqueous layer to pH = 5.5 with concentrated HCl (~ 13 mL).
7. Extract with ether (3 x 100 mL).

a. Carboxylic acid product is protonated under acidic conditions and is in the organic layer.

8. Dry organic layer over $MgSO_4$ and remove solvent.

Characterization

Yield ~ 80%.

^{1}H NMR (500 MHz, $CDCl_3$): δ 7.34-7.12 (m, 2H), 6.90-6.53 (m, 3H), 3.51 (q, J=7.0Hz, 2H), 2.94 (s, 3H), 2.43 (t, J=7.2 Hz, 2H), 1.94 (p, J=7.3 Hz, 2H).

^{13}C NMR (126 MHz, $CDCl_3$): δ 179.07, 149.18, 129.22, 116.72, 112.64, 52.07, 38.52, 31.46, 21.90.

ESI-MS in ACN:H_2O:HAc: 193.3 g/mol $[M]^+$.

Synthetic procedure for N-(carboxypropyl)-Methlyene Blue (MB') (3).

Table A1.4. Reagents for the synthesis of N-(carboxypropyl)-Methlyene Blue (MB′).

	Reagents	**Molecular Weight (g/mol)**	**Moles (mmol)**	**Mass (g)**
1	2-amino-5-(dimethylamino)phenyl thiosulfonic acid	247.31	9.7	2.40
2	4-methyl phenylamino butanoic acid	193.24	9.7	1.87
3	50% w Ag_2CO_3 on Celite	275.79 (Ag_2CO_3)		10

Important:

- MB' is soluble in DMSO, DMF, Methanol, ACN (from most to least).
- Does not NMR well until COMPLETELY dry due to resonant structures.
- MB' has an exceptionally large extinction coefficient so solutions must be exceptionally dark.

1. Combine equimolar amounts of **1** and **2** in equimolar in a 500 mL flask.

2. Dissolve in Methanol:H_2O 200 mL : 80 mL and mix solution.
3. Heat the solution just below refluxing (~60 °C).
4. Slow step-wise addition of **3** over 15-30 min.
5. Reflux reaction for 2 hr.
6. Let reaction return to room temperature.
7. Vacuum filter the reaction mixture through Celite and wash with methanol.
    a. Pack a Buchner funnel with Celite prior to filtering reaction and wash with methanol.
8. Remove solvent and dry load reaction mixture onto 0.4 Silica gel.
    a. Re-suspend reaction mixture in minimal methanol and toluene.
    b. Add silica, remove solvent and place under vacuum overnight to remove any trace solvent.
9. Pack a dry column with high grade Silica (*4*).
    a. **Safety**: Wear a mask the full time working with this silica to avoid inhalation.
    b. Load silica roughly 3 to 4 fingers high and vortex to pack the silica.
    c. Add dry loaded Silica on top of packed column.
    d. Add an additional 6 inches of Celite, attach aspirator and a 500 mL flask.
10. Run column.
    a. Start with 20 mL portions of $CHCl_3$:MeOH:HOAc (100:15:1.5) to elute impurities.
    b. Completely dry column between changing solvent and collection flask otherwise column will crack.
    c. Step-wise increase Methanol component until the blue band elutes.
11. Remove solvent, transfer to a vial, and use ether washes to remove as much water as possible. Date and store in the freezer.

Characterization

Yield ~ 20%.

ESI-MS in MeOH:H_2O:HAc (1:1:0.1%): 356.3 g/mol $[M-H]^+$.

Synthetic procedure for MB′-NHS ester (Figure A1.2) (3).

Table A1.5. Reagents for the synthesis of MB′-NHS ester.

	Reagents	**Molecular Weight (g/mol)**	**Moles (mmol)**	**Mass (mg)**
1	Methylene Blue ‘ (MB′)	357.47	0.022	8
2	*N*,*N*′-Dicyclohexylcarbodiimid (DCC)	206.33	0.045	9.3
3	N-Hydroxysuccinimide (NHS)	115.09	0.045	5.2

1. In a scintillation vial combine **1**, **2**, and **3**.
2. Add a minimal amount of DMF (~0.5 mL) to solubilize MB′.
3. Cover with aluminum foil and let stir at room temperature overnight.
4. Remove DMF and re-dissolve in 20 µL of DMSO per 1 mg MB’.

Characterization

ESI-MS in MeOH:H_2O:HAc (1:1:0.1%): 453.3 g/mol $[M-H]^+$.

Important: The carboxylic acid (356 g/mol), methyl ester (370 g/mol), and NHS ester (453 g/mol) will all be present in MS if activation was successful.

Figure A1.2. Synthetic Scheme for NHS-ester activation of MB′.

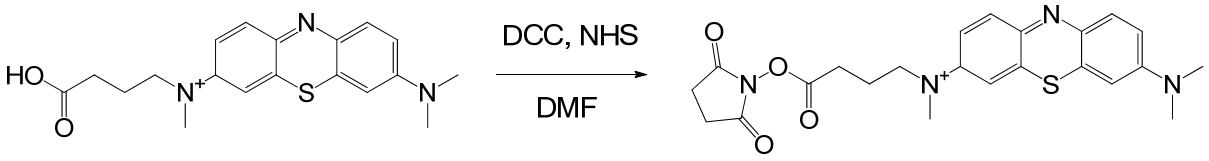

REFERENCES

1. Chen, H., Herkstroeter, W.G., Perlstein, J., Law, K.Y., Whitten, D.G. *J. Phys. Chem.* **1994**, *98*, 5138.

2. Wagner, S.J., Skripchenko, A., Robinette, D., Foley, J.W., Cincotta, L. *Photochemistry and Photobiology* **1998**, *67*, 343.

3. Pheeney, C.G., Barton, J. K. *Langmuir* **2012**, *28*, 7063.

4. Pedersen, D.S., Rosenbohm, C. *Synthesis* **2001**, *16*, 2431.

APPENDIX II

Probe-oligonucleotide synthesis and purification

INTRODUCTION

The procedures here are modified from those published previously (*1, 2*). See Figure A2.1 for the schematic of DNA synthesis and purification.

MATERIALS AND METHODS

Materials

All phosphoramidite reagents were purchased from Glen Reagents, including potassium carbonate solution. Ammonium hydroxide (NH_4OH), dithiothreitol (DTT), Nile Blue (NB), and all solvents were purchased from Sigma Aldrich and used without further purification. NHS-ester modified Methylene Blue (MB′) was synthesized based on protocols presented in Appendix I.

Step 1: Oligonucleotide Synthesis

Standard Conditions (Natural, Thiol-, or Amino-modified DNA)

1. Check waste, all liquid reagents, and phosphoramidites. Ensure that there is enough reagent for the # of columns x # of bases being synthesized.
2. Use Change Bottle command for changing liquid reagents.
3. Use Autodilution command for the dilution of solid reagents.
    a. For expensive phosphoramidites (thiol, amino, or any other modifiers) dilute the 100 µmoles into 1.2 ml to yield enough phosphoramidite for six columns. Stop the autodilution within the last 3 sec of the pressurization. This stops the priming of the lines.
4. Run set up.
    a. Load your sequence.

Figure A2.1. Schematic of DNA synthesis and purification.

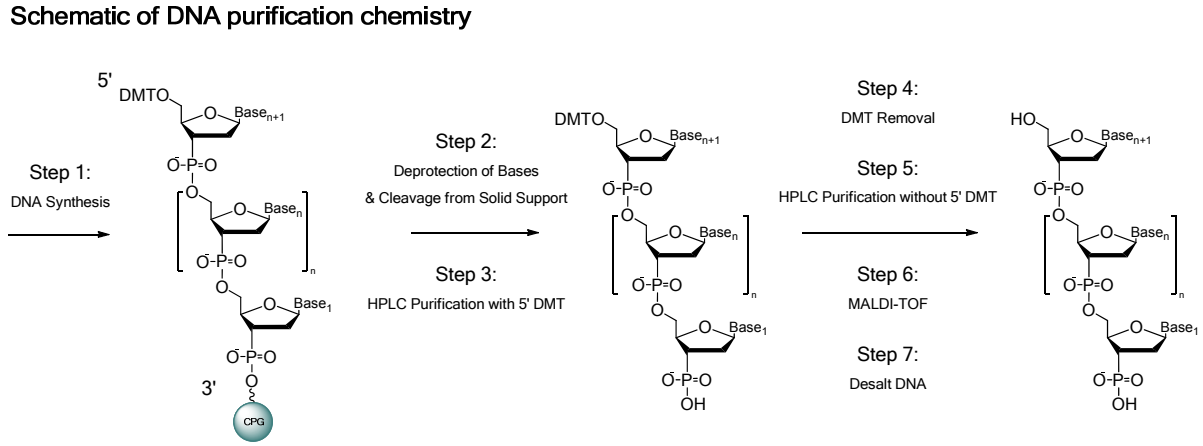

b. Load the cycle, either 1 μM-PO-fix (when the lines have been primed) or 1 μM-PO-fix-cpg (when the lines have not been primed - stopped during pressurization).
c. Ensure that the cleavage and DMT removal options are turned off, and that the trityl limits are set to 0% and 85%.

5. When finished check that the trityl yield was > 92% and place columns on lyophilizer.

Ultra-mild Conditions (Nile-Blue Modified DNA)

1. Use ultramild protected A & G bases (Pac-dA-CE and iPr-Pac-dG-CE respectively).
2. Switch to ultramild Cap A (THF/Pyridine/Pac_2O).
3. Use ultramild protected columns if your first base is A or G; otherwise standard columns are sufficient.

Step 1A: Solid Support Coupling (Nile Blue)

1. Vortex and sonicate 9 ml anhydrous DCM (dichloromethane), 1 mL DIEA (N,N-Diisopropylethylamine), and 150 mg NB in a glass vial to thoroughly mix.
2. Fill a 1 mL syringe with NB coupling solution and connect to one side of column. Plunger solution into column to dispel air inside column and attach a second empty syringe to the other side of the column.
3. Mix coupling reaction by pushing the solution between the two syringes. This must be done in a fume hood behind the shield.
4. Wrap in parafilm and tape and secure onto shaker and let reaction proceed for 24 hr (Figure A2.2). After 2 hr re-mix the reaction solution using the syringes in a fume hood.
5. Discard coupling syringes and use 5 mL syringes to wash off excess NB.
    a. Dichloromethane (DCM) 5 times with 5 mL; until only a light blue color persists.

Figure A2.2. Nile Blue coupling reaction to NHS-Ester modified DNA.

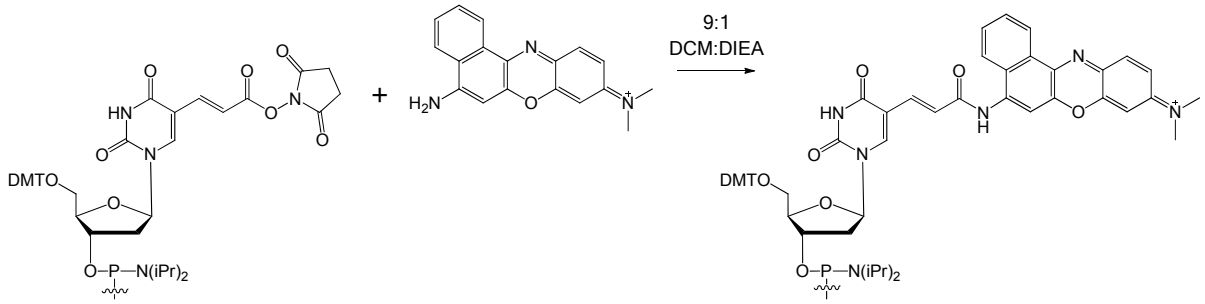

b. Methanol 2 times with 5 mL; wash as quickly as possible and be prepared to immediately quench with Acetonitrile (Methanol cleaves DNA from the CPG).
c. Acetonitrile (ACN) 5 times with 5 mL.

6. Dry columns on the lyophilizer.

Step 2: Deprotection and cleavage from solid support

Standard Conditions: Natural, Thiol-, or Amino- Modified DNA

1. Transfer solid support to a 1.7 mL eppendorf.
2. Add 800 µl of NH4OH, vortex, and clamp lids.
    a. Use fresh NH_4OH, stored at 4°C.
3. Place on 60 °C hot plate for 8 hr.
4. Refrigerate solution for 15 min to cool NH_4OH.
    a. **Important:** NH_4OH tubes are unsafe to be opened while hot and DNA sample will be lost.
5. Once cooled: vortex, pipette supernatant into filter tubes, and centrifuge to filter.
6. Add an additional 400 µl NH_4OH to the solid support.
7. Vortex, pipette supernatant into filter tubes, and centrifuge to filter again.
8. Dry NH_4OH solution on the speed vacuum.

Ultramild Conditions: NB Modified DNA

1. Follow the same procedure as above but replace NH_4OH with Potassium Carbonate and allow the reaction to sit at room temperature for 12 hr.

Step 3: HPLC Purification - DMTON

Standard Conditions: Natural, Thiol, and Amino DNA

1. Add 600 µl of 5.0 mM phosphate buffer to dried samples from speed vacuum.
2. Re-suspend DNA, and transfer to a filter tube.

3. Centrifuge for roughly 10 min and transfer into HLPC vial.

Ultramild Conditions: Nile Blue modified DNA

1. Run a Nap5 size exclusion column on NB-modified DNA to remove small molecules prior to HPLC.
    a. See DMT removal of Thiol-modified DNA for procedure for Nap 5 column.
2. Elute samples directly from Nap5 column into HPLC vial.

Instrument preparation

If it's the first time purifying DNA by HPLC create the necessary methods and sequence before turning on the pump:

Start Method (###START):

Time (min)	ACN	50 mM NH_4OAc Buffer	Flow rate
0	100 %	0 %	2.0 mL/min
15	5 %	95 %	2.0 mL/min

DMT ON Method (###DON):

Time (min)	ACN	50 mM NH_4OAc Buffer	Flow rate
0	5 %	95 %	2.0 mL/min
30	75 %	25 %	2.0 mL/min
35	5 %	95 %	2.0 mL/min

Monitor DNA at 260 nm & 280 nm; NB and MB at 580 or 600 nm.

End Method (###END):

Time (min)	ACN	50 mM NH_4OAc Buffer	Flow rate
0	5 %	95 %	2.0 mL/min
15	100 %	0 %	2.0 mL/min
20	100 %	0 %	2.0 mL/min

Sequence table

Vial 91	Wash	##START		10ul
Vial 91	Wash	###DON		10ul
Vial #	Sample name	###DON		10ul for analytical 600ul for collection
Vial 91	Wash	###END		10ul

Always run an analytical first to determine sample purity and retention time.

1. Load the Start Method & update your sequence.
2. Detach last column used and replace caps. Join inlet and outlet with metal adaptor.
3. Fill all solutions (Line B: ACN and Line C: 50 mM Ammonium Acetate Buffer) & update solvent volumes by right clicking solvent bottles on instrument diagram.
4. Turn on the pump. Pump 100% ACN for 5 min, until pressure stabilizes.
5. Replace metal adaptor with column and let the pressure stabilize – document column pressure at 100% ACN, as column ages and ultimately fails this will be marked by an increased initial column pressure.
6. Check sequence parameters.
    a. Subdirectory = initials, Operator = initials, Prefix = date
7. Start Run.
    a. When collecting samples, DO NOT collect either front or end shoulders. Only collect the main peak.
    b. Typical Retention times: Natural ~12 min, Thiol ~20 min, Amino ~ 15 min, NB ~ 20 min.
8. Freeze in liquid nitrogen and place samples on the lyophilizer.

Step 4: DMT removal

Standard Conditions: Natural, Amino, and NB modified DNA

1. Prepare 80% acetic acid with 20% H_2O.
2. Add 250 µL to each dried sample from lyophilizer.
3. Vortex and centrifuge for a few minutes to force liquid from the sides into solution.
4. Let reaction proceed for 25 min.
    a. Might see slight orange color from DMT group.
5. Transfer solution to a 1.7 mL eppendorf.
6. Add 1 mL Ethanol to quench the reaction and vortex.
    a. Keep Ethanol in refrigerator such that it is chilled to aid in DNA precipitation.
7. Puncture cap with a needle and place on speed vacuum to dry.

DNA modified with 5' Thiol-modifier (perform directly before running HPLC)

1. Re-suspend dried samples in 50 µl pH ~8.4 50 mM Tris HCl buffer.
2. Add 30 mg DTT (so final [DTT] = 100mM), vortex & centrifuge.
3. Let reaction proceed for 45 min.
4. Prep a Nap5 size exclusion column.
    a. Remove top and bottom caps and place over a collection beaker.
    b. Prime column with 3.0 mL 5.0 mM Phosphate Buffer.
        i. Buffer runs through column by gravity and filter should be dry before proceeding to next step.
5. Load sample onto column knowing exact volume (~70 µL).
6. Add ~420 µL phosphate buffer to move the DNA to the base of the column but not elute it. Volume determined based on column capacity of 500 µL (500 µL – 70 µL = 430 µL).
7. Place Nap5 over HPLC vial and add 600 µL of phosphate buffer to elute DNA.

Step 5: HPLC Purification – DMTOFF

Sample preparation

1. Add 600 µl of 5.0 mM Phosphate buffer to dried samples unless it is 5′-Thiol modified DNA which can be used directly from the Nap5 column.
2. Vortex samples, transfer to a filter tube, and centrifuge.
3. Transfer into HLPC vial.

Instrument preparation

1. Same procedure as DMTON except for the method and retention times.
    a. DMT OFF Method (###DOFF):

Time (min)	ACN	Buffer
0	5 %	95 %
35	15 %	85 %
40	5 %	95 %

    b. Retention times: Natural ~12 min, Thiol ~15 min, Amino ~ 15 min, NB ~ 30 min.
    c. If DNA peak elutes in the first 8 min of the method update your method to be isocratic for the first 7 min, held at 5% ACN & 95% Buffer as the DNA is eluting within the dead volume of the column and therefore not being purified.
    d. Don’t bother running analyticals for DMTOFF of MB and NB modified DNA on PLRPS columns as they don’t typically work.

Step 6: Mass Spec

1. Matrix-assisted laser desorption/ionization time of flight (MALDI TOF) mass spectrometry to verify the identity of the oligonucleotide.
2. Use IDT to predict the molecular weight (MW) of the desired DNA sequence.

a. Correct MW of 5′ thiol modfied strand by subtracting 133 g/mol to account for disulfide cleavage in the spectrometer.

Step 7 & 9: Desalt DNA

1. Add 100 µl H_2O to dry lyophilized samples, vortex & centrifuge.
2. Transfer to a 1.7 mL eppendorf.
3. Add 1000 µl of cold Ethanol to eppendorf.

a. Keep Ethanol refrigerated to aid with precipitation.

4. Add 50 µl of 3 M NaCl to the tube formerly containing the dried sample and transfer to eppendorf.
5. Vortex, freeze in liquid nitrogen, and centrifuge in the cold room for 25 min.
6. Pipette off supernatant.
7. Wash pellet with 400 µl of 70% EtOH/H_2O (chilled).
8. Vortex, centrifuge (1 min), and pipette off supernatant.
9. Wash pellet with 400 µl of 100% EtOH (chilled).
10. Vortex, centrifuge (1 min), and pipette off supernatant.
11. Place pellet of DNA on the speed vacuum to dry.

Step 8: In solution coupling of MB' to Amino modified DNA

*** Most important information:*

- *Use Amino-modified DNA with DMT group removed.*
- *Reaction is buffered to pH 8.3-8.5 by 0.1 M $NaHCO_3$ (Figure A2.3).*
- *MB'-NHS is freshly activated in DMF but the DMF must be completely removed for the coupling reaction to proceed.*
- *Nap5 column to remove excess MB' in order to protect the HPLC column.*

Figure A2.3. In-solution coupling of NHS-ester modified MB with amino-modified DNA.

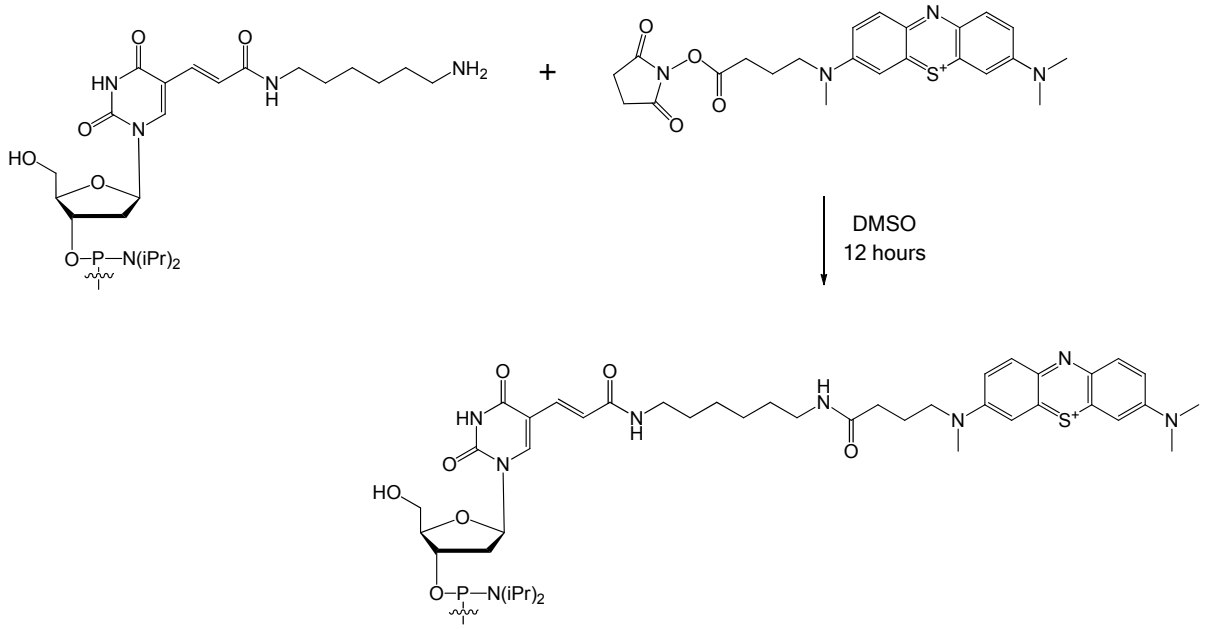

1. Re-suspend desalted DNA pellet in 200 µl of 0.1 M $NaHCO_3$.
2. Add ~ 50 µL of MB'-NHS in DMSO (see Appendix I).
3. Place on shaker and cover with aluminum foil and let shake overnight.
4. Purify MB′-DNA prior to HPLC with a Nap5 size exclusion column.
    a. Load sample onto column knowing exact volume (~250 µL).
    b. Add ~ 230 µL phosphate buffer.
    c. Add 800 µL of phosphate buffer to elute DNA into an HPLC vial making sure to collect the first blue band.
    d. See DMT removal of 5'-Thiol-modifed DNA for further details.
5. Purify by HPLC using the same protocol as DMTOFF.
    a. Collect the peak that has absorbance at 260 nm, 280 nm, and 600 nm (Figure A2.4).
    b. Freeze and dry samples on the lyophilizer.

Step 10: Quantify and Anneal DNA

Important: Re quantify ssDNA after every freeze thaw cycle.

1. If DNA is dry, re-suspend in ~200 µL 5.0 mM Phosphate buffer.
2. Quantify DNA by UV-Vis.
    a. Turn on both lamps on the UV-Vis and let warm up.
    b. Blank UV-Vis with 400 µL phosphate buffer.
    c. Make diluted samples for each ssDNA stock.
        i. Add 1 µl – 5 µL of ssDNA in 400 µL phosphate buffer and vortex.
        ii. Absorbance at 260 nm must be between 0.1 and 1.
    d. Use the same cuvette for all samples and place in the UV-Vis in the same orientation each time. Wash cuvettes with methanol and water between each sample and dry thoroughly.

Figure A2.4. Analytical HPLC traces for MB' modified DNA purified using the DMTOFF method. MB'-modified DNA is identified by the presence of a peak at all three wavelength monitored (260 nm, 280 nm, and 600 nm). As an inset the full spectrum of MB'-modified DNA is provided.

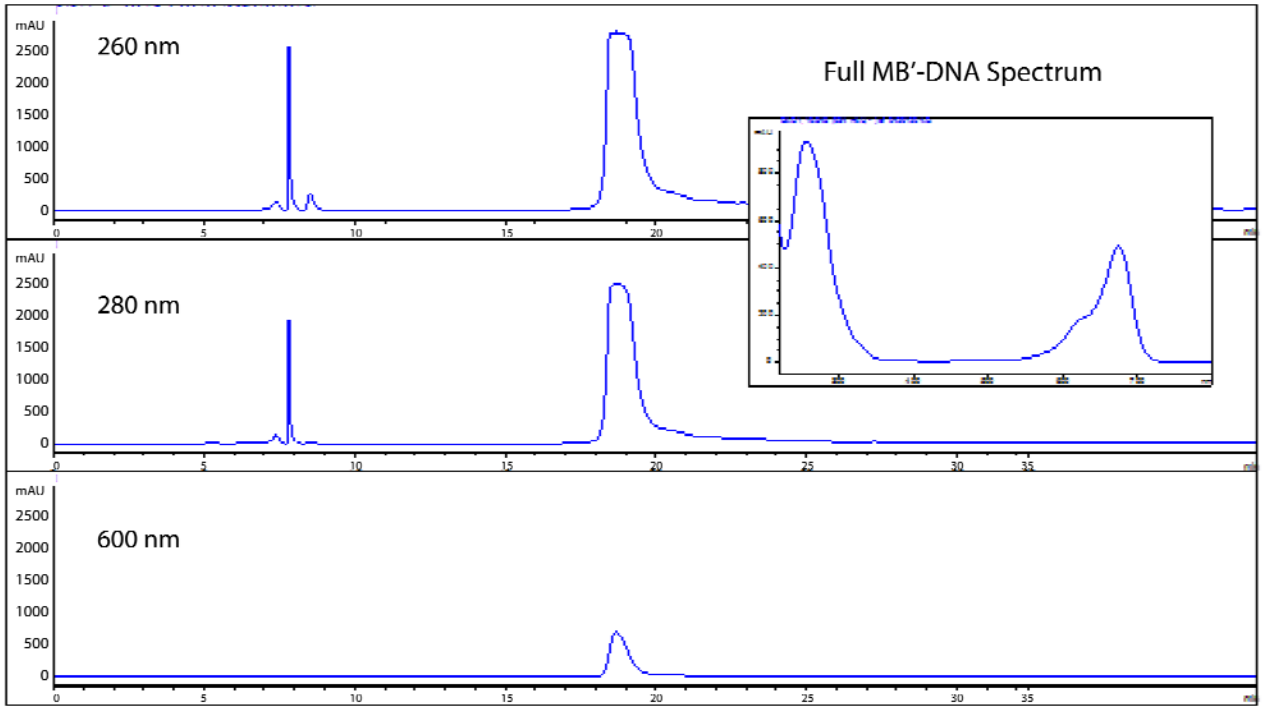

3. Calculate ssDNA stock concentrations.
    a. Use IDT to determine the extinction coefficient of your DNA.
    b. If NB or MB use the appropriate correction factors.
4. Prepare stocks of 50 mM double stranded (ds) DNA in 5.0 mM Phosphate Buffer.
5. Bubble Ar for 1 min into solution to thoroughly de-oxygenate the solution.
6. Place on Thermocycler (File #9) to anneal DNA.
    a. Heats to 90 °C, holds for 5 min, and then slowly cools over 90 min.
    b. After the cycle is complete, store in freezer.

REFERENCES

1. Slinker, J., Muren, N., Gorodetsky, A., Barton, J.K. *J. Am. Chem. Soc.* **2010**, *132*, 2769.

2. Pheeney, C.G., Barton, J. K. *Langmuir* **2012**, *28*, 7063.

APPENDIX III

Multiplexed Chip Fabrication

INTRODUCTION

The procedures here are modified (*1*) and augmented (*2*) from previously literature precedence. See Figure A3.1 for images of various multiplexed chips patterns that have been fabricated using the below procedures.

MATERIALS AND METHODS

Materials

Silicon (1-0-0) wafers with a thickness of 500-550 μm, single side polished, and any dopant were purchased from Silicon Quest International. Photoresists (Shipley), SU-8 (Microchem), and all developers were provided by the Kavli Nanoscience Institute (KNI). All deposition metals were purchased and maintained by the KNI at purities > 99.99%. Transparency masks were purchased from CAD/Art Services.

General Fabrication Procedures and Troubleshooting

See Figure A3.2 for the step-wise patterning of deposited metal and SU8 coating. The most common problem encountered during fabrication is undesired features in the photoresist or SU8 coatings. If this occurs the most liable cause is that the wafers were insufficiently dehydrated; alternatively it can also be caused by contaminated photoresist/SU8. When troubleshooting the photoresist/SU-8 quality, it is critical to realize that the bake, exposure, and development parameters are not independent of one another. Baking cures the photoresist/SU-8, slowing the development. Exposure to UV either solubilizes or stabilizes the resist, depending on the polarity, by speeding up or slowing down the development, respectively. Finally, the development time should ideally be 30 – 60 sec for even development of feature. For example, if the features are over developed,

Figure A3.1. Images of devices fabricated using standard photolithography of various patterns. Devices for use in two different infrastructure assemblies are presented. Chips with Pt counter and reference electrodes integrated into the device were prepared for use in both assemblies.

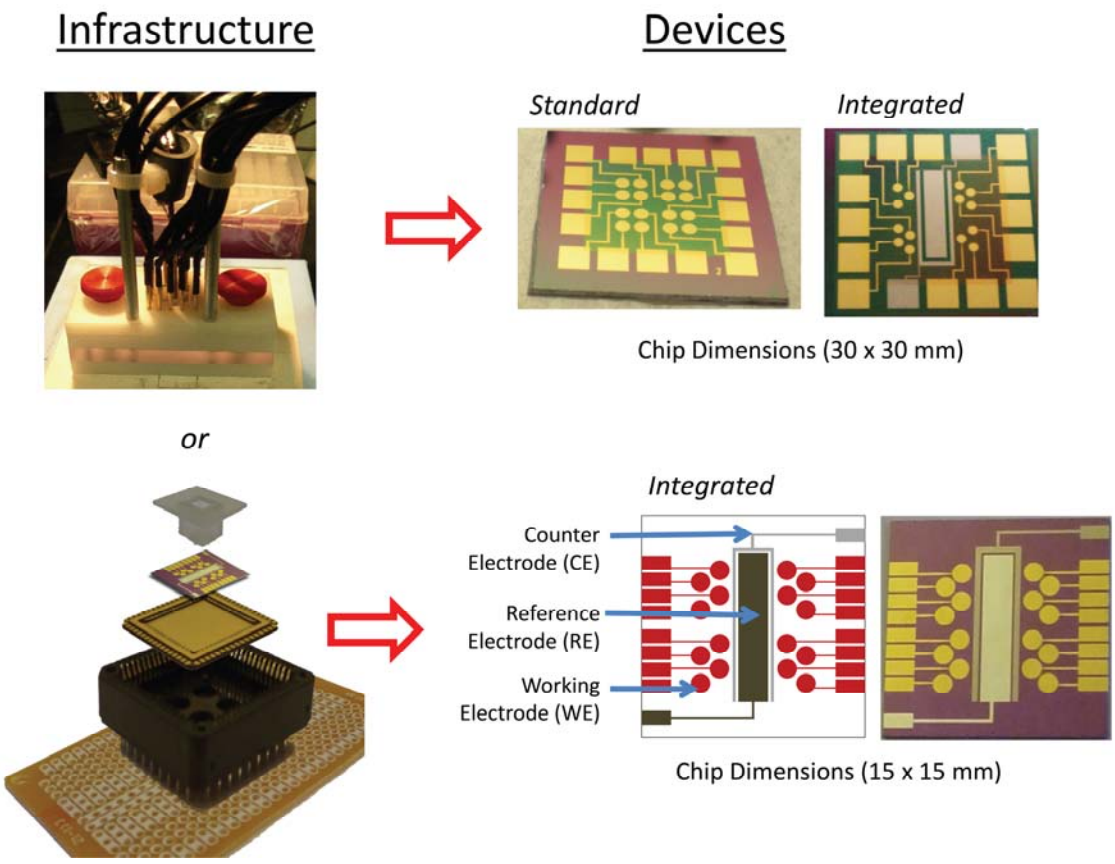

Figure A3.2. Depiction of the step-wise procedure for the deposition of metal features and coating of SU-8 on thermal insulated SiO_2 wafers.

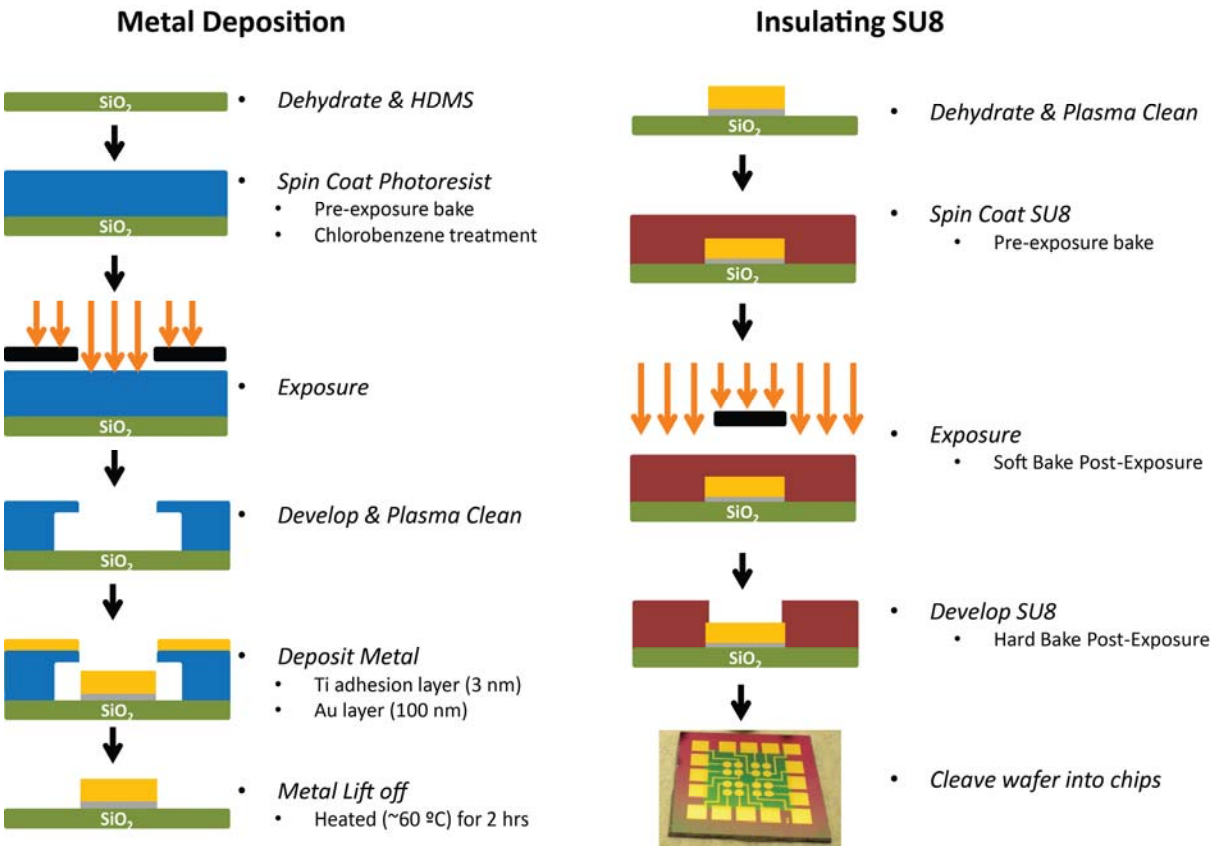

instead of shortening the development time, the pre-bake time can be extended or the exposure time adjusted, which will result in the same overall affect.

In general the overall quality of the SU8 layer is the most critical component to ensure successful electrochemistry. Defects in the SU8 layer have been seen to result in minimal or no signals generated from the immobilized DNA. If the devices are not yielding signals and there are no defects in the SU8, other possible causes are the adhesion of the metal and the cleanliness of the surfaces. Poor metal adhesion can be identified by the ability to easily scratch off the deposited metal. This can be fixed by increasing the HMDS incubation time and/or the thickness of the Ti adhesion layer. Finally, plasma cleaning chips directly before assembly with DNA for 5 min with O_2 (100 W at 1 Torr) can rescue chips if the problem is quality of the Au surface. Plasma cleaning chips directly before assembly with DNA is also useful for generally increasing signal sizes by ~10 - 20%.

Patterning with Positive Photoresist

1. Dehydrate wafers; bake wafers (140 °C) in either oven or hot plate for 30 min or 10 min minimum respectively.
    a. Dehydration temperature is dictated by needing to be at least 20 °C above the highest temperature used during the process.
2. Let wafers cool and then place wafers in HMDS chamber for 5 min.
3. Spin coat wafers with 2 µm of positive photoresist (MicroPosit S1813).
    a. Use Laurel 2 and program E (2500 rpm for 30 sec for 2 µm thickness).
    b. Center/balance wafer in laurel and then turn on vacuum to immobilize.
    c. Pipette photoresist S1813 from middle of the bottle onto center of the wafer, ensuring there is enough photoresist to fully coat the features on the wafer.

   d. Close lid and spin; when spinning is done check that the wafer is coated, then release from vacuum, check that the back of wafer is clean of photoresist, and if there is photoresist use a swab to remove with solvent.
   e. If after spinning the photoresist does not cover the necessary features do not bake wafer. PG remover, Photoresist Developer, or Nanostrip will all work to remove the photoresist and restart the process including the dehydration.
4. Soft bake wafers on a hot plate at 115°C for 1 min.
   a. Make sure to equilibrate hot plate prior to use because ideally temperature is within ± 1 ºC.
5. Undercut photoresist by soaking in chlorobenzene for 5-10 min.
   a. **Safety**: Chlorobenzene is highly carcinogenic, therefore always keep petri dishes covered with lids and thoroughly dry with N_2 gun while under the fume hood. If fumes start to persist throughout the solvent room, stop and find a staff member in the KNI.
6. Expose photoresist to UV light using contact aligner (Karl Suss)
   a. Load the 5” mask holder and 4” wafer holder
   b. Turn on monitor and pump and check that the lamp is on channel 2 for the g-line. Load mask and the soft contact program.
   c. Edit program parameters: alignment gap of 20 µm, exposure time of 30 sec, and WEC type of contact.
      i. Exposure time based on g-line intensity to deliver a dosage of 150 mJ/cm^2, adjust as needed if lamp power is changed to keep dosage constant.
   d. Load wafer, align, and expose.
      i. Rough alignment can be performed without microscope. Press F1 then enter to move microscope out of the way.

ii. Return microscope using same commands to perform fine alignment. Typical centered alignment positions are y = 12 and x = 5.

e. Follow commands to unload wafer.

7. Develop photoresist with MF-CD26 developer for ~ 30 sec.
    a. Quench development by rinsing with water for 1 min.
8. Thoroughly dry with N_2 gun and ideally proceed to metal deposition within 24 hr.

Metal Patterning

1. De-scum wafers by plasma cleaning for 2 min by O_2 (100 W at 1 Torr).
2. Proceed to metal deposition using CHA (Ti = 30 Å and Au = 1000 Å).
    a. Sign into CHA log file and record required fields, including: initial pressure, base pressure ($5x10^{-7}$ psi), and crystal life (needs to between 25-30).
3. Open recipe folder (Ti_Au deposition) in excel, load desired parameters, save, and then close.
    a. Pressure: $5x10^{-7}$ (no higher than $1x\ 10^{-6}$).
    b. Material file: Ti = 2 and Au = 5.
    c. Rate: Ti = 0.5 Å /sec and Au is 1.0 Å/sec.
    d. Thickness: Ti is 15 Å and Au is 1000 Å.
    e. Crucible: Ti is 2 and Au is 5
4. Load samples (up to 42 wafers with orbital sample holder) and start chamber pump down. Wait for pressure to reach base pressure, turn on high voltage, and engage the autostart.
5. Upon completion of process proceed directly to metal lift off using PG remover. Lift off all wafers at once using a 4 L beaker of PG Remover heated to ~60°C.
    a. Metal lift off takes ~ 1hr to fully developed all feature and remove any residual photoresist.

b. Once metal lift off is complete wash wafers in acetone followed by water and dry with N_2 gun.

Patterning with SU-8 (Negative Photoresist)

1. Dehydrate wafers by baking at 180 °C for at least 10 min.
2. De-scum wafers by plasma cleaning for 2 min by O_2 (100 W at 1 Torr).
3. Spin coat wafers with 2 μm of negative photoresist SU-8.
    a. Use Laurel 1 and program F (3000 rpm for 30 sec for 2 μm thickness).
    b. Center/balance wafer in laurel and then turn on vacuum to immobilize.
    c. Pipette SU-8 2002 from middle of the bottle onto center of the wafer, ensuring there is enough photoresist to fully coat the features on the wafer.
    d. Close lid and spin; when spinning is down check that the wafer is coated, then release from vacuum, checking that the back of wafer is clean of photoresist, and if there is photoresist use a swab to remove with solvent.
4. Pre-exposure bake on hot plate at 95 °C for 1.5 min.
    a. **Important**: Verify SU-8 coating prior to baking as once the SU-8 is baked it is exceptionally challenging to remove. Nanostrip and plasma cleaning are the best options for trying to remove cured SU-8.
5. Expose SU-8 to UV light using contact aligner (Karl Suss) by the aforementioned procedure.
    a. Differences: use channel 1 (i-line), alignment gap of 20 μm, exposure time of 25 sec for a total dosage of 160 mJ/cm^2, and WEC type of contact.
6. Post-exposure soft bake on hot plate at 95°C for 1.5 min
7. Develop excess SU-8 with SU-8 developer in solvent room.

a. Soak each wafer for 60 sec in SU-8 developer, rinse in isopropanol, soak for an additional 10-20 sec in SU-8 developer, and perform a final rinse isopropanol rinse.
    i. Check quality of SU-8 development under the microscope and if SU-8 is under developed soak wafer for an additional 10 sec in developer.

8. Hard bake wafers at 150 °C for 15 min to cure SU-8.

REFERENCES

1. Slinker, J., Muren, N., Gorodetsky, A., Barton, J.K. *J. Am. Chem. Soc.* **2010**, *132*, 2769.

2. Pheeney, C.G., Arnold, A.R., Grodick, M.A., Barton, J.K. (2013) *J. Am. Chem. Soc.* in press.